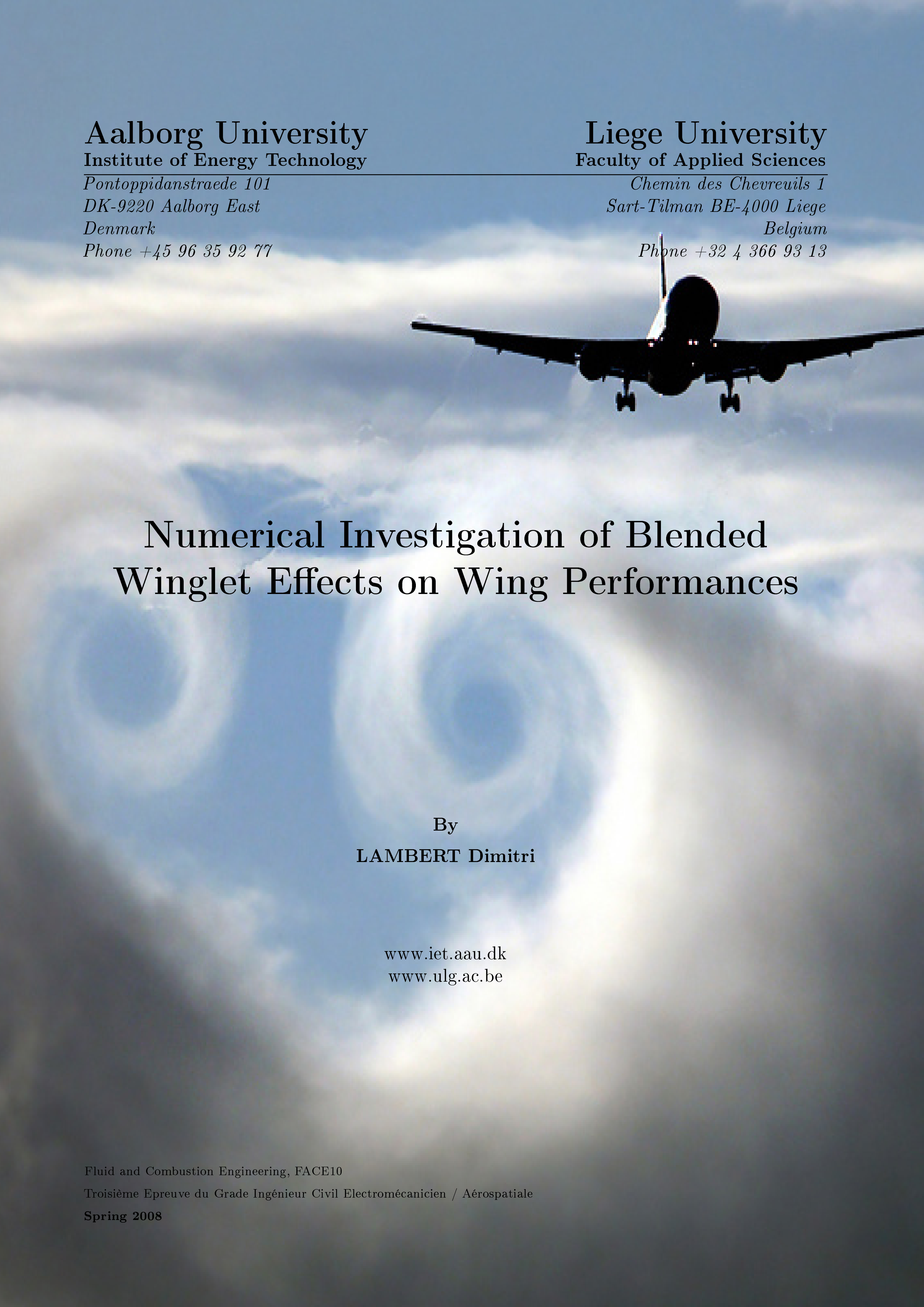

Aalborg University
Institute of Energy Technology
Pontoppidanstraede 101
DK-9220 Aalborg East
Denmark
Phone +45 96 35 92 77

Liege University
Faculty of Applied Sciences
Chemin des Chevreuils 1
Sart-Tilman BE-4000 Liege
Belgium
Phone +32 4 366 93 13

Numerical Investigation of Blended Winglet Effects on Wing Performances

By

LAMBERT Dimitri

www.iet.aau.dk
www.ulg.ac.be

Fluid and Combustion Engineering, FACE10
Troisième Epreuve du Grade Ingénieur Civil Electromécanicien / Aérospatiale
Spring 2008

Numerical Investigation of Blended Winglet Effects on Wing Performances

LAMBERT Dimitri

....

Project period

February 4 - June 3, 2008

Printing

8

Number of pages

98

Supervisor
Lasse Rosendahl
IET, Aalborg University

Since decades fuel never stops rising. Civil aviation market is very sensitive for profitability. Several ways are possible to reduce aircraft fuel consumption. One of them is the wingtip device. Winglet has been proven. But there is still one big challenge: to simulate the aerodynamics around it. Different types of winglet are modelled in the present work: the simple winglet, the blended winglet and the shifted downstream winglet. The blended winglet is the most fitted to the wingtip to prevent auxiliary vortex to be born at the junction.

Although there exist different analytical models to solve the flow around a $3D$-wing, none of them can include wingtip device effects. This investigation is then lead numerically. Two models are built according to a thickness difference.

Winglet brings effectively higher performances regarding lift and drag. Pressure gradients around the wing are well preserved until the wingtip, keeping the wing operational on its whole span. They prevent vortex and then allow the fluid flow to stay quite homogenous and unchanged at the wintip. But if the angle of the winglet is too sharp, an auxiliary vortex could be created. Thanks to wingtip devices the vortex lets feel weaker along the span because it is generally displaced to the winglet tip.

Models built are two extreme cases about winglet geometry but could give a first general idea on how winglets influence the general aerodynamics around the wing.

Contents

I Report 3

1 Background 4

1.1 Introduction . . . 4
1.2 State of the art . . . 5
1.3 Winglet theory . . . 6
1.3.1 Recall on simple wing flow . . . 7
1.3.2 Generalities . . . 7
1.3.3 Simple winglet . . . 9
1.3.4 Blended winglet . . . 9
1.3.5 Shifted downstream winglet . . . 10
1.4 Objectives . . . 10
1.5 Trends and experimental characteristics . . . 11
1.5.1 Drag and Lift . . . 11
1.5.2 Vortex pattern . . . 12

2 CFD Simulations 14

2.1 Different models and geometries . . . 14
2.2 Mesh quality . . . 16
2.2.1 Conclusions on 2D elements: . . . 16
2.2.2 Conclusions on 3D elements . . . 18
2.2.3 Is the mesh refined enough? . . . 20
2.3 Settings in Fluent . . . 20
2.3.1 Models . . . 20
2.3.2 Boundary conditions . . . 21
2.3.3 Solver . . . 21

3 Results 22

3.1 Forces and Moments . . . 22
3.1.1 Lift and Drag . . . 22
3.1.2 Moments . . . 30
3.1.3 Conclusions on forces and moments . . . 31
3.2 Pressure . . . 33
3.2.1 Distribution along the wing span . . . 33
3.2.2 Distribution along the chord . . . 35
3.2.3 Conclusions on pressure . . . 36
3.3 Velocity . . . 37
3.3.1 X-component . . . 38
3.3.2 Y-component . . . 42
3.3.3 Z-component . . . 45

3.3.4 Conclusions on velocity . . . 48
3.4 Vortex pattern . . . 50
3.4.1 Case without winglet . . . 50
3.4.2 Case with simple winglet . . . 53
3.4.3 Case with blended winglet . . . 54
3.4.4 Case with shifted downstream winglet . . . 56
3.4.5 Conclusions on vortex . . . 56
3.5 Mesh Independancy . . . 58

4 Conclusions and Discussions **59**
4.1 Assumptions and Limitations . . . 59
4.2 Final Conclusions . . . 60
4.3 Further Work . . . 61

II Appendices **62**

A Fluent Program **63**
A.1 Basic equations in Fluent . . . 63
A.2 Models . . . 64
A.2.1 Solver . . . 64
A.2.2 Turbulence . . . 66

B Modeling procedure **70**
B.1 Cooper scheme . . . 70
B.2 2D geometry . . . 71
B.3 3D geometry . . . 72
B.4 Quality Analysis . . . 73
B.4.1 2D elements in the Full-3D-Model . . . 73
B.4.2 2D elements in the 2D-wing-in-3D-environment Model . . . 77
B.4.3 Conclusions on 2D elements: . . . 78
B.4.4 3D elements in the Full-3D Model . . . 79
B.4.5 3D elements in the 2D-wing-in-3D-environment Model . . . 80
B.4.6 Conclusions on 3D elements . . . 81

C Data extraction **83**
C.1 Along the wingspan . . . 83
C.2 Along the chord . . . 84

D Pressure figures **85**

E Velocity figures **89**

F Vortex pattern figures **93**

III Bibliography **96**

Part I

Report

Chapter 1

Background

1.1 Introduction

Fuel price are always in mind. Since decades, price never stops rising. Especially in civil aviation, fuel price is a crucial factor for rentability. Engineers still work to optimize aircrafts. One big feature come out this last ten years in civil aviation is the wingtip device. This little device placed at the end of the wing aims to eliminate, or at least, to reduce induced drag. This induced drag comes from a secondary flow due to the pressure gradient between upper and lower surface. Its name is the *winglet*.

The effect of the winglet has been proven. For instance, the Boeing 747-400 can save 9.5 tons at take off, only thanks to its winglets. That means about 2.5 % of drag reduced ([1]). For the Boeing 737 Next Generation, performances are well improved, but especially for medium range rather than for short range (less than one hour trip). Indeed, due to the weight penalty, short range trip shoudn't have benefits with winglet ([2]).

Also from [2], climb performances are rather enhanced, then cruise altitude might be higher and thus drag is lowered by reducing time spent in traffic congestion: "*With Blended Winglets, we can now climb direct to 41,000 feet where traffic congestion is much less and we can take advantage of direct routings and shortcuts which we could not otherwise consider*".

But there is still a unresolved challenge: detailed numerical modelling of the vortex structures around an airfoil. This complex three dimensional motion is in different ways quite complicated. In section 1.2, state-of-the-art computations are discussed where models are quite difficult to be found to fit with reality and therefore, this is the aim of this work. Based on an experiment done in a wind tunnel to investigate effets of blended winglet on wing performances ([8]), complete three dimensional computations are run in order to validate this experiment. In the simulations in the present work, a NACA 4412 profile is used, and the results are compared to available data from literature and simple aerodynamic models. Furthermore, data from airfoils fitted with winglets are also brought for comparisons. It has not been possible to obtain data for a NACA 4412 airfoil with a winglet, but only for a NACA 5012 airfoil. These general features from experiment are detailed in section 1.5.

Differences from NACA 4412 and NACA 5012 are found thanks to the NACA four-digits profile code (please refer to section 2.1 for detailed recalls). Maximum thickness is the same for both wings (12 % of the chord). It is the only common feature. The wing in experiment has a maximum camber situated at leading edge and has one percent more than the one used in the present work which is situated at 40 % of chord from leading edge.

1.2 State of the art

Civil aviation is very sensitive to fuel price changes. Nowadays, it is not believable to get a fuel price as low as in the 60's. Figure 1.1 presents the evolution of the fuel price through years and the discrepancies between oil discovery and production.

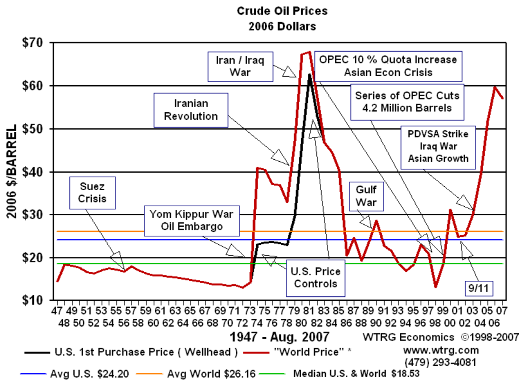

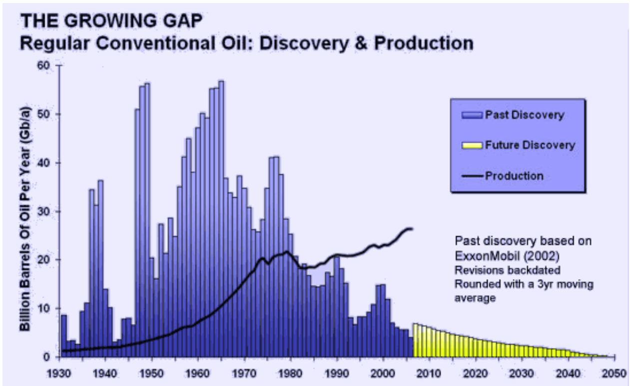

Figure 1.1: Left: Fuel price evolution from [3] - Right: oil discovery/production evolution from [4]

Obviously from these, because of huge demands of the market and the decrease of production, fuel price is not about to fall. From right picture, it seems that the price has already reached higher, but current situation is on the same track to reach the top.
In civil aviation market, fuel price is a crucial element for profitability. If it rises, tickets prices rise and passenger numbers might decrease. Fuel consumption is then a key factor. To reduce it, two main ways are possible: enhance engine performance and/or aerodynamic performance. Scheme is illustrated on figure 1.2.

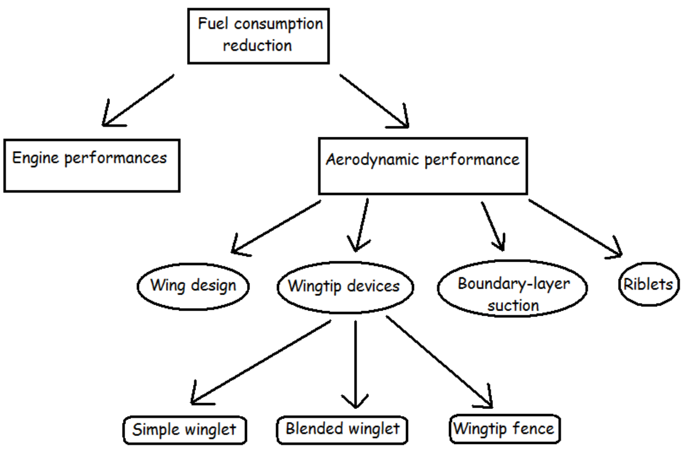

Figure 1.2: Ways of drag reduction

Of courses there are different devices to reduce drag at engine performances level but they are not mentioned here. Under aerodynamic performances level what can reduce drag? Good wing design, wingtip devices (or winglet), boundary layer suction and riblets can be mentioned. By order, a well-designed wing produces lower drag; winglets prevent secondary flow and then vortex (induced drag); sucking boundary layers allows to have more kinetic energy and then limitate the risk of flow separation; and riblets allow reducing skin friction and then drag.

This work aims to investigate numerically effects of winglet on wing performances. The main part is to underline the influence of a specific winglet which is the blended one.

Effects of these winglet (and especially the blended one) are well-know from constructors like Boeing, Airbus and so on. But numerical prediction of wingtip vortices (see in section 1.3) are still a challenge in computational fluid dynamics. According to [5], it is because "*besides predicting the development of the strong vortex itself, one needs to compute accurately the flow over the wing to resolve the boundary layer roll-up and shedding which provide the initial conditions for free vortex*". One of the principal characteristics to capture when modeling near-field vortex is that "*...as the vortex rolled up, the pressure on the axis progressively fell, leading to an increase in the axial velocity above that in the free stream as one moved radially inwards to the vortex centre*". The main challenges in modeling trailing vortex flow's development is that, as already cited above, the boundary layer (on both surfaces of the wing) have to be computed very accurately since they are the initial condition for the vortex computation. In consequence, the model of turbulence has to be chosen in order to be able to resolve this complex boundary layer ([5]).

Winglets are quite highly efficient devices to reduce induced drag but another important parameter is weight penalty ([6]). Indeed, adding a winglet means more weight to be flown and more bending stresses at the root of wing, so more fuel is consumed. A compromise has to be found. For example, according to [6], "*Leyser [7] has shown that wing tip devices with anhedral provide lower induced drag reductions in comparison with devices using dihedral. Unlike that, the present study has been carried out considering weight increase .../... . Taking an advantage of the dihedral of the wing, a winglet with anhedral may provide a greater equivalent drag benefit than the design with dihedral by reducing the wing root bending moment*".

In conclusion, winglets are well a state-of-the-art device to reduce induced drag on aircrafts, but they have to be studied with all factors (weight, manufacture cost, ...). At this CFD standpoint, modeling vortex in trailing flows are still a challenge because of the need of solving very accurately boundary layers at lifting surfaces which are intial conditions for the vortex computation.

1.3 Winglet theory

The winglet is the name for the physical device attached to the tip of the wing. Different types of winglet exist but they have the same purpose: reducing induced drag. First winglet principle is detailed then particular cases like wingtip fences or blended winglets are focused.

1.3.1 Recall on simple wing flow

Fluid flow pattern around a simple wing alone is presented on figure 1.3 left and the wingtip flow feature on the right.

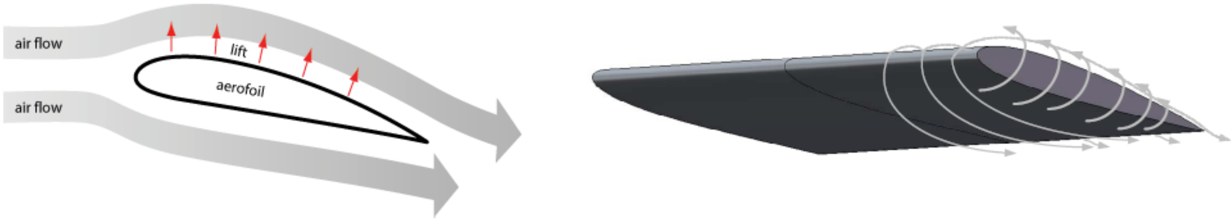

Figure 1.3: Flow around simple wing and its wingtip from [8] and [10]

When a wing profile is not symmetrical (or when there is a non zero angle of incidence), a velocity difference is uphold between upper and lower surfaces. This creates a pressure difference and a circulation around the wing: lift is generated. At wingtip, fluid from high pressure surface tends to go to low pressure. There is a secondary flow at wingtip (as illustrated on figure 1.3 right) that leads to vortex creation. Induced drag comes from this wingtip vortex.

1.3.2 Generalities

Lift of a wing is produced by high pressure on the lower surface and low pressure on the upper surface. Each of these components acts in increasing lift direction. As the well-known Bernouilli equation, the fluid has a trend to go from high to low pressure. Because every wing on aircrafts are non-infinite, at the wingtip, the phenonemon occurs. It creates a flow from the lower to the upper surface. From this point, the vortex is generated and can vanish into the traling wake of the wing. This pattern is clearly visible on figure 3.4.

Figure 1.4: Vortex illustration by *NASA Langley Research Center (NASA-LaRC)* [10]

The rotation sense is easily deductible from this picture. This illustrates well the path from low to high pressure. Increasing aspect ratio is one manner to lower these vortices. Theoretically an infinite span wing has no vortice. But rising span means higher bending moment at root and this is not in the same direction as weight saving. The intermediate way to prevent the fluid going this way is to block it physically: the winglet is born. Its main purpose is to stop (or rather decelerate) the fluid and then reducing induced drag. Figure 1.5 illustrates that over the normal wing, secondary flow is able to form the vortex while the winglet reduces this fluid vortex motion. On the actual wing, it is necessary to uphold a velocity - hence pressure - difference between the upper and lower side of the wing in order to create lift. For the winglet, this is not so, and a smoother approach to even pressures can be obtained on this part. Thus, as one approaches the new wingtip (i.e. the tip of the winglet), the strength of the vortex can be much reduced, causing a much lower flow into the trailing vortex.

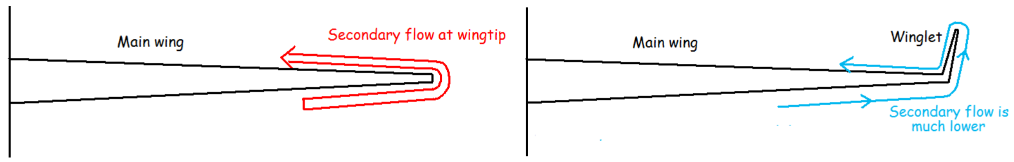

Figure 1.5: Influence of the winglet on the secondary flow

In addition to this reduction of incuded drag, the winglet itself produces a kind of additional thrust. Indeed, the winglet is, in a certain mode, the lengthening of the wing. The profile of the winglet could be the same as the wing profile (and could even be more cambered than the wing itself [9]) , namely it produces lift and drag. On figure 1.6, an above view of the wing and winglet is presented.

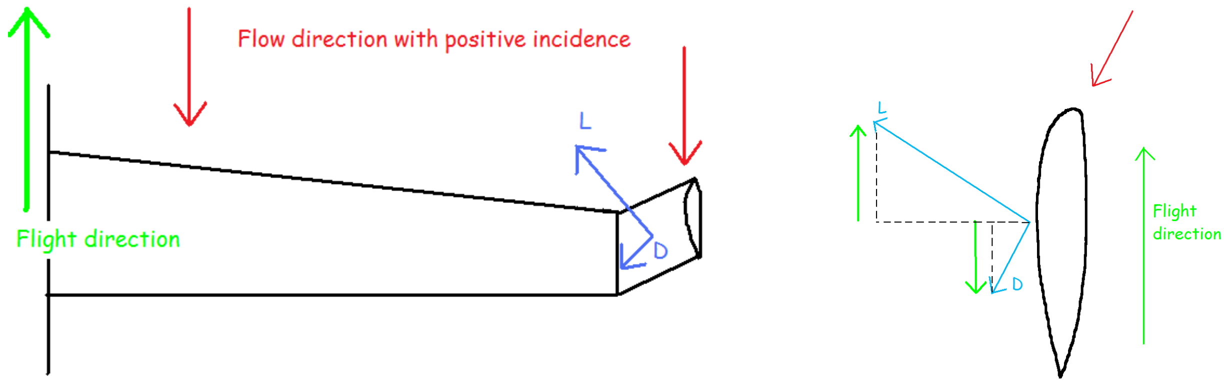

Figure 1.6: Acting forces on winglets (above point of view)

Because the profile of winglet could be the same, at a such angle of incidence, the winglet generates lift and drag. Of course, these forces are not in the plane parallel to the wing. But it is obvious to imagine that the component perpendicular to the wing is nearly negligible since the angle of the winglet tends to 90° (Figure 1.6 left).

Concerning the decomposition in the wing plane (Figure 1.6 right), each lift and drag produces component in the flight direction and towards the fuselage. But the ones towards the fuselage are exactly compensated by the same winglet on the other wing. These forces are then not discussed.

Drag of the winglet has a component to augment wing drag while its lift has a component to counter wing drag. For a well shaped winglet, lift is bigger than drag. It is why winglet generates a kind of thrust from itself. In addition of limiting the wingtip vortices, the winglet produces a little thrust. This reinforces the fact that the device reduces the total drag.

1.3.3 Simple winglet

Roughly speaking, the simple winglet is added at the wingtip "without care". This winglet could be simply seen as a plate stuck to wingtip. Figure 1.7 shows examples of this type of winglet.

Figure 1.7: Sharp winglet: Left: 747-400 of Northwest Airlines by Carlos Borda - Right: A340-200 of South African Airways by Michael Van Bosch

This means that between the wing and winglet, there is a corner with a sharp angle. As seen on figure 1.5, the boundary layer of the secondary flow might be subjected to adverse pressure gradient. Then a smaller auxiliary vortex is born, beginning from this junction.

Drag reduction is well present but not optimal due to this new little vortex. Advantage is the low cost of manufacture and assembling. Indeed this is less time and cost consumming than building a perfect fitted winglet to the wing (as the blended one, section 1.3.4). Moreover, the simple winglet itself is surely lighter because there is no smooth transition (winglet is smaller).

1.3.4 Blended winglet

The blended winglet, as its name indicates, is perfectly fitted to the wing. In this case, the corner at the junction is avoided. Examples are presented on figure 1.8.

Figure 1.8: Blended winglet: Left: 737NG of Ryanair by Michel Lambert - Right: 737NG of Virgin Blue Airlines by David Morrell

This smooth transition presents the advantage of limiting the risk of too high adverse pressure gradient that could lead to a creation of a small vortex (flow separation). In this case there is no small vortex at the junction. Advantages are not free. The cost of manufacturing a fitted winglet is bigger and its weight is higher as well. Indeed, such a winglet and its smooth transition are heavier than a simple one stuck at wingtip.

1.3.5 Shifted downstream winglet

Another way to prevent the risk of a flow separation due to high adverse pressure gradient at the junction is to create a winglet that is shifted downstream. Examples are displayed on figure 1.9.

Figure 1.9: Wingtip fence: Left: A380 of Airbus Industrie by Martin Boschhuizen - Right: A319 of EasyJet Airline by Sam Lambert

This kind of winglet is also well-known as *wingtip fence*. Indeed, it is like a barrier at wingtip that blocks secondary flows. The winglet shifted downstream leads to the same effect as the blended winglet: the fluid cannot be separated. In this case, there are the advantages of blended winglet and the weight is still limited because the wingtip fence is rather small compared to the blended one.

1.4 Objectives

This work aims to validate experimental observations ([8]) done in a wind tunnel where effects of blended winglet were investigated. As earlier stated, only trends and main characteristics are retained. In section 1.5, main results and tendencies are mentioned. Numerical tools are used. All flows are simulated in Fluent program[1].

Simulations are done with a NACA 4412 profile instead of a NACA 5012 as in experiment. A different profile from the one of experiment was chosen to have data base references in 2D while tested profile does not. Of course, observed trends should be similar and the main goal of this present investigation is to confirm these.

The main challenge in this work is to go further in vortex modeling. Indeed, vortex are still complicated to model due to this complex three dimensional motion and also due to initial conditions in case of an airfoil. Vortices generated by an induced volicity start from upper and lower surface of the wing: they are initial values. As stated in section 1.2, some model problems are still unresolved.

[1]Please refer to appendices A to know more about Fluent

This work can be seen as the continuation of the exprimental work done in the wind tunnel by doing a complete three dimensional computation with and without different types of winglet (see section 1.3). In the report of the experiment, a pre-study of the model to use has been done and this was helpful for these present computations.

1.5 Trends and experimental characteristics

Cases in experiment ([8]) were run for different types of winglets and various angles of incidence. Then one can find here only results related to angle of incidence sensitivity and vortex pattern. Beyond these trends, more accurate analysis were done in the experiment. And also in this work, deeper analysis are done to compare winglets and behaviours of vortices in each cases. Characteristics below, reported from experiment, are, in a certain way, the starting point for deeper interpretations in the present report.

1.5.1 Drag and Lift

The lift and drag coefficients are plotted on figure 1.10. One can find their final results for effects of winglets on drag and lift.

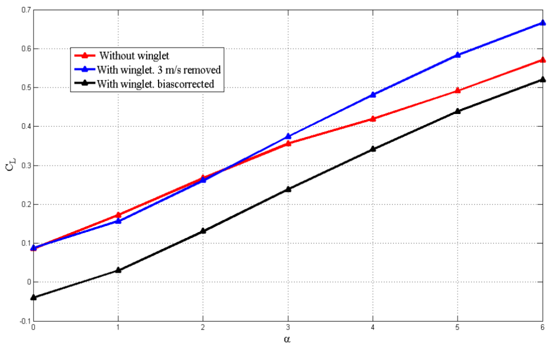

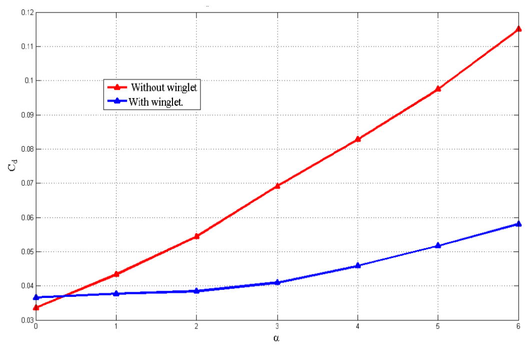

Figure 1.10: Comparison of lift (left) and drag (right) coefficients with and without mounted winglet (from [8])

For each evolution, they worked with confidence intervals. For lift (left graph on figure 1.10), they got an accuracy problem at low airspeed. For $3\,m/s$, they had to remove measurements due to unrealistic high values. Following if these data are taken in account or not, lift evolution with winglet is translated upwards or downwards while the lift evolution without winglet lies between those two previously cited evolutions. Then they couldn't conclude whether the lift is modified by the winglet or not.

On the contrary, drag evolutions (right graph on figure 1.10) are more clear. Obviously winglet reduces drag considerably. At low angles of incidence (α), it looks at the same level, but when α increases, drag has a tendency to stay moderate. This moderation through α seems to be the expected drag reduction since they start from the same level at low angles of incidence. (Note that in case of drag, measurements from low airspeed, $3\,m/s$, are already removed)

1.5.2 Vortex pattern

Thanks to a hot-wire anemometer (CTA), which is traversed by fluid flow, they could measure the axial and tangential velocities (mean and fluctuating values) in a grid situated behind the wing (at given distances). Then they could display vortices patterns on different planes behind the wing. On each plane, the orthogonal velocity was depicted in order to detect vortices. Displays are made at 30 mm, 60 mm and 90 mm behind the wing at 6 m/s and 14 m/s, namely Reynold number of 40788 and 95172. Only results at 14 m/s are kept for comparisons because they are more accurate and closer to simulations done in the present work. Figure 1.11 presents the evolution of the vortex through the three cross sections in the case without winglet.

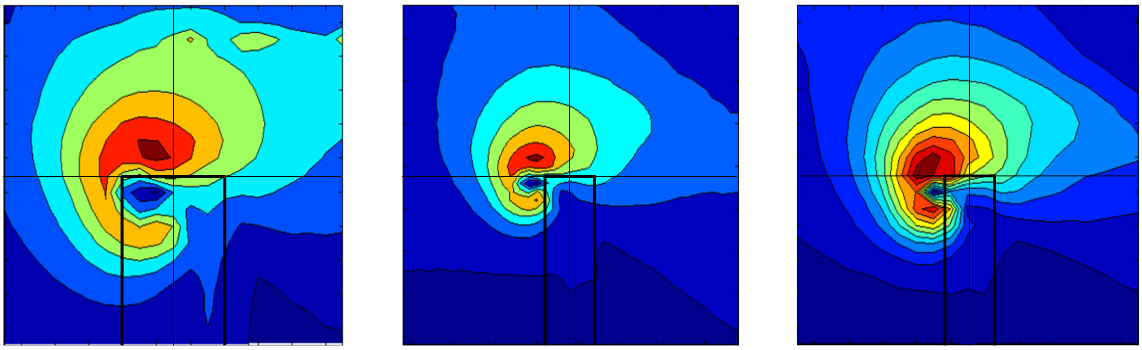

Figure 1.11: Evolution of the vortex through cross sections (30, 60 and 90 mm behind the wing) in the case without winglet (from [8])

Please note that first display on figure 1.11 shows an area of 40 x 40 mm while the two last ones show an area of 80 x 80 mm. They reported a decreasing average orthogonal velocity from first to last cross section, meaning a vanishing and extending vortex (be careful with the differences in scale area!). Figure 1.12 shows the same evolution but in the case with winglet. Please still note the differences in scale! The first one shows an area of 40 x 40 mm while the two last ones display an area of 80 x 80 mm.

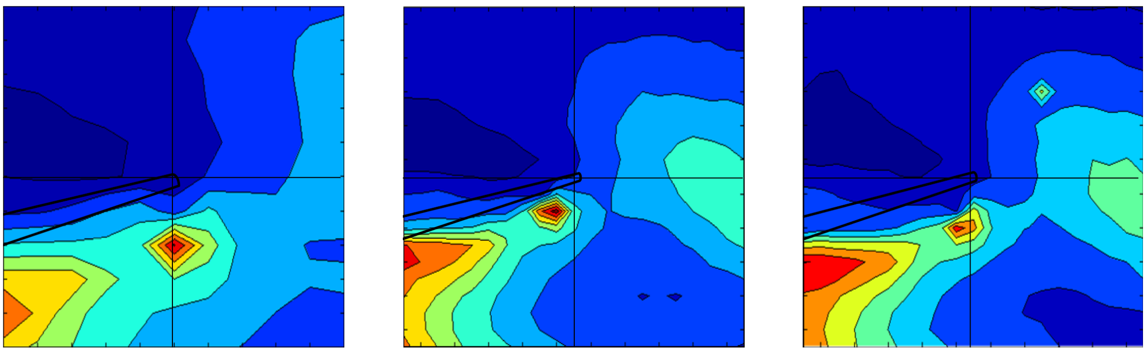

Figure 1.12: Evolution of the vortex through the cross sections (30, 60 and 90 mm behind the wing) in the case with winglet (from [8])

The average orthogonal velocity is reported being lower than in the case without winglet. For example in the cross section at 30 mm behind the wing, it decreases from an average of 6 m/s to 3.9 m/s. One can conclude that strength is lower in this second case. About the pattern itself, it seems the vortex is much smaller (be careful in scale differences!) than the previous case but they reported "*vortexes shed from the middle of the winglet, causing the vortex real area to be larger than shown. A larger measuring area would propably reveal an area of vortices behind the middle of the winglet, however the vortex strength still seems to be reduced*".

Indeed, if one has a look at average and maximum velocity values, one can conclude that energy involved in vortices behind winglet is less than behind the wing alone.

Chapter 2

CFD Simulations

2.1 Different models and geometries

Different models:

This work aims to investigate numerically effects of blended winglets on wing performance. Since these simulations are the continuity of the experimental work done by [8], a full 3D-simulation is required to investigate deeper the so-called *blended winglet*. By the way, it is not only compared with the simple case without winglet, but also with other well-known types of winglet presented in section 1.3: the shifted downstream winglet (wingtip fence) and the simple one (with sharp angle).

Due to the complex geometry of the winglet, some assumptions are done. Goals of simulations (and then geometries) are focused exclusively on discrepancies of performances due to the different winglets. To simplify, only one feature of winglets that distinguishes them between each other is retained. This feature is the junction between winglet itself and the wing. Effectively, this particular region is crucial since it could create an auxiliary vortex and then lower the drag reduction gained by winglet. In broad outline, one can find on figure 2.1 this difference between each of them.

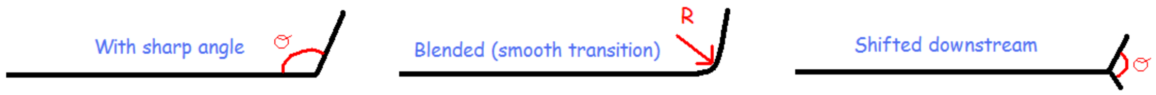

Figure 2.1: Retained feature to differentiate winglet types: comparison

This comparison shows the only difference selected between each case for the investigation. So, everthing else like detailed chord variations along winglets, thickness variations, ... are not taken in account.

Considering the way geometries are built (please refer to appendices B.3), the angle between the winglet and the wing (or the horizontal) is limited to about 60°. Indeed due to too highly skewed elements, convergence is not possible beyond that angle. Then decision is taken to make, in addition to the full 3D-model, a 3D model with a 2D wing. Namely, still in a three dimensional environment, the airfoil and the winglet are just drawn as simple plates. This kind of model allows to increase the angle of the winglet up to 80°! This angle is more realistic for a real winglet ([11]).

Of course, both of these models are used for analysis. The full 3D-model is capable to give more detailed behaviours about what occurs in a real 3D wing case, and even though the 2D-wing-in-3D-environment model allows to observe 3D effects as well, it highlights much more effects of winglet since its angle is closer to reality. More than 100 simulations are run, but due to lack of precision or non convergence, some of them are thrown away. One can find in table 2.1 a summary of selected cases for each model.

	Full 3D-model	2D wing in 3D	2D simulation
Wing alone	x	x	x
Simple winglet	x	x	
Blended winglet	x	x	
Wingtip fence		x	

Table 2.1: Summary of simulations done

Each case is run for an angle of incidence from 0° to 10° by step of 2°, except for 2D simulations: from 0° to 16°. That means a total of 51 simulations spread into 8 different models which are also spread into three different environments.

Numerical geometries:

The chosen profile is NACA 4412. It has two common digits with the profile of experiment ([8]) which was NACA 5012. Then at least the maximum thickness is the same in both wings (12% of chord according to NACA four digit profile). Recall that for such NACA profile (for example $WXYZ$), the first figure, W, indicates the percentage of the maximum of camber, the second one, X indicates the distance of the maximum camber from the leading edge in tens of percents of the chord, and finally the two last ones, YZ indicate the maximum thickness of the wing in percentage of the chord. [10]

On figure 2.2 are presented numerical domains in which simulations are run. This is build in Gambit (please refer to appendices A and B.3).

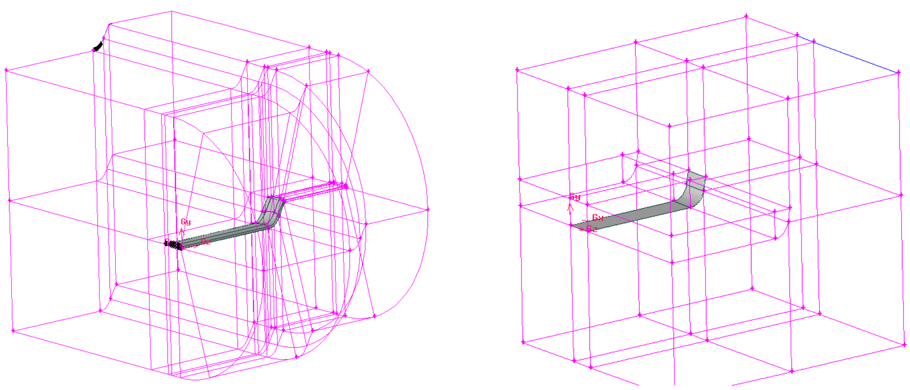

Figure 2.2: Numerical domains in Gambit: Full 3D-model and 2D-wing-in-3D-environment model (case of the blended winglet)

In the full 3D-model, inlets are curved because it is easier to draw and mesh with this configuration. In the opposite, in the 2D-wing-in-3D-environment model, the domain is simply cubic. Each external surface is assigned as *far field pressure*, except for surfaces on the side of fuselage. These are assigned as *symmetry*. Please refer to section 2.3 for more informations about those boundary conditions. All internal faces are set as *continuum fluid* by default.

In the full 3D-model the profile is completely drawn, but in the 2D-wing-in-3D-environment model the wing profile is not represented since the wing is a simple plate. 2D and 3D wings are depicted on figure 2.3. This zoom in shows clearly the profile of the wing taken in account in the full 3D model (right) compared to the simple plate instead of the real wing in the second model (left).

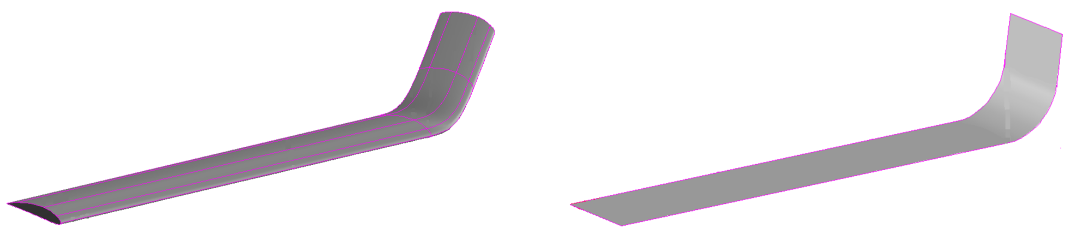

Figure 2.3: 3D and 2D wing in the case of blended winglet

Please note that any chord or thickness variations are applied in both models and those profiles of the wing (NACA 4412 or just a line in the 2D case) are kept for the winglet. In other words winglet is the prolongation of the wing with another given direction (according to which winglet is considered). One can also observe the difference in angle of winglet between both models. Recall that in full 3D-model the angle is limited to 60° while 80° is reached with the second model.

2.2 Mesh quality

Only conclusions about the mesh quality are presented here. Please refer to appendices B.4 to read detailed mesh analysis.
It is divided in two parts: 2D and 3D elements. One can see 2D conclusions like the good starting point before generating the whole 3D mesh (and geometry). They are as important as final 3D conclusions because they tell a lot about the main reason of the rather good quality of the 3D mesh. 3D elements conclusions confirm that main features of 2D meshes are retained.

2.2.1 Conclusions on 2D elements:

Full-3D Model:

The 2D mesh quality analysis is performed since the whole 3D mesh is generated from this 2D domain. So it is important to have a rather good quality mesh before building the 3D one. If the 2D discretization is well made, then the 3D one depends only on the third dimension discretization. Thanks to the four criterions used in the analysis, some conclusions can be underlined.

The area criterion confirms places where mesh is more refined. These places are indeed regions of interest, namely the near-wing regions and trailing wake (figure 2.4). The four corners and areas before the wing are not relevant in this investigation.

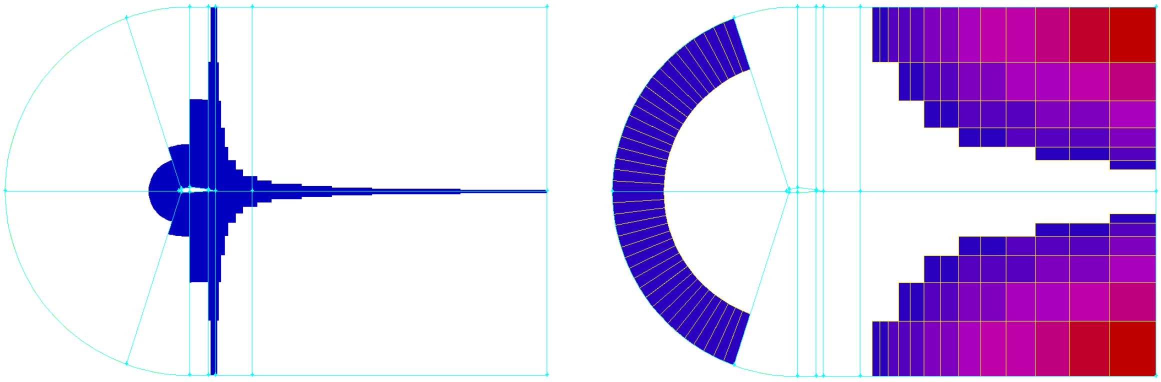

Figure 2.4: Left: smallest area regions (from $0\,m^2$ to $0.02\,m^2$) - Right: largest areas region (from $0.3\,m^2$ to $2\,m^2$)

The aspect ratio and stretch criterion give informations on lengths and regularity of elements. Aspects ratio works with lengths ratio. All regions of interest are kept in acceptable range (maximum of 100 recommanded by [12]), except for the four last cells at the wing boundary. They go up to 400 for the very last one (figure 2.5). This is quite large but it comes from a kind of compromise.

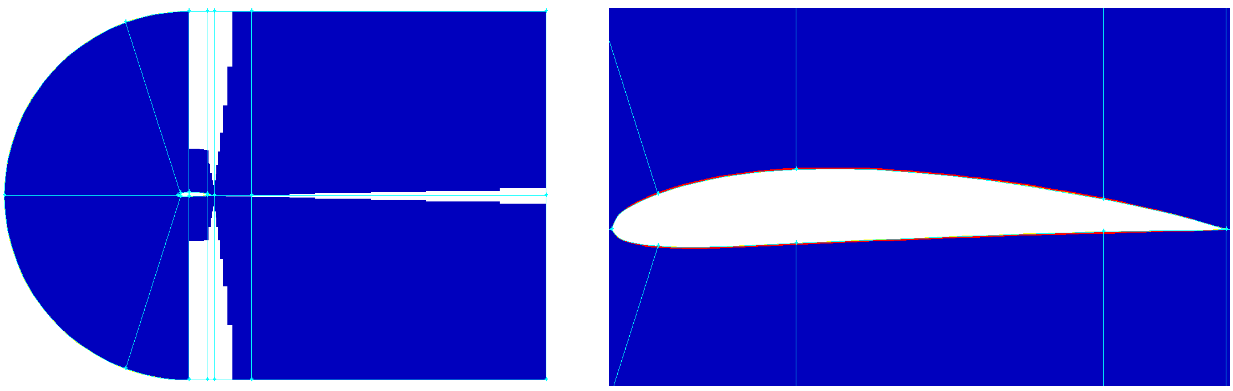

Figure 2.5: Aspect ratio (from 0 to 20): Left: general view - Right: zoom onto the wing

The stretch criterion evaluates the regularity of each element. This criterion is not the best respected. Indeed the average value is 0.8563 and nearly 50 % (43 % on figure 2.6) stand beyond a value of 0.9. But fortunately regions of interest (near-wing and the beginning the trailing wake) get reasonable values between 0 and 0.5.

Finally the EquiAngle Skew measures a kind a regularity as well. This criterions is the most respected in the 2D mesh. Indeed more than 82 % stand below 0.1 which is the recommanded average value by [12] for a high quality mesh.

The 2D mesh is globaly well created. Except for the stretch criterion which is, in average

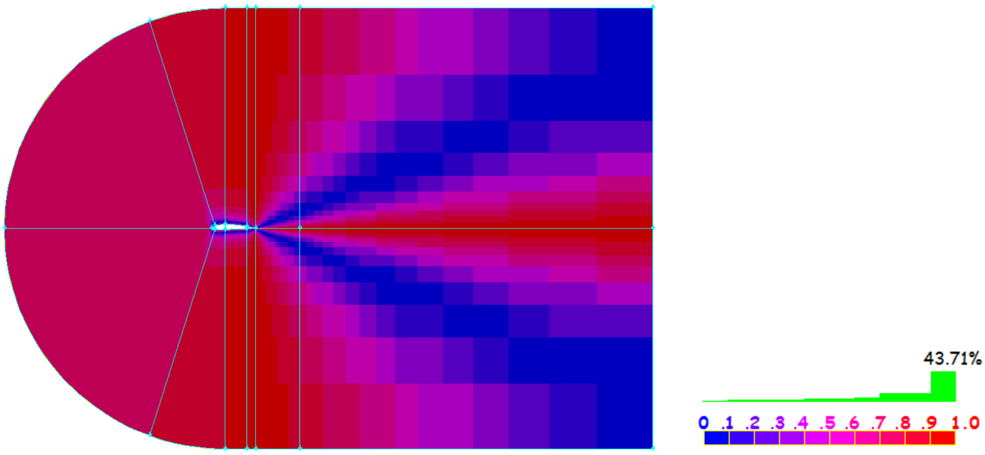

Figure 2.6: Stretch repartition and its legend

but not localy, too high. Every other stays in very acceptable ranges to get a good quality mesh.

<u>**2D-wing-in-3D-environment Model:**</u>

The purpose of this model is rather for confirming or reinforcing trends than for getting accurate results. But a good starting 2D mesh is even essential than in the previous model.

Aspect ratios are acceptable in average, although they are a slightly too high in last cells near the wing (up to 2000). It is a pity that good shaped elements are not optimally allocated (Stretch).

The EquiAngle Skew is very very good, except for a few elements near the blended winglet (worst elements reach 0.96!). Regions with this kind of elements are subject to accuracy problems (please refer to the blended case in section 3.4). Otherwise, the average values tell that meshes are *good* to *excellent*, according to [12].

2.2.2 Conclusions on 3D elements

<u>In the Full-3D Model</u>, one can distinguish the case with winglet and the case without. They are different from the partial curved path. In the case without, it is a straight line, otherwise it is curved at the level of winglet. This curve leads to some modifications in features of meshes and especially in quality.

Without winglet, the aspect ratio (AR) reaches very high values but only in the far trailing wake. Otherwise, it stays at an acceptable range according to [12] (at about 100 in average).

Even if it stays quite low, regions of interest are not optimally deserved by elements with high AR (stretch criterion). EquiAngle Skew (EAS) is very good with an average value of 0.025. Like in the 2D mesh, it should be 0 (perfect elements). But an additional mesh, other than the 2D extracted mesh, is created. It is the mesh after the wingtip along the thrid dimension path. It is filled by quadrilateral elements with poorer quality ($[0.96 - 1]$). Fortunately those elements are not present in the trailing wake where accurate solutions are needed since this investigation studies *induced drag by wingtip vortices* which develop mainly after the wing (figure 2.7). This space is also present in cases with winglet (after the winglet thus).

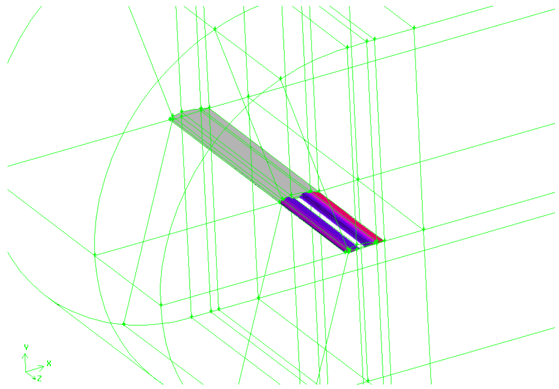

Figure 2.7: Stretch in $[0.96 - 1]$

With winglet, AR and stretch criterions examinated in the case without winglet are still correct. Only the EAS gets changes due to the curved path in the third dimension.

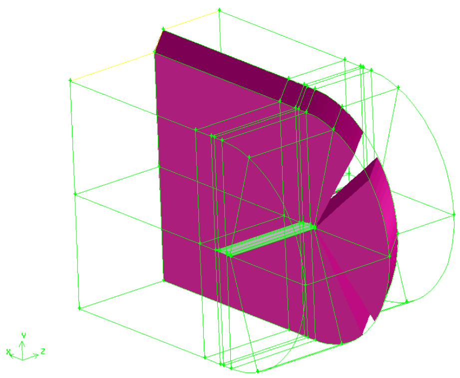

Figure 2.8: EAS of $[0.6 - 0.7]$ for the simple winglet

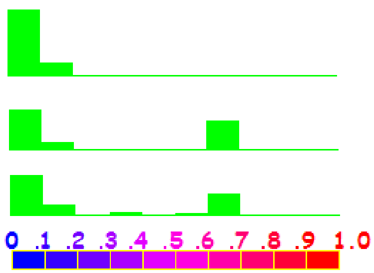

Figure 2.9: EAS distribution for the case withtout winglet, simple and blended winglet (from top to bottom)

At the winglet position on the extracting path, elements have non optimal values as shown on figure B.18. This is confirmed by the comparison between EAS values distribution of cases of figure B.19. A new peak appears in the case with winglet. This is the winglet region. Range of these values is $[0.6 - 0.7]$, which is fair according to [12]. One should take this as a compromise once again, because keep in mind that average EAS for each case is below 0.4 which is the maximum recommended value for high quality mesh in 3D.

Meshes are rather good. They have kept main characteristics of the 2D mesh, except around winglet regions (when the case) where EAS is poorer and spaces after the wing tip (or winglet tip) where EAS is bad. Fortunately this should not affect calculations in a large way.

In the 2D-wing-in-3D-environment Model, mesh characteristics in this model are the same as in the 2D analysis since the extracting path is only a straight line.

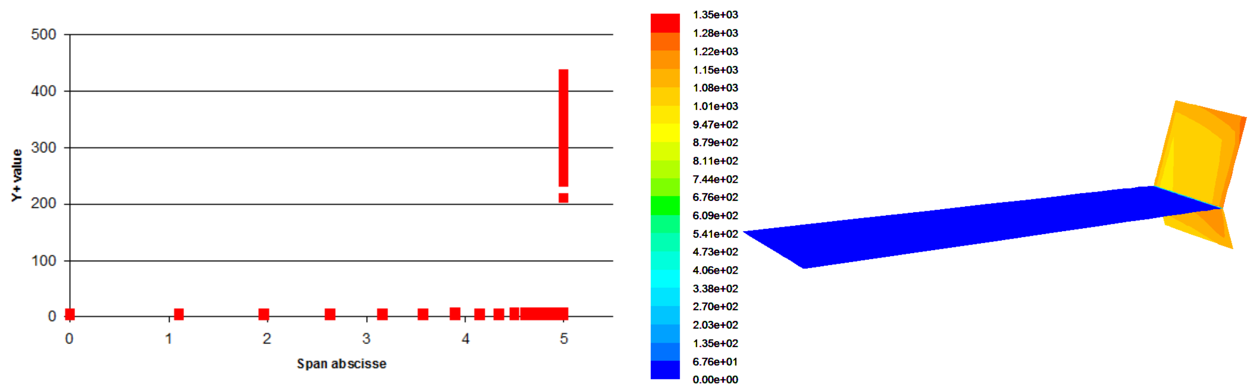

Figure 2.10: Left: Sudden variation in Y^+ value at wingtip in case without winglet - Right: repartition of Y^+ values in 2D-in-3D model (case shifted D.)

2.2.3 Is the mesh refined enough?

According to section A in appendices, viscous model used is the SST$k-\omega$. When option "transitional flow" is enable, near-wall model approach is preferred. Then value of Y^+ must be ≈ 1. Table A.4 summarizes Y^+ values on wing and winglet for each case.

	Full 3D-model	2D wing in 3D	2D simulation
Wing alone	95 %	95 %	100 %
Simple winglet	95 %	35 %	–
Blended winglet	97.5 %	35 %	–
Wingtip fence	–	21 %	–

Table 2.2: Percentage of elements having Y^+ in $[0-10]$

In the Full-3D-model, only a few elements have very high Y^+. They lie at wingtip or winglet tip. The wing (or winglet) side has comparable value of the tip (up to 600!). Figure 2.10 left shows the sudden $Y+$ variation at wingtip of the case without winglet. It is exaclty the same behaviour at winglet tip instead of wingtip.

In the 2D-wing-in-3D-model, only the wing without winglet has very good Y^+ value. But when winglet are placed, it decreases drastically. But in case of blended winglet, on the wing it self, value rise up to about 1000! While in the two other cases, value on wing stays acceptable (below 100). For example, one can see depicting on figure 2.10 right of repartition of Y^+ on the wing with shifted downstream winglet. Except in case with blended, all cases are similar. In blended case, all values are quite high (even on the wing).

2.3 Settings in Fluent

This section is related about what is set in Fluent like models, boundary conditions and solver.

2.3.1 Models

For detailed comments and explanations about models used in Fluent, please refer to appendices A.2. For each case, the same model is used. Indeed it is more relevant to compare effects of changes in geometry if one keeps the same model between each trial. The model is very simple since one works with simple air:

- viscous model: SST $k - \omega$ with all parameters kept by default
- Materials: Ideal-gas simple air
- Viscosity law: Sutherland
- Ambiant pressure and temperature: Standard atmosphere ($101325\,Pa$ and $300\,K$)

2.3.2 Boundary conditions

The main boundary condition used is *pressure farfield*. Indeed every exterior boundaries are set as pressure farfield, except for the fuselage side (side at which is attached the wing). This boundary is used to simulate free-stream condition at infinity. It is possible to set velocity components, Mach number, pressure and temperature. Pressure and temperature are kept at standard atmosphere.

Mach number is calculated thanks to Reynold number: 300000. This number is chosen in purpose to be able to fit with data from books (among others [19]). From Re, the deducted Mach number is: 0.1314412 since for air $\gamma = 1.4$ and $R = 287.3\,Jkg^{-1}K^{-1}$. Then the speed of sound can be written:

$$a = 20.05\sqrt{T}\,ms^{-1} \tag{2.1}$$

Two components of the velocity are entered in the panel. These are calculed following angle of incidence (from 0° to 10°) with appropriate cosinus and sinus.

Symmetry can be used to simulate mirror condition or to avoid having viscous effects at this boundary. Effectively in the case of a wing, one cannot set a velocity at the fuselage (unphysical) but at wall neither (due to undesired viscous effects). The only solution is to use symmetry condition.

Obviously wing and winglet are set as walls since one needs to inforce non-slip condition at this place. This creates a development of boundary layers which are crucial in drag calculation.

Everything else which is not set particularly is considered as *continuum fluid* by Fluent.

Inputs	Value	Inputs	Value
Reynold	300000	Ambiant temperature	$300\,K$
Mach Number	0.1314412	γ	1.4
Velocity	$45.8\,m/s$	Ambiant pressure	$101325\,Pa$
Model A	Full-3D	Model B	2D-wing-in-3D-environment

Table 2.3: Boundary conditions summary for each case in both models

2.3.3 Solver

Second order discretization upwind is used to solve the problem (Please refer to appendices A.2 for more informations) with a *pressure based* solver (or segregated one).
Each farfield boundary is initialized with velocity value. Then iterations are run.

Chapter 3

Results

Four parts are distinguished for results: Forces (lift, drag) and Moments, Pressure coefficient and distribution, Velocity pattern and Vortex pattern. For each section, both models are investigated. Especially the *2D-wing-in-3D-environment* one is used to reinforce effects of the winglet since it has more sharp winglets with a higher angle between the horizontal and the winglet itself (please refer section 2.1).

From now, the Full-3D model is called **model A** and the 2D-wing-in-3D-environment is called **model B**. This is easier and lighter to read.

3.1 Forces and Moments

3.1.1 Lift and Drag

For each case, data from each angle of incidence are extracted, worked and then presented in comparisons. For model A, *data from litterature* are depicted on graphs since data for the NACA 4412 is readily available in the litterature.

The main purpose of winglets is to reduce total drag, especially induced drag, coming from vortices generated at the wingtips. And moreover, blended winglets should reduce still more drag since they have a smooth transition avoiding the creation of an auxiliary vortex. Figure 3.1 presents comparisons for lift and drag coefficients (model A).

Comparison with data from litterature:

At the first sight, one can see that C_l is rather convincing while C_d isn't so much. Indeed discrepancies in C_L between data from litterature and the case without winglet is about 0.2 on a range of 1.3. This means an error of 16 % on lift. While the biggest gap in C_D is about 0.045 (between case without and data from litterature) on a range of 0.06, namely an error of 75 %. This is unacceptable. [21] informs that for 3D wing, induced drag is proportional to C_L^2 and might be given by (3.1) where δ is a small value, constant for a given wing. Profile drag (from fuselage, ...) can also be expressed by (3.2).

Then total drag can be written like equation (3.3). This is found by doing the sum. The resulting coefficient by this sum is called *Lift-dependent drag* which can be seen as "*the difference between the drag at a given lift coefficient and the drag at some datum lift coefficient*".

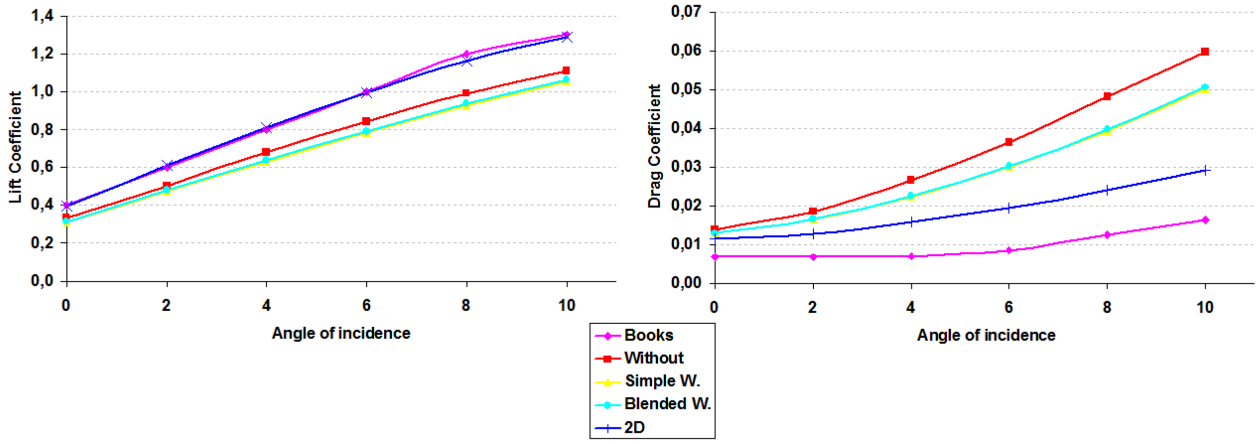

Figure 3.1: Model A: Lift and drag coefficients comparison

$$C_{D_V} = \frac{C_L^2}{\pi(AR)}(1+\delta) \qquad (3.1)$$

$$C_{D_{prof}} = a + bC_L^2 \qquad (3.2)$$

(3.3) is valid only if the datum lift coefficient is taken to be zero.

$$C_D = C_{D_0} + kC_L^2 \qquad (3.3)$$

where C_{D_0} is the drag coefficient at zero lift and kC_L^2 is the lift-dependent-drag coefficient.

Taking an idealized case in which C_{D_0} is independent of lift, one can deduct that $C_D \propto C_L^2$ is a good approximation for total drag.

If the error on the lift coefficient is about 0.2 and if drag coefficient is proportional to C_l^2, then one might expect to have an error of about 0.04 on drag. Whatever the sign of the error on lift, the difference on drag will be positive due to the square. Figure 3.2 illustrates the interval of error on drag related to the offset on lift.

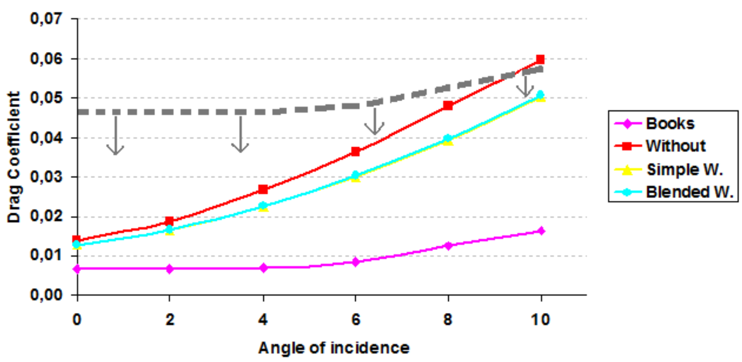

Figure 3.2: Model A: Error in drag coefficient (without winglet) due to the offset in C_L

Drag coefficient from simulation in the case without winglet should thus lie below the grey line according to the offset of the lift. Finally one can see that drag is not so bad calculated at all! Despite that, there is still a large gap between numerical's and litterature. The blue line (called $2D$ on figure 3.1) is a simple $2D$-simulation. One can see there is still a large gap between this and litterature.

Moreover, numerical drag still increases with angle of incidence and finally overruns the grey line (at $\alpha = 10°$) because in 3D wing, one has to take induced drag in account which is proportional in a second order to C_L, namely to α. This induced drag is obviously not represented with the 2D data.

Drag-related-error is quite coherent with the lift error. But one can still wonder why there is an error on lift. One has to keep in mind that data from litterature are for a 2D wing (actually a 2D cross section). This might explain the 8 % discrepancy in C_l. Effectively, in 3D wing due, to wingtip vortices, a downwash velocity is created. This has a tendency to reduce the effective angle of incidence and then the lift. At the same velocity, if lift decrases then its coefficient also does since $C_L = \frac{L}{\frac{1}{2}\rho S V^2}$.

In regard to this, decision is made not to take data from litterature as reference, but rather the case without winglet. This case is then the basic configuration to which all comparisons are applied and explained.

Effective drag reduction:

Looking at figure 3.1, one can wonder if there is a real drag reduction. There is effectively a drag reduction but there is also a lift reduction. A linking could be done between these two reductions. If one decreases, the other one should as well. So one might be lead to think there no effective drag reduction. To ensure there is effectively a drag reduction, let's do another error analysis.

The use of winglets should not bring about lift reduction, but only reduction in drag. Let us consider there is an error on the lift between cases with winglet and the *reference case* (which is now the case without winglet from simulation). The largest gap between them is about 0.056 or about 5 % in a relative way. Since quadratic proportionality between C_L and C_D is assumed, one should expect to get about 0.003 for the largest error in drag coefficient. Figure 3.3 shows the interval of confidence.

Lower and upper bounds of this interval for the drag without winglet are depicted. There is then a real drag reduction when adding winglet since any drag path lies in the interval of confidence of the case without winglet. The bigger is the angle of incidence the higher is the drag reduction. Figure 3.4 depicts relative drag reduction when adding simple winglet at the wing alone and when changing simple winglet to blended one.

The yellow curve illustrates percentage of gain of drag when adding the simple winglet compared to drag of the case without. Even if in absolute, drag reduction is still more important as angle of incidence increases, it is not the case in a relative way. Maximum reduction is 18 % at α of 8°, while maximum absolute reduction seen on figure 3.3 is at angle of 10°. It means that even if drag increases with α, the gain in drag when adding winglets seems to stay

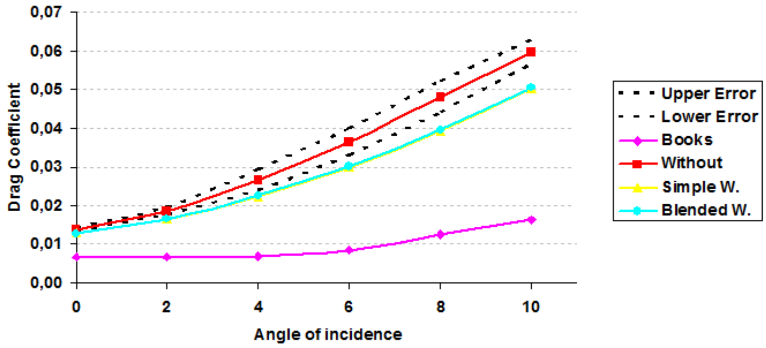

Figure 3.3: Model A: Error in drag coefficient (winglet cases) due to the offset in C_L

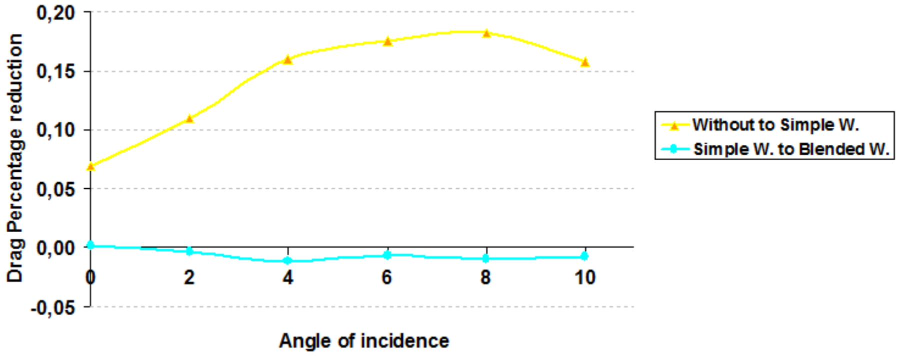

Figure 3.4: Model A: Percentage of drag reduction when adding simple winglet or changing simple winglet to blended one

constant from a given angle of incidence. Average drag reduction is 14 % which is not bad at all.

When replacing simple winglet with the blended one (blue curve), results are very surprising. This goes against expectations. Indeed the blended should decreases still little more the drag (or increase drag reduction), but one can see that there is a negative drag reduction, namely an increase of the drag. Like argued in chapter 2, the model B aims to highlight this trend not visible in model A.

Origins of forces:

Fluent allows to decompose force into *pressure* and *viscous* forces. The first one contains, among others, the induced drag and the second one is mainly the skin friction drag.

It seems clear that the lift is mostly generated by pressure force. Numerical's reports that viscous lift is part of less than 0.1% of total lift. This obviously totally negligible. However there is a trend that worths to be mentioned. It is illustrated on figure 3.5.

Firstly while contribution of viscous lift is very small, it is not zero! Secondly, one can see that viscous lift lowers with angle of incidence to be negative from a given one. Figure 3.6 shows sort of strategic regions on wing. At low angles of incidence, the blue region is subject to acceleration of fluid, then creates a upwards force (parallel to edges) and at high α, the

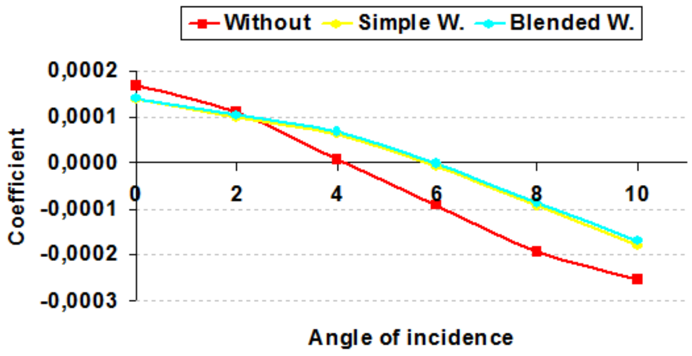

Figure 3.5: Model A: Viscous lift comparison

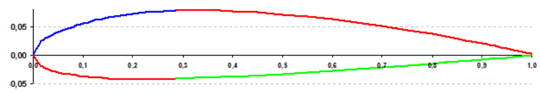

Figure 3.6: Model A: Strategic regions on wing

green region makes more friction, creating a parallel force to the downwards edge since there is an high angle of incidence. This might explain this inversion in viscous lift.

As figure 3.5 informs, from $\alpha = 2°$, viscous lift in case with winglet is higher than without. This might come from that when α increases, fluid runs the winglet still more in height rather in width (equals to chord length in this investigation). Of course and once again, this contribution is very negligible and changes really nothing in lift coefficient, but this trends had to be mentioned.

About drag, as one will see, with no angle of incidence, pressure and viscous drag are in the same order. Once incidence increases, pressure drag widely surpasses the viscous one. Figure 3.7 presents these two evolutions.

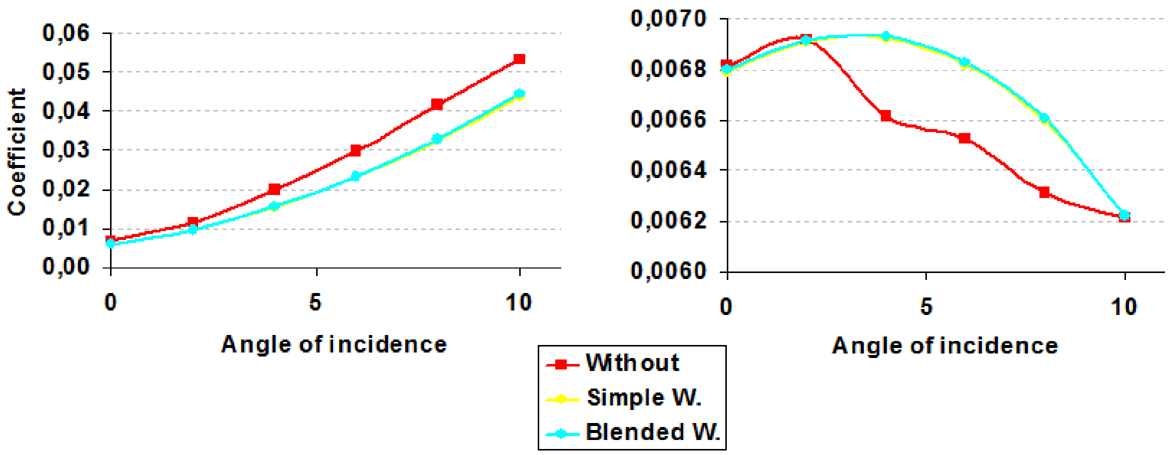

Figure 3.7: Model A: Pressure and viscous drag respectively (be careful at the scale: the one on right figure is ten times less than the one left figure)

Pressure drag in the case with winglet is significantly lower than without. Obviously this comes mainly from the reduction in induced drag done by winglet. It is confirmed with viscous drag. Indeed it is slightly (scale!) higher when the winglet is added. This means that the total drag reduction seen on figure 3.4 is only due to induced drag reduction. Fortunately, it is the purpose of winglets.

Viscous drag with winglet is greater than maximum 5 % of the drag without. Seen the order of accuracy of the present work, one can easily take 5 % discrepancy as something constant.

Once again, there is no observable differences between the case with simple and blended winglet.

Model B:

Model is is briefly presented since its purpose is to try to underline several benefits/effects of different winglets. In this case, in addition to simple and blended winglet, the shifted downstream winglet is also analysed. Figure 3.8 presents results for the lift and the drag for model B.

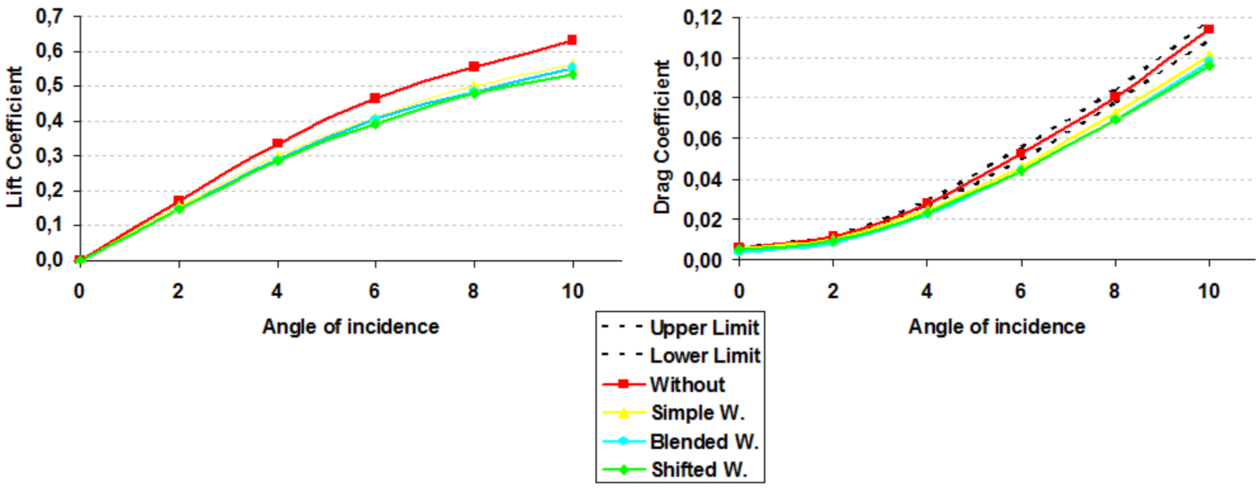

Figure 3.8: Model B: Lift and drag coefficients comparison

Lift is still lower with the winglet. Right figure shows, in addition to the drag coefficients comparison, intervals of confidence for drag without winglet. Indeed, this interval is built assuming no lift variation when adding winglets. One can see that there is an effective drag reduction because any of drag curve lies in this interval. It is difficult to distinguish differences betweeen each curve. Figure 3.9 enables to clarify differences between each case.

The left graph presents drag reduction reported to each case. The yellow curve shows drag reduction when passing from the case without winglet to the case with simple winglet. The reduction is quite constant.

The blue one is reported to the case with simple winglet. So when adding the blended, the reduction is still higher: about 33 % more than with the simple winglet at $\alpha = 0°$. Then gain decreases with angle of incidence. Blended winglet is really more interesting than simple simple winglet since with no incidence, blended one can save more than 30 % drag of simple winglet.

About the shifted downstream (or S.D.), results are surprising. Exceptations are to have the same behaviour as the blended one. But when removing the blended and adding the S.D., the green curve reveals a negative reduction (about 37%!) , meaning it is much less powerful than the blended.

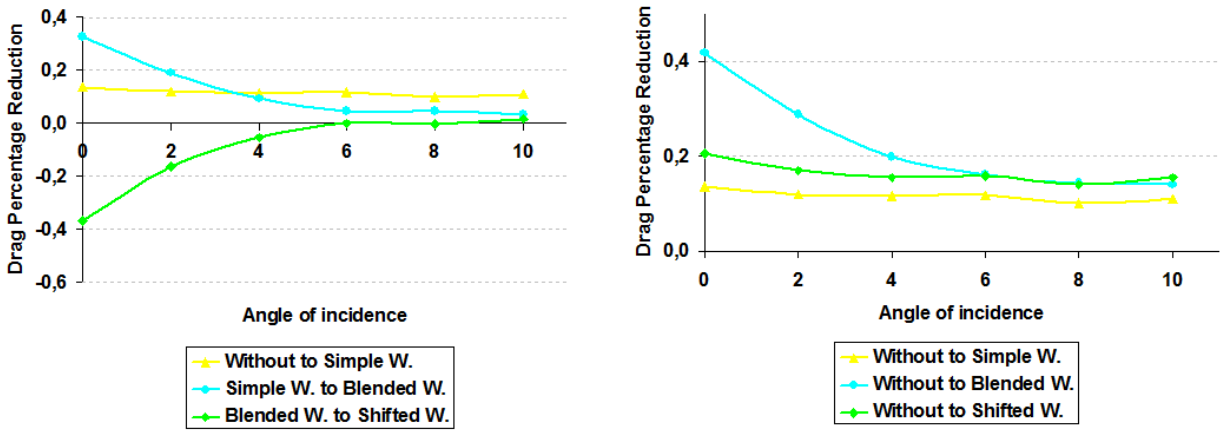

Figure 3.9: Model B: Drag comparisons reported to the case *without*, to the case with *simple* and to the case with *blended* (Left) - to the case *without* only (Right)

All these trends are confirmed by right graph. It shows absolute comparisons with the case without winglet. Certainly the blended winglet is the most powerful with a reduction up to 42 % then decreasing with angle of incidence to be stabilized at about 15 % where it joins the S.D. one. S.D. winglet is out of expectations since theoritically it should give comparable results as the blended one. Simple winglet is very constant (about $11 - 12\,\%$), but a little bit lower than the two other ones.

Origins of the lift is not surprising: Only from pressure forces and very negligible from viscous ones (order of 10^{-4}). About drag, it is depicted on figure 3.10. With no angle of incidence, there is obviously no pressure drag but only viscous drag. At low angle of incidence (2°), viscous and pressure drag are nearly equal and then when α increases, pressure drag surpasses widely viscous one to be nearly negligible (when $\alpha = 2°$, viscous drag is about 45 % of total drag while at $\alpha = 10°$ it becomes only $1 - 2\,\%$ of total drag).

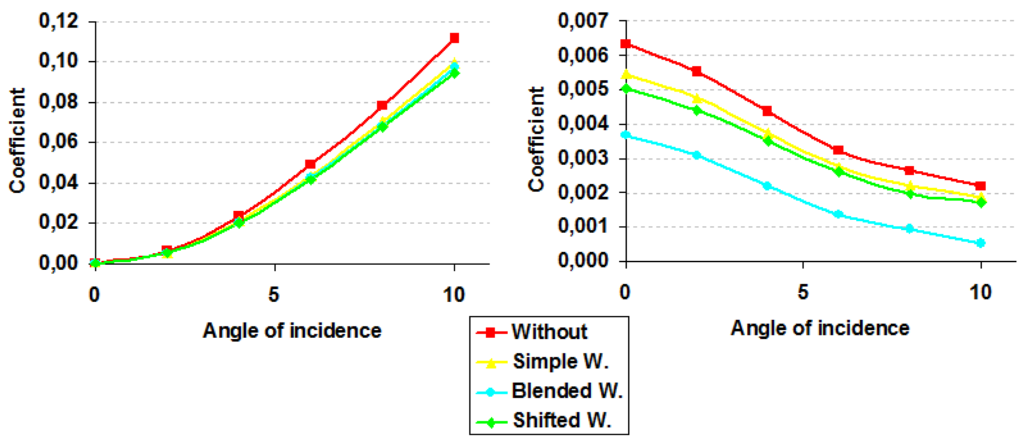

Figure 3.10: Model B: Pressure and viscous drag respectively

Pressure drag is lower when winglet is placed since induced one is lowered by purpose. Differentely of model A, viscous drag cannot be assumed as constant. Although viscous drag has a decreasing proportion of the total drag, at low angle of incidence it does have a great (even greater than with no angle of incidence!) proportion.

At $\alpha = 0°$ viscous drag of blended w. is nearly twice below the one of the case without. At high angle of incidence, it rises to more than 4 times below, but at this incidence, viscous drag is negligible compared to pressure drag. In a smaller way, it goes the same for other winglets: about 1.15 (simple) and 1.25 (shifted downstream) time lower.

As reported in section 2.2.3, Y^+ values are not totally optimal on the whole wing when the blended winglet is placed (in model B). Then, lift could be widely modified by the mesh problem. Moreover, the EAS (EquiAngle Skew) is about 0.96 around this winglet. It means that vortex could be pretty bad simulated (please refer to section 3.4). Force components in the case of blended winglet in model B should be carefully interpreted.

Comparisons with experimental's:

Recall lift and drag evolution found in the experiment [8]. Graphs on figure 3.11 are already discussed in section 1.5.

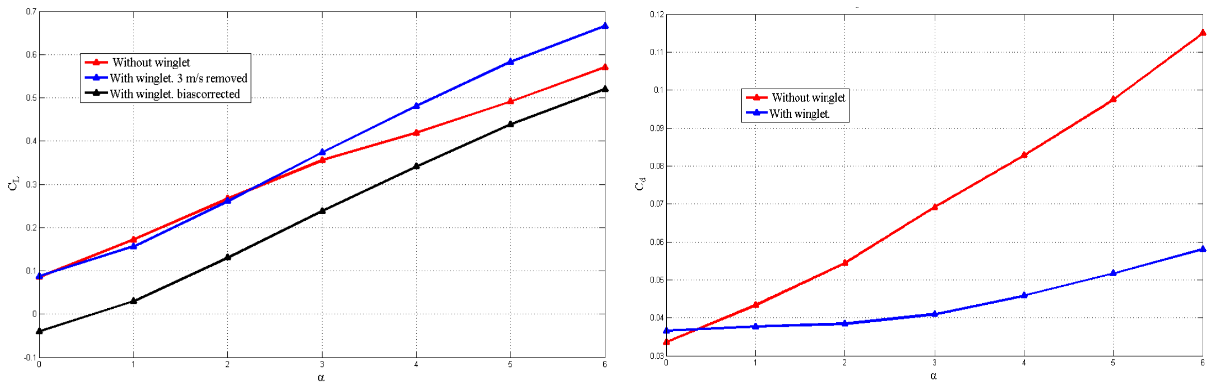

Figure 3.11: Lift and drag evolution found by the experiment

On one hand, they could not conclude anything on the lift since the lift evolution with winglet is between the two lift evolutions without winglet. Indeed due to the experimental feature, they got two different evolutions following they kept or removed some data.

In the present numerical investigation, lift with winglet is always lower than the one without any device. Obviously if winglet reduces drag and lift at the same time, interests would be very small. So it why lift is always considered to be the same as the one without winglet. This assumption is done by considering any trend found in the experimental work and by a logical way of purpose.

On another hand, experimental drag was considerably reduced when winglet was mounted. At $\alpha = 6°$ drag was reduced twice. Numerical's don't show such reduction. About $16-17\,\%$ of reduction is observed at this angle of incidence. This is the maximum one for model A as seen of figure 3.4. The positive slope of drag reduction through angle of incidence is well simulated in this model. But any difference are highlighted between winglets.

For the model B, reduction rises up to $42\,\%$ (absolute way) with the blended winglet. But the observed trend is in the opposite way as the one found in the experiment. Indeed maximum drag reduction in numerical's is at low angle of incidence and then decreases to be stabilized near 17 % from 6° of incidence (figure 3.9). While experimental's reveals no influence of winglet on drag at low angle of incidence. Other winglets investigated in this work have constant effects on drag. No one has an increasing effect with α. But one has to keep in mind that the wing in model B is a simple plate and thus could not behave like a real wing profile.

This trend might come from that simulations report a much lower viscous drag at low angle of incidence (Righ graph on figure 3.10) and at these angle, viscous drag is as important (even more important for $\alpha = 0°$) as pressure drag.

3.1.2 Moments

Adding winglet increases moment in different ways. First at root of the wing, bending moment is more important since winglet is mounted at the furthest distance from root (already discussed in section 1.3). Secondly winglet generates lift which has a component acting in the same direction as the wing lift itself. Here are presented only moment creating bending at wing root, namely moment in the x-direction.

The left graph on figure 3.12 depicts bending variation through angle of incidence for all three cases and the right one shows its relative increase.

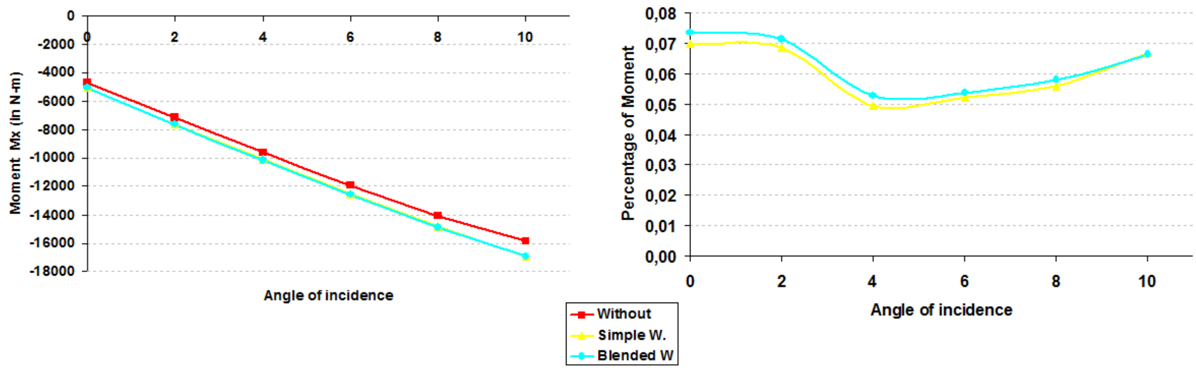

Figure 3.12: Model A: Left: Absolute variation of bending moment at root - Right: Relative increase of bending moment at root reported to the case without winglet

In this model, bending moment is the x-direction moment. It is measured at root of the wing. This gives a general idea of stresses at root and relative increase when adding winglet. On left figure, one can see that bending moment increases with angle of incidence (increases in negative number). It is normal since lift (or rather the resultant force) still rises.

Right figure shows the relative increase of the bending moment when adding the simple or blended winglet. This is reported to the case without winglet. Once again, in this model, differences between winglet is not so clear (less than an half percent between cases). Although the increase is well distinguished when winglet is added: about an average of 6 % more when there is a winglet. It could come from forces generated from the winglet itself and its own weight. But in these models, weight is not modelled. So increase in bending moment only comes from winglet lift. Actually if the weight was taken in account, the bending moment should be lower since lift and weight act in the opposite direction.

Figure 3.13 presents relative increase of the bending moment in the second model (B). With this model, one can see differences between winglets. Clearly, the blended one leads to the lowest increase in bending moment at the root of the wing. The higher one is when the shifted downstream (S.D.) one is placed. Between them lies results for the simple winglet. Maybe the bending moment of the S.D. one is greater because the downstream part is run by the secondary flow. This fact can lead to a new moment around this axis even if, at the first think, it seems to be very negligible.

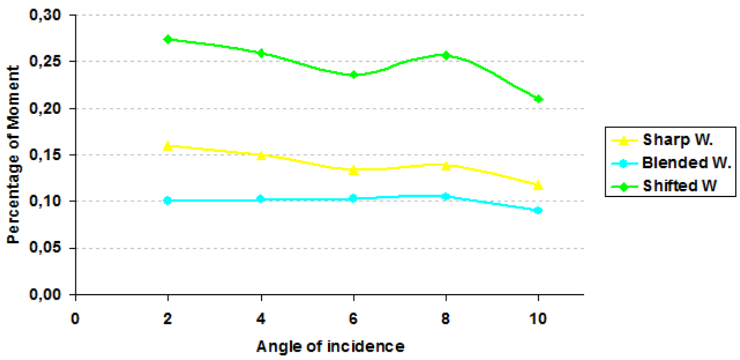

Figure 3.13: Model B: Relative increase of bending moment at root reported to the case without winglet

Once again, one has to keep in mind Y^+ values, not only on wing but also on winglet in model B. Indeed, except in case of blended winglet, each wing gets quite good values of Y^+, while winglets get non optimal values. If they have those kinds of Y^+ values (section 2.2.3), their lift could not be simulated properly and then lead to imprecise bending moment. Although this problem, the shifted downstream could still have the highest moment since, even if boundary layers are not so well simulated, the fluid flow still runs the downstream part creating additional moment.

3.1.3 Conclusions on forces and moments

Generally forces are well simulated. For each model, lift is slightly lower than expected but when doing a kind of error evaluation, drag is revealed to be well reduced thanks to winglets. Model A can not give differences between winglet themself, while model B does. But a surprising result comes out from it. The shifted downstream winglet seems not to be so efficient as expected. Since each wing in both models (except the wing with the blended winglet in model B) gets good Y^+ values, wing lifts should not be affected.

When comparing with experimental results, numerical's are quite convincing about lift and drag. But once again, even if model B can distinguish effects of different winglets, the trend of drag is totally in the opposite of the experiment: drag decreases with angle of incidence. This might come from model B is run with plate rather than 3D wing. Behaviour is then totally modified.

Bending moment are generally higher than without winglet. Effectively, winglets generate their own lift and then contribute to bending moment. Model B leads to differences between winglets, but due to non optimal Y^+ values on winglet in this model, one can not conclude surely about lift effect from those winglets. However it seems that the shifted downstream leads to the highest moment thanks to its downstream part.

3.2 Pressure

This section aims to investigate pressure distribution on and around the wing. Pressure at wingtip is especially focused in order to determine/confirm effects of winglet. Two "windows" are available to see pressure distribution on a wing. The first one is the distribution along the wing span, namely from the fuselage (not modelled in the present work) to the wing (or winglet) tip. And the second one is displaying pressure field around wing at a given cross section along the span, namely in the fluid flow direction.

3.2.1 Distribution along the wing span

Figure 3.14 depicts pressure distribution along the span of the wing in the case of simple winglet in model A. Pressure is taken on the upper surface of the wing, at chord equals to 0.3 (on one meter long chord).

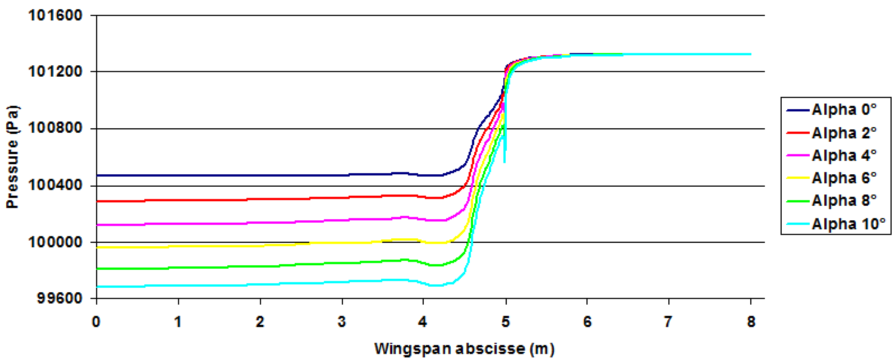

Figure 3.14: Model A: Pressure distribution along the span for all α in the case of simple winglet

Note that x-axis is the distance from fuselage. In the case of simple winglet, the wingtip is situated at $4.5\,m$ and the winglet tip at $5\,m$. Since data are extracted at constant chord, pressure is constant from the fuselage (zero-abscisse) to the near-winglet region. Then pressure begins to increase to reach the atmosphere pressure. Obviously as long as α rises, pressure decreases still more and more on the upper surface. But whatever is the pression on upper surface, reference atmosphere is always reached after the wing (or winglet) tip since it is a far-field pressure. Evolution through angle of incidence presented on figure 3.14 is the same without or with any winglet. α-pressure evolution is not more interesting as previously mentioned.

If one compares pressure distribution when adding winglet or not, one obtains figure 3.15.

Extreme values of α are taken since other intermediate values are situated in between these curves (as mentioned regarding figure 3.14). Pressure field is exactly the same on the wing. Obviously because it is the same wing profile. At the winglet junction, pressure starts to increase earlier in the case without winglet. Indeed winglet acts like a fence to prevent secondary flow to be created. This flow, in the case without winglet, could be the origin of this earlier pressure increase. But when the pressure starts to rise with winglet, it goes much faster than in the case without. As one will see later, there is a low pressure zone at the winglet junction.

At each wingtip there is pressure lost. For the blended case, there is second peak at the

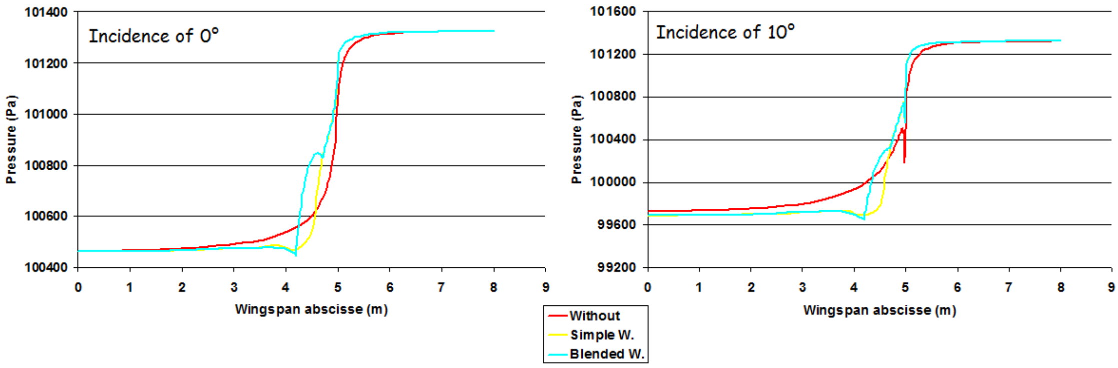

Figure 3.15: Model A: Comparisons of pressure distribution along the span between cases at $\alpha = 0°$ and $\alpha = 10°$

middle of the winglet. It has to be forgotten. It comes from data extraction in the span direction which is not perfectly done. For a short explanations, please refer to appendice C. Then at $\alpha = 10°$, the winglet tip is clearly featured by this big pressure lost. This comes from the vortices ignition. (All CFD-displays are available in appendices D).

Indeed, pressure distribution along the wing span are measured at chord equal to $0.3\,m$ (on $1\,m$ long). This is quite early to expect to see entire vortices created. If one has a look at what happens a little bit further (at $0.8\,m$), pressure lost is much more important. This is because vortices are almost totally created. Figure 3.16 shows these pressure contours for all cases in model A. Scale is from lowest value (about $96000\,Pa$) to $101000\,Pa$ which is indeed a lower pressure compared to reference pressure ($10125\,Pa$).

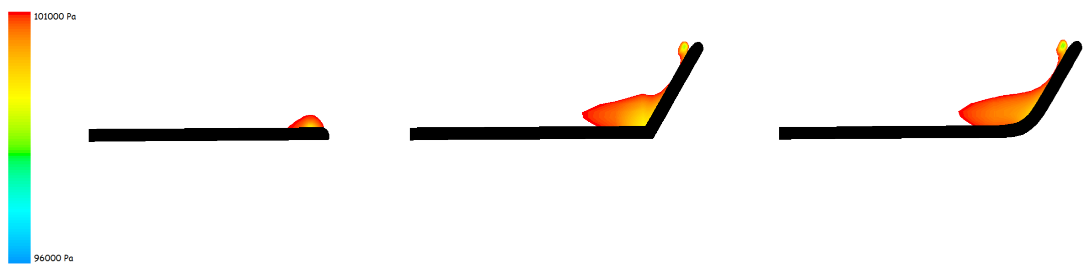

Figure 3.16: Model A: Comparisons of pressure contours around winglet at chord equal to $0.8\,m$ and $\alpha = 10°$

When no winglet, there is simply a pressure lost corresponding at the beginning (creation) of the vortex. When the simple or blended winglet is added, there are two pressure peaks. The first one is at the junction and the second one at the winglet tip. The second one (at winglet tip) corresponds to the one in case without winglet, namely when vortex is creating. The first one (at winglet junction) is because at those points, upper surfaces of wing and winglet create low pressure. Adding both contributions, one gets lower pressure. The pressure lost is even higher in the case of simple winglet ("more yellow"). This is coherent since contributions of both wing and winglet are concentrated at one point (the junction).

The model B for the pressure analysis is not as useful as expected. Indeed it is not a real wing profile but rather a simple plate. So pressure distribution is pretty constant along span. The comparison of pressure distribution can be found in appendices D. Winglet in this model has almost no incidence, so there is any pressure gradient between surfaces of winglet. In this case, vortices are only generated at wingtip (please refer to section 3.4).

3.2.2 Distribution along the chord

This distribution is very important because it informs about potential flow separation. Indeed if along the chord, one gets large pressure gradient, this could lead to an earlier laminar-turbulent transition. Once there is a flow separation, one can lose lift (namely earlier stall).

[21] indicates, in a schematic way, that there are adverse pressure gradients near the leading edge at a cross section close to the wingtip in the case of simple winglet. With the blended and shifted downstream, they report that it is like without winglet, namely a smooth transition between pressure levels. While with a simple one, there is sudden jump of pressure. This jump is reported as highly risked in terms of flow separation.

Unfortunately results for these features are less convincing. Again due to the lack of accuracy in data extraction (in the x-direction this time) from Fluent (please refer to C), only case with simple and blended winglet are depicted. Figure 3.17 shows pressure profiles along the chord.

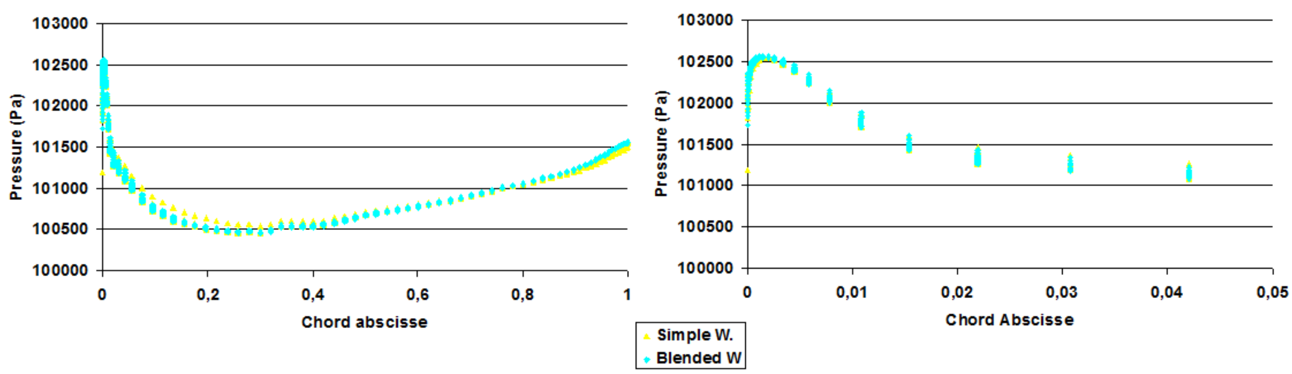

Figure 3.17: Model A: Pressure distribution along the chord for case with winglet only (from 0 to 1 and from 0 to 0.05 (near leading edge region))

Any trend is highlighted in this present work. But a potential adverse pressure gradient might be "invisible" because all points depicted on this figure are for all cross sections (along the wing span). Please refer to appendices for more information about data extraction. To try to dectect a potential trend, let have a look at figure 3.18.

It seems obvious that pressure is pretty similar for every winglet (Please note that when no color = atmosphere pressure). Cross sections are taken just at the wingtip (before the winglet starts). That confirms results of figure 3.17: No significative difference. In the case without winglet, field pressure is less "strong" since at the wingtip pressure should be the same on the upper and lower surface. One feature is that when winglet is added, wing is still operational to produce lift until its end (still low or high pressure on both surfaces). In appendices D, all colorful maps are placed and one can observe trends of pressure in cross section along the wing and winglet span.

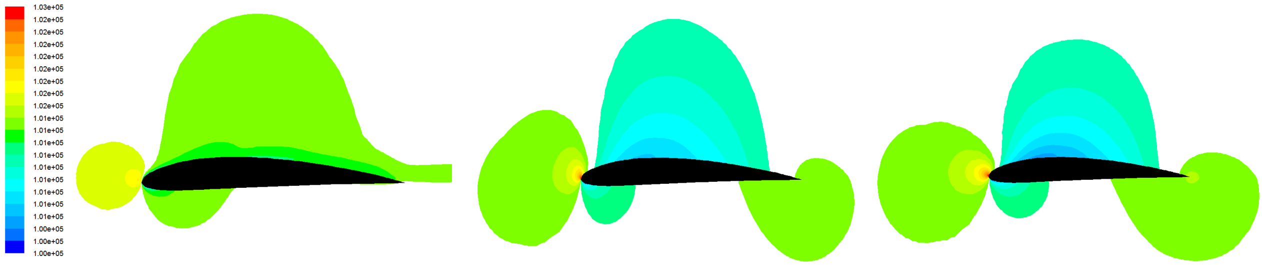

Figure 3.18: Model A: Displays of pressure field in each near-wingtip cross section for cases without, with simple and blended winglet respectively

Model B is once again less useful since all data graphs are totally unreadable because of the previously cited feature in Fluent. But still in the same appendices, one can have a look at results and pressure field comparisons.

3.2.3 Conclusions on pressure

Pressure field is analysed in two ways: along the span and along the chord.

The first one indicates trends when winglet is placed. Indeed winglet leads to a stronger pressure transition (on the upper surface). The purpose of winglet is to prevent secondary flow and then "fluid mixing" that could lead to a vortex at the wingtip. So it is normal to have a later and stronger increase in pressure. But due to the lack of precision in data extraction, no other feature can be highlighted.

The second one could indicate potential adverse pressure gradient that might lead to flow separation and then stall. Once again, imprecision in data extracting leads to simple analysis and no deep observation. Feature from [21] is not underlined since pressure evolution with simple winglet is the same as the one with blended winglet. But, as expected, pressure stays at low level (or high level if lower surface) until the end of the wing. Then performances are increased.

3.3 Velocity

In this section, velocities around and behind the profile are investigated. It aims to know which effects has winglet (or not) on profile flow and behind the wing itself. Thanks to velocity patterns, it is possible to know more about secondary flow, vortex generation, ... This part is divided into three logical sections: one for each component of velocity X, Y and Z. Each component can bring essential information about the wing performances.

Since the two models have not necessary the same components direction, let us take the following convention:

- X-component: direction of drag (rolling moment)
- Y-component: direction of lift (yawing moment)
- Z-compoment: direction of cross-wind (pitching moment)

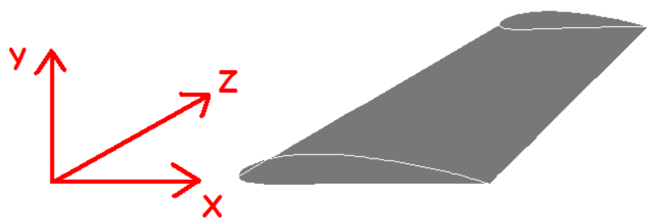

Figure 3.19: Axis convention for velocity analysis

Those three axis are illustrated on figure 3.19. X-component is related to lift performance, Y and Z-components are related to vortex components. So they tell a lot about vortex creation. Moreover Z around the wing itself can inform about the intensity of the potential secondary flow. For each component, generalities are presented, then observations of the given component along the span and finally in the trailing wake at different given cross sections from wingtip (at middle wing ($2\,m$), at $0.5\,m$ from wingtip and at wingtip).

When measuring along the span, all components on the wing are obviously equal to zero according to the non-slip condition. It is why an intermediate distance is found to be out of the boundary layers but not too far still to capture features around the wing. Data are extracted along the span at $0.3\,m$ from upper and lower surfaces respectively (please refer to appendices E to find a depicting of this path). Figure 3.20 depicts paths along which components are measured. There are five paths along which data are extracted: three in the trailing wake and two along the span (note there is only one path along the span drawn on the figure). Data from all paths are not always deeply analysed. If not, one can find all graphs in appendices E.

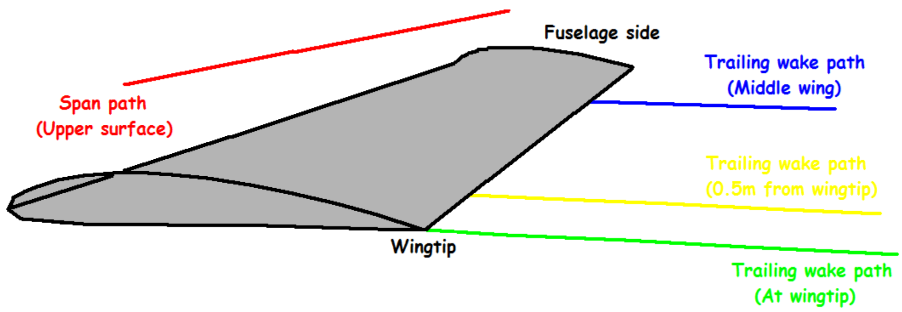

Figure 3.20: Paths along which velocity components are extracted

3.3.1 X-component

Generalities:

According to 3.19 this is the direction of the fluid flow. This component gives an idea of the lift since they are linked by the square of the velocity. Limits of this component for each case are presented in table 3.1.

	Without	Simple W.	Blended W.
Upper limit	59.4	59.4	59.8
Lower limit	-7.0	-17.8	-17.8

Table 3.1: Model A: Limits of X-component velocity for each case at $\alpha = 0°$ in m/s (round to one decimal places)

In general, for $\alpha = 0°$, upper limit or maximum X-component of velocity is quite similar for each case. Indeed, it is the same profile, same boundary conditions, same model and same incidence. This similarity in upper limit for this component is kept through all angles of incidence. While lower limits are slightly different. Figure 3.21 and 3.22 allow to conclude an important assumption.

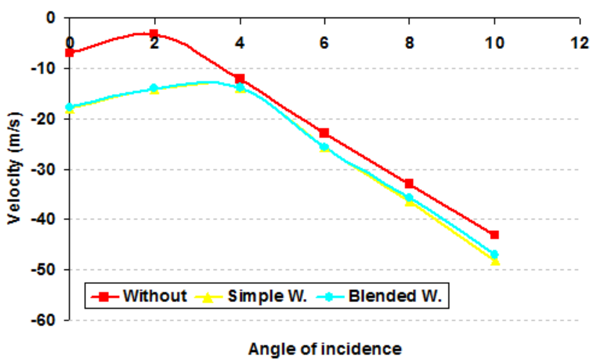

Figure 3.21: Model A: Evolution for lower limit for x-component through angle of incidence

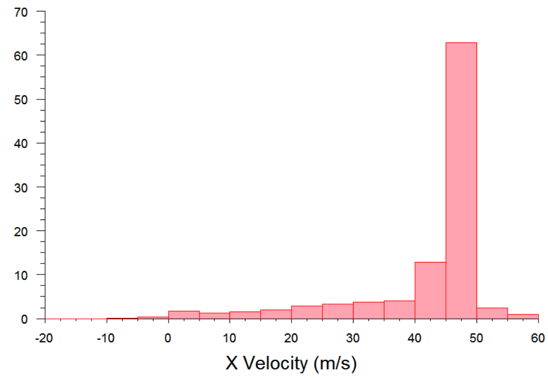

Figure 3.22: Model A: repartition of X-component velocity in the case of blended winglet at $\alpha = 0°$

The first one indicates that, even if lower limits are slightly different between cases, the trend through α is pretty the same. Moreover except when no incidence or a few (2°), values are almost completely similar. The second one ensures that one should not take care about the negative velocity (which could be a disaster for lift performance) since it contributes in a very minute way. Indeed figure 3.22 informs of the percentage distribution of velocities in classes. The main class is $[45; 50]\, m/s$ and the percentage of negative velocities is then very negligible (about $0.4\,\%$ to be precise).

Negative velocities are situated are the stagnation point of wing. Left figure 3.23 illustrates this thanks to vectors colored by negative X-components. It is like if particles of fluid rebound all along the stagnation point. Right figure shows vectors for a negative range of $[-7; -17.8]$. This allows to see where are situated those extra vectors compared to the case without winglet. It seems that range of negative vectors is more wide because of the winglet. Indeed this extra range with winglet is exclusively situated at stagnation points of the winglet.

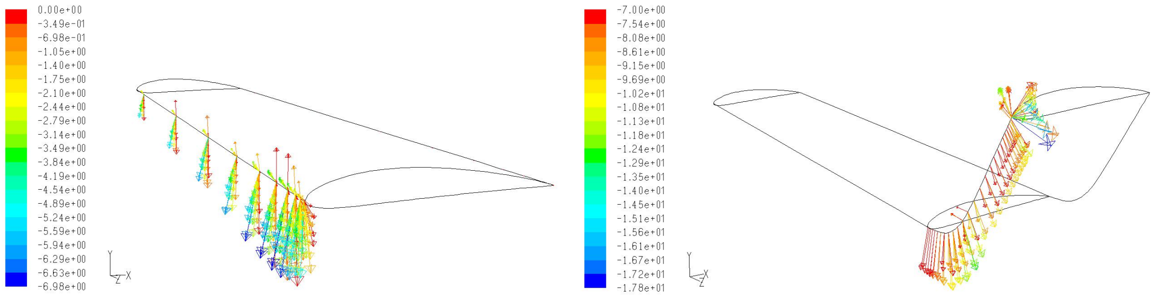

Figure 3.23: Model A: Vectors at the stagnation point colored by negative X-components in the case without and with blended winglet

	Without	Simple W.	Blended W.	Shifted W.
Upper limit at 0°	45.8	45.8	45.8	45.8
Lower limit at 0°	0	0	0	0
Upper limit at 10°	56.2	59.4	58.0	55.2
Lower limit at 10°	−25.2	−26.9	−25.4	−25.5

Table 3.2: Model B: Limits of X-component velocity for each case at 0° and 10° in m/s (round to one decimal places)

Table 3.2 reports limit values for X-component velocity for the model B at 0° and 10° of incidence. These two angles are highlighted because at 0°, nothing happens since it is a simple plate. The upper limit is exactly equals to the boundary condition[1] and the lower limit is 0 since any vortex or complicated motion is initialized. For $\alpha = 10°$, one can think it is the case in model B, comparable to the one in model A at 0°, since it seems to involve the same velocities (around the wing). This fact is confirmed with the lift coefficient. For this model, there is no significative difference if winglet or not, although without winglet the lowest negative value is pretty equal to cases with winglet. (Recall that in model A, there is a wide gap between those)

This is because origins of negative velocity in the models are different. While in model A, it comes from stagnation point, in model B origins can be found in figure 3.25. Indeed, to get a pressure difference between lower and upper surfaces, the wing must have a certain angle of incidence. But the fluid can not stay attached to the wing since it is not profiled at all. Simple plate generates a too high adverse pressure gradient due to the sudden change in flow direction and then boundary layers separate from the wing (or the plate actually). Figure 3.24

[1] $45.8\, m/s$ or $Mach = 0.1314412$

shows differences between both models in X-component velocities. In the model B, blue region indicates the low to negative velocities while in model A this kind of region is pretty small (especially at low angle of incidence). This low velocities region can also be seen on figure 3.25 where only negative component velocity are displayed. One can observe that the entire wing is covered by vectors of negative direction. These lie in this "blue region". Please remark that vectors have, in addition to be in negative X-direction, other components such Y and Z and create a certain trend near the wingtip. These components are discussed later.

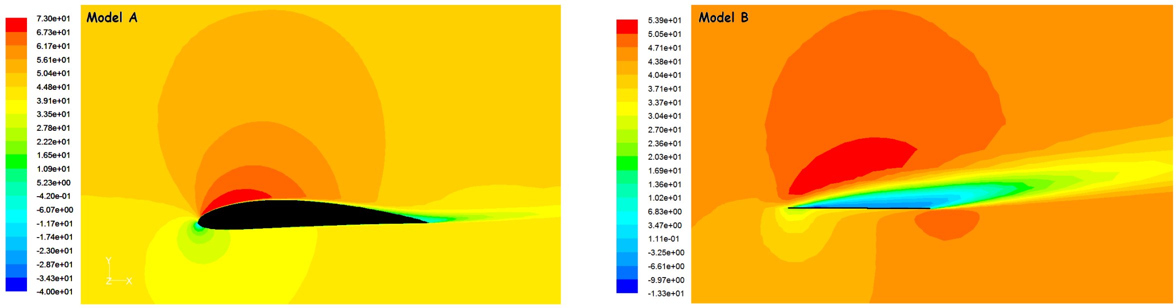

Figure 3.24: Comparison of the "blue region" between both models at $\alpha = 10°$

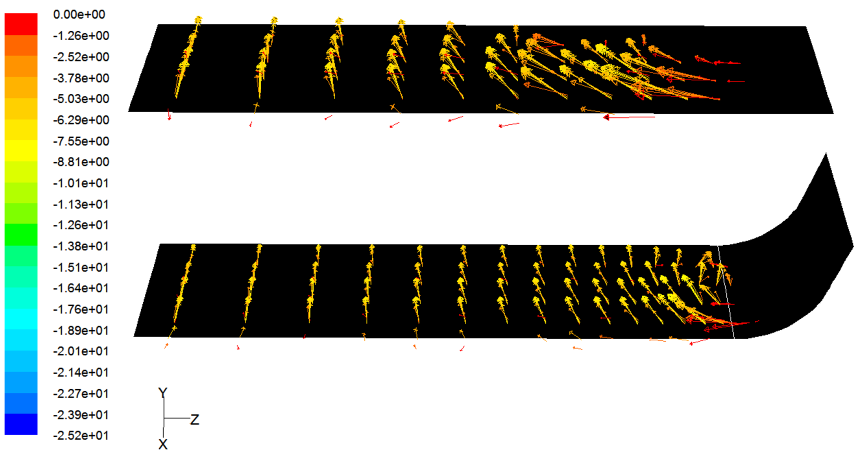

Figure 3.25: Comparison of the "blue region" between both models at $\alpha = 10°$

Along the span:

Figure 3.26 compares velocities between both models along the span.

It seems clear that trends are totally similar in both models. Values are quite constant through span except near/at the wingtip. Please be careful at the wingtip abscisse. Table 3.3 summarizes abscisses for each case in both models.

In the case without winglet for both models, velocity seems to decrease significantly near the wingtip. This could be the consequence of the "mixing" due to vortex creation. In model A, when winglet is placed, there is no change in velocity while in model B, both cases with simple and shifted downstream present a lost in velocity at wingtip. This is because the last

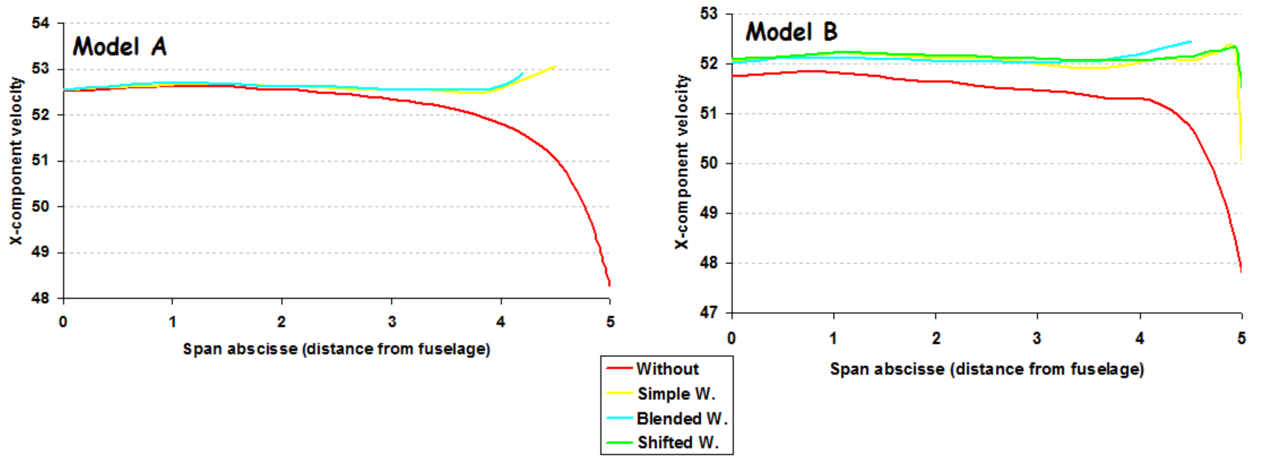

Figure 3.26: Comparison of X-component variation along the span for both models on the upper surface (at 0° and 10° in model A and B respectively)

	Without	Simple W.	Blended W.	Shifted W.
Model A	5	4.5	4.2	–
Model B	5	5	4.5	5

Table 3.3: Wingtip abscisse along the span for all cases in both models (in m)

node lies in the boundary layers of the winglet. Since the blended one has smoother transition, the last node is pretty far from the winglet itself. Indeed the viscous model used in this investigation allows to simulate the boundary layer up to the linear part thanks to a near-wall-model (please refer to section A). So this sudden lost in velocity should not take in account while the "long" lost in the case without winglet is a real one. This lost of velocity is very observable on figures placed in appendices E. These are diplays of the wing at different chord abscisses. And one can see lost in X-component as long as vortex is creating.

One can see that there is no significative discrepancy between case of blended winglet and other cases in model B. That might mean that lift (section 3.1) is correctly simulated despite that Y^+ problem discussed in section 2.2.3.

In the trailing wake:

Figure 3.27 shows the evolution of this component from the trailing edge to $1\,m$ behind the wingtip for model A. One can find all other evolutions in the trailing wake (middle wing and $0.5\,m$ from wingtip) in appendices E. This is interesting because one can see that at middle of the wing, evolution for all three cases is totally similar and as close as one approaches to the wingtip, the case without winglet gets steeper increase.

It seems that the vortex at wingtip has a sudden tendency to increase relative speed of fluid. But quicly after the trailing edge, the component goes back to the same level as other cases (boundary velocity). One can not conclude that potential vortex increases significantly flow speed. This increase is quite negligible, especially behind the wing (no more lift produced). Otherwise vortices would not be disadvantageous!

Model B analysis doesn't bring more information but its evolution can be found in the same

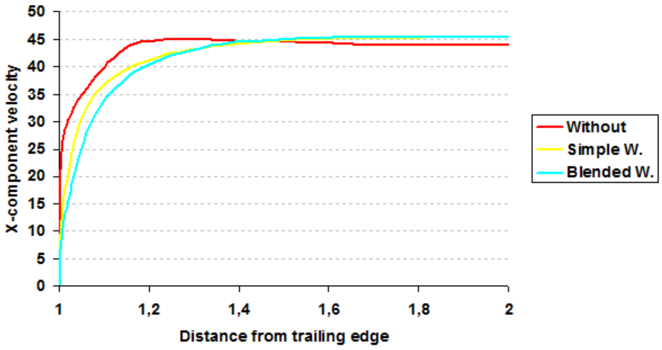

Figure 3.27: Model A: Comparison of X-component variation in the trailing wake at the wingtip at 0°

appendices.

3.3.2 Y-component

Generalities:

According to 3.19, this component is the vertical one. It could give information on the vortex[2] but also on the acceleration when fluid passes over the profile. In general, limit values of this component are similar in each case since profile is the same. One can find table with them in appendices E. Limits are generally high (up to $85\,m/s$ and down to $-40\,m/s$) but, as depicted on figure 3.29, main class of velocity is $[-10; 10]$. Extreme values are situated at leading edge of the wing because it is where fluid goes up (or down if lower surface) to be accelerated and then create a lower pressure. Corresponding extreme values analysis is performed in Z-component section 3.3.3.

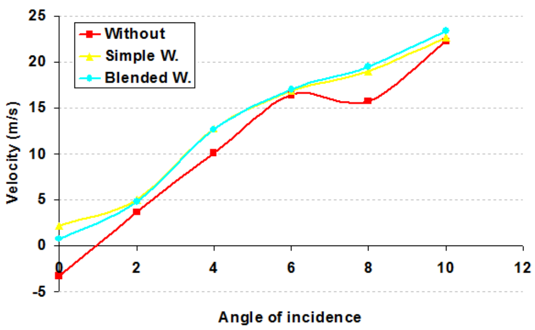

Figure 3.28: Model A: Average value of Y-component through angles of incidence

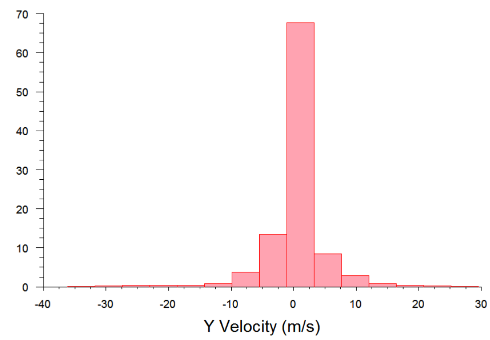

Figure 3.29: Model A: repartition of Y-component velocity in the case without winglet at $\alpha = 0°$

Figure 3.28 indicates the average value of this component for each angle of incidence. There is no difference between cases. Obviously when α increases, velocity in this direction rises.

For model B, any difference is found compared to model A. Average value is the same for each winglet. Absolute values of velocity are lower but this comes from that in model B, the wing is not profiled at all. So flow doesn't get big acceleration in vertical direction.

[2]please refer to suitable section 3.4

Along the span:

Only evolution on the lower surface is interesting since fluid has a trend to go on the upper surface. Then velocities on it are subject to larger variations. Figure 3.31 recalls what happens at the wingtip. And figure 3.30 indicates evolution on the lower surface in model A.

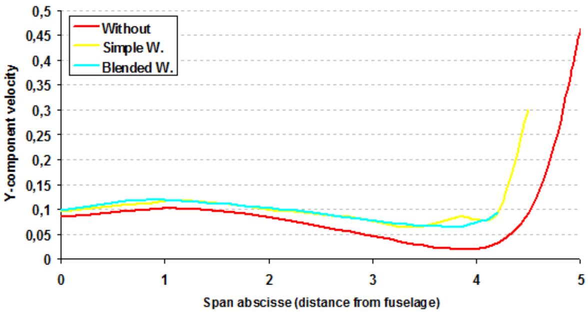

Figure 3.30: Model A: Evolution Y-component on the lower surface at $\alpha = 0°$

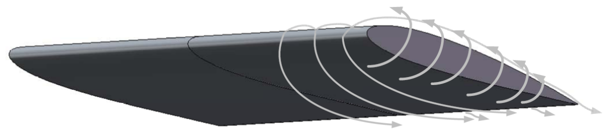

Figure 3.31: Wingtip fluid motion when creating vortex (from [8])

Value are positive since path of extracting data is at $0.3\,m$ chord, thus still in the accelerating part (for this component) of the profile. At the wingtip[3], fluid accelerates suddendly to mix with low pressure fluid. Thus there is a jump in vertical velocity to allow this motion. This is clearly visible for the wing without winglet while when the winglet is placed, the jump is very limited. In the case of simple winglet, there is also a big jump, but this is because fluid still wants to go to low pressure region and then it follows the winglet path which is nearly vertical. In the case of blended, there is no jump at all since it has a very smooth transition.

In model B, only evolution on upper surface is extracted from Fluent. Depicting can be found (with the one of model A) in appendices. There is no clear tendency on upper surface of model B. It is more chaotic at wingtip than in model A. Effectively in model A on upper surface, this component logically decreases when vortex appears or when fluid has to run on winglet going upwards (simple one). Once again, the blended case presents same order of values than other cases although there is some mesh problems (Y^+) over this wing in model B.

In the trailing wake:

Figure 3.32 presents evolution of component in the trailing wake at the wingtip level for both models. Other evolutions in trailing wake of model A (at middle wing and $0.5\,m$ from wingtip) are placed in appendices E. It is possible to see that the trend is suddendly inverted to become the one on figure 3.32 right. This tendency is that in the case without winglet, Y-component becomes still lower (or more negative) since the generated vortex lets feel still more. This aspect of vortex feeling along the span is treated in section 3.3.3 where the Z-component is discussed.

Indeed in model A, velocity behind the wing without winglet is totally inverted compared to cases with winglets. It is positive due to the fluid motion at wingtip as seen on figure 3.31. While when winglet is placed, this fluid motion is prevented and then Y-component

[3] Once again please be careful at the wingtip abscisses for each case

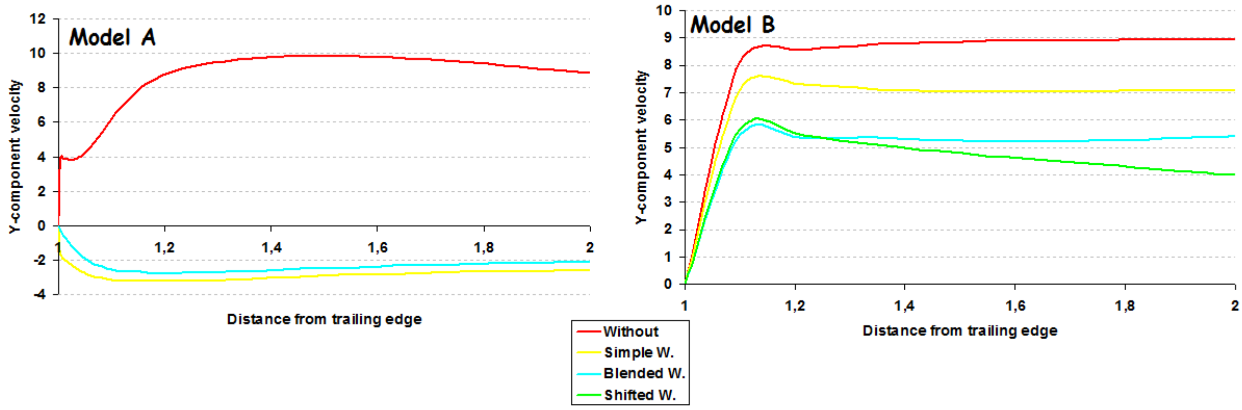

Figure 3.32: Comparison of Y-component variation in the trailing wake behind the wingtip at 0° and 10° for model A and B respectively

stays negative like it is the case earlier on the upper surface. This trend to stay negative after the trailing edge comes from this phenomenon: negative velocities on upper surface are more important in absolute way than the positive ones on lower surface. Figure 3.33 illustrates that phenomenon in the case of simple winglet where one can see that Y-velocities variation are much more important on upper surface and that the trailing wake path (red line) is still in negative values. In the case without winglet, values stay positive but in a decreasing manner because vortex is extending and the trailing path (along which data are extracted) lies still more and more in the heart of the vortex where velocity is still smaller and smaller. This is displayed on figure 3.34.

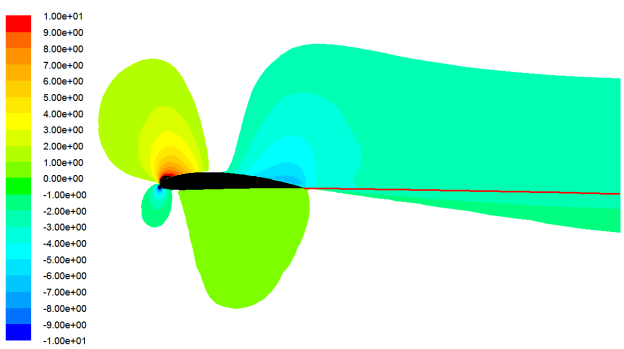

Figure 3.33: Model A: Difference of Y-component between upper and lower surface in the case of simple winglet at $\alpha = 0°$

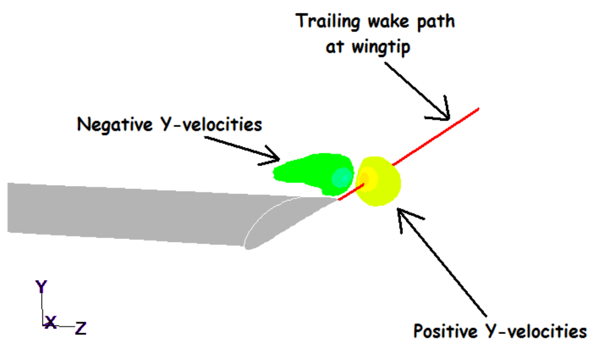

Figure 3.34: Model A: Vortex capture at $0.3\,m$ behind the wing: positive Y components stay along the trailing wake (case with simple winglet at 0°)

In model B, one gets something quite different. Indeed each component is positive unlike in the model A. Recall that in model B, wing is a simple plate and then fluid cannot stay attached at the wing as long as there is an angle of incidence. Since fluid does not fit totally with the profile, it could not create a negative component (at least not so important). Moreover, due to incidence of 10°, it is logical that fluid goes up (velocity in far-field has a Y-component to create the incidence). Figure 3.35 shows the trailing wake behind wingtip with the simple winglet in model B with the red line of the trailing path. And effectively, trailing path lies in positive components. In the case without winglet it is also in positive components since there is a wingtip vortex (same origin as model A) and moreover the phenomenon earlier explained reinforces this tendency. In case with winglet, there is also a vortex at wingtip, but smaller than without winglet (please refer to section 3.4). It is why Y-component is the biggest in the case without winglet.

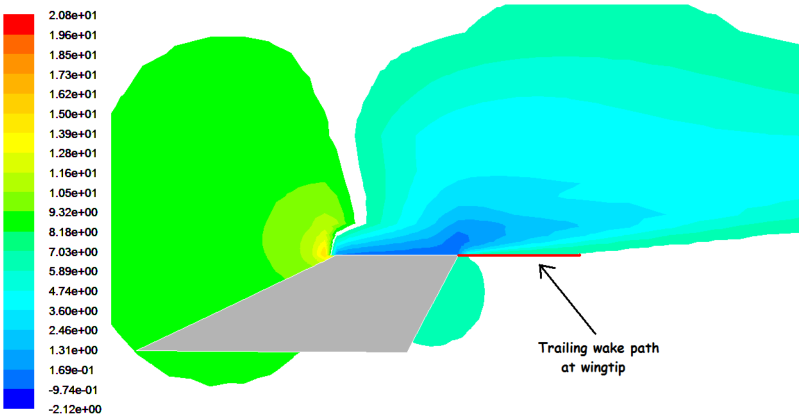

Figure 3.35: Model B: trailing wake in the case of simple winglet at 10°

Displays of trailing wake with winglets (in appendices E) can suggest an explanation of why there are differences in values between those cases. Effectively, the highest Y-velocity is in the case with simple winglet, then in the blended and finally in the shifted downstream one. Having a look at these colorful maps could lead to the conclusion that as large is the surface of the winglet as low is the velocity behind it (and as high is the upwards velocity at the leading edge). Another explanation is that each winglet has, at the junction, a little vortex. And since Y-component is a component of the vortex exterior boundary[4], this gives a window of the intensity or a picture of the location of the vortex (more information about location of vortex in section 3.4). Indeed simple winglet presents the strongest vortex (except when no winglet), and the blended and shifted D. have vortex a slightly detached from wingtip (so component are lower). Section 3.4 will show that vortex in case of blended winglet in model B is unphysical. This is the addition of highly skewed elements around the winglet in this case and the non optimal Y^+ values over winglets in model B.

3.3.3 Z-component

Generalities:

Z-component is, according to 3.19, parallel to the wingspan. In addition to reveal how the vortex behaves[5] (like Y-component), this component gives information about the secondary flow on the wing. It is the previous step of vortex formation. About wing performances, this could inform on the cross-wind flow, but in this investigation, any is simulated.

Once again, distribution of this component (in both models) contains one main class of $[-5; 2]\,m/s$ while limits are very large (up to $56\,m/s$). It is not possible to extract relevant information about trends throug angles of incidence since ranges in vortices are much more below extreme limits of the whole domain. But while extreme values for Y-component are spread everywhere in the domain, Z-ones are concentrated at strategic regions like negative

[4] please refer to section 3.4

[5] please refer to suitable section 3.4

X-ones are (section 3.3.2). Figure 3.36 depicts these regions in the case without winglet and with blended one.

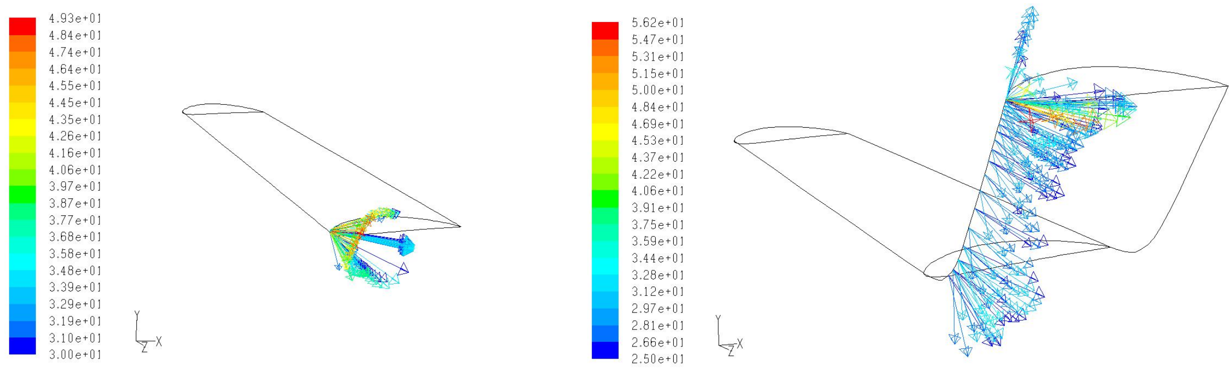

Figure 3.36: Model A: Vectors colored by extreme positive values ($[30-50]\,m/s$) of Z-component in case without and with blended winglet respectively at $\alpha = 0°$

These strategic points are, in case without winglet, at leading edge of the wingtip and, in case with winglet (blended depicted here), along the whole leading edge of the winglet itself. When no winglet, particles going downwards (following the profile near wingtip) are quicly sucked by the motion of fluid going to the upper surface. This leads to high velocities in this direction. When there is a winglet, it is the same phenomenon (vertical velocity creation due to the profile). But winglet is nearly vertical, so velocity direction has the same angle and then becomes nearly horizontal (instead of vertical). Actually Y-component and Z-component are totally linked. When one has high values on the wing, the other has high values on the winglet since winglet is a wing-like but with about 90° inclination.

In model B, the simple plate is not profiled at all and then is not subject to so high vertical velocities (or horizontal on winglet). Then ranges of Z-velocities (like Y-velocities) are moderate: up to $15-17$ against 50 in model A.

Along the span:

Figure 3.37 depicts Z-component along the span for both models. Theses evolutions are taken on the upper surface. Please refer to appendices E for evolution in model A on the lower surface.

In both models, the component seems to decrease along the span. This could be normal since as one approach the wingtip the secondary flow should get stronger and then component should fall[6]. But in model A, at wingtip when there is no winglet, it rise up to $0\,m/s$. Effectively, evolution presented here are taken at chord of $0.3\,m$ (on $1\,m$ long). So it might be a little bit too early to see effective differences between case. Although in model B, in the case without winglet, component falls drastically while when winglet is place, it stays at same level but in a chaotic manner. This could be due to the influence of non-optimal Y^+ values over winglets. Moreover in model A, cases with winglets seem to fall even faster than the case without. Beside that, evolution on lower surface (appendices) shows an large increasing in component which is coherent with reality of secondary flow. But this can not be surely trusted according to previous comments and because position of 0.3 chord is really to early to capture

[6] because origin of the coordinate system is at fuselage side

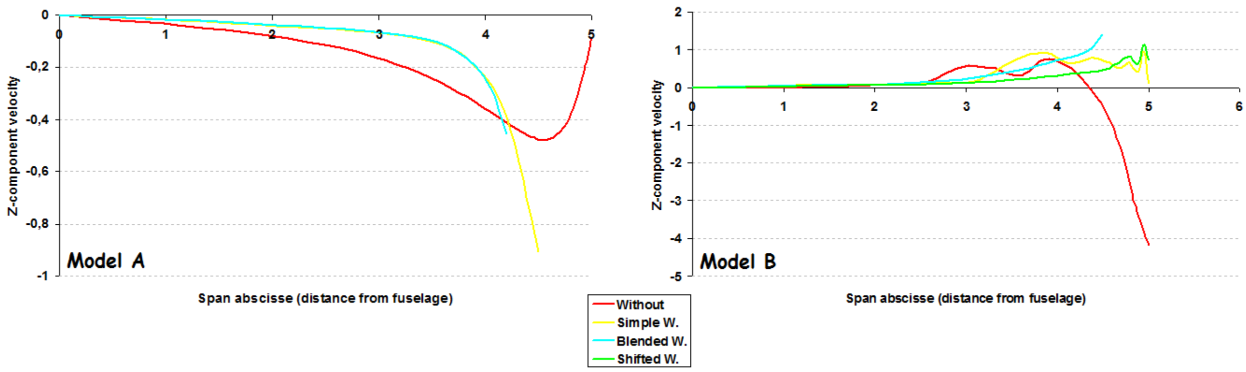

Figure 3.37: Evolution of Z-component on upper surface of both models at $\alpha = 0°$ and $\alpha = 10°$ respectively

any phenomenon of vortices creation.

Figure 3.38 illustrates the presence of a rotating motion in Y-plane[7], namely parallel to the wing. Left one shows the Z-distribution at wingtip along the chord and the right one depicts the Z-component field seen from $0.3\,m$ above the wing (exactly same height as upper surface path for span evolution). On left figure, it is clearly observable that as far as one is from the leading edge, as big (in negative values) is the component. That means secondary flow is still more important when approaching to trailing edge. Then vortex is still more created. On right figure, one can see there is, in addition to the vortex rotation motion in plane perpendicular to the wing, another rotation motion in Y-planes. This motion is concentrated at the middle chord of the wingtip (center is indicated by the red cross).

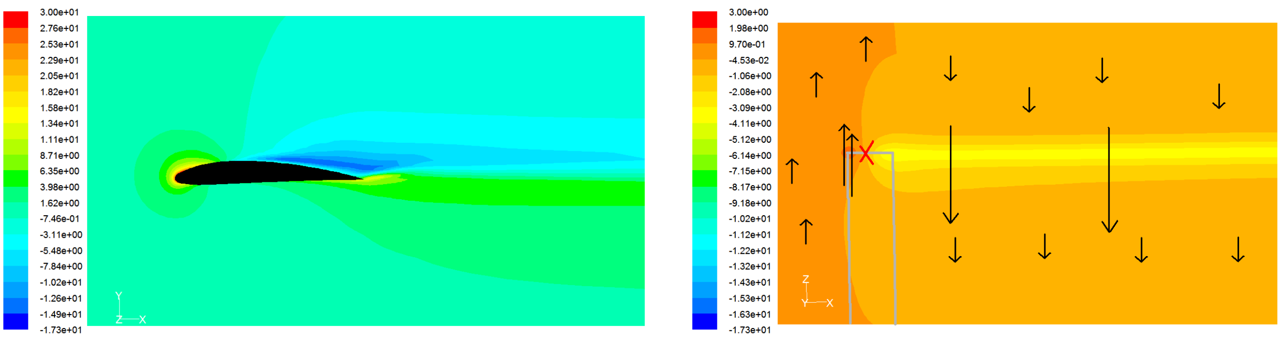

Figure 3.38: Model A: Illustration of rotation motion in Z-plane at $0°$: Left: Z-component field along the chord - Right: Z-component in the Z-plane $0.3\,m$ above the wing

In model B, the same rotation is observable (in appendices). But be careful that at constant Z-plane with incidence, center point rotation is translated along the trailing vortex!

In the trailing:

Figure 3.39 presents only results for the evolution of the component in the trailing wake at level of wingtip. For evolutions at middle wing and $0.5\,m$ from wingtip in model A, please refer

[7] plane with constant Y

to appendices E.

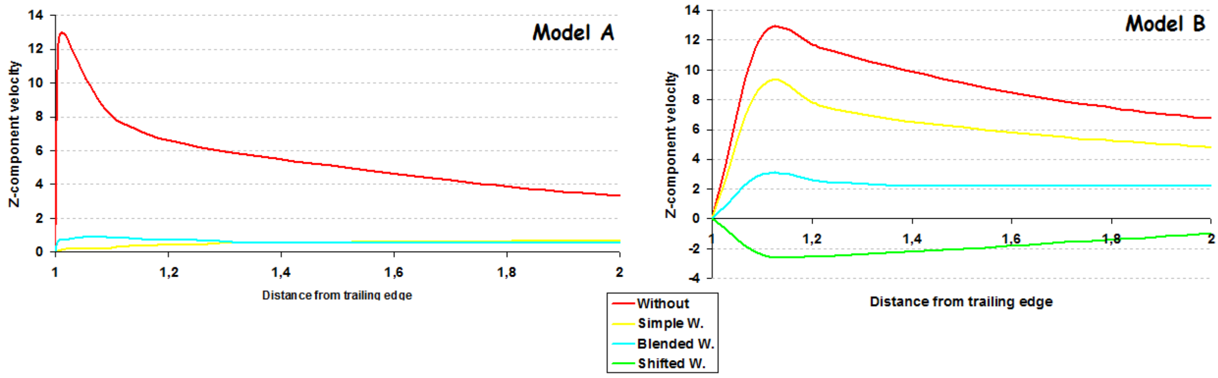

Figure 3.39: Comparison of Z-component variation in the trailing wake behind the wingtip at 0° and 10° for model A and B respectively

Once again, for model A, component in case without winglet is quite high in the trailing wake since it is in the vortex. It stays in positive values because trailing path lies in this region[8]. When winglets are placed, vortex is situated higher in position so the trailing path doesn't lie really in the vortex itself (appendices). It is why components are much more below the one without winglet.

In model B (right figure 3.39), it is more choatic. Like Y-component, one can say that fluid doesn't fit with the profile and then brings complicated flow structure[9]. Differences between cases could be due to vortex position, auxiliary vortex intensity or complicated flow mixed with surface area. Indeed, the simple winglet presents a vortex at wingtip while the blended and S.D. ones have also a vortex but a slightly below. So Z-components are negative. In vortex, positive components are below and negative above. It is why if vortex is slightly below, one lies a little bit more in lower Z-components. But please refer to vortex section 3.4 for more detailed analysis. Once again, vortex behind the blended winglet could be imprecise (section 3.4) and Y^+ values on winglets of model B could also lead to some discrepancies.

3.3.4 Conclusions on velocity

This section analyses velocities over and behind the wing only and compares velocity profiles with and without winglet. Each component can bring information about different performances of the wing. From that it is possible to establish globale performance variations when winglet is placed.

X-component gives information about lift itself since this is the component parallel to the wing and then which generates low pressure on upper surface. In model A, winglet seems not to influence widely this component. Indeed along the span it is quite constant except at wingtip when there is a vortex (case without). When a vortex is created, the wing is maybe slightly less efficient because high component values are only on a smaller span distance than with a winglet. In the trailing wake behind wingtip, this component is not really affected

[8] It is pretty the same explanation as in Y-component section, so please refer to appendices for these colorful displays

[9] please refer to Y-component section

neither. It is coherent because vortex creates a motion in planes perpendicular to the wing. In model B, extreme negative values are situated on the wing because its trailing wake is much more different than a normal profiled wing. Since data were extracted at $\alpha = 10°$ in model B, trailing path does not lie in this wake. So no trend is found. Along the span, same conclusions as model A are taken.

Y-component and Z-component are, at certain levels, linked. The Y-component suddenly increases at wingtip due to fluid motion from lower to upper surface. Winglet seems to limit this trend. In the trailing wake high components reveal that there is a vortex behind the wing alone while with winglet, there is nothing behind the wingtip (surely behind the winglet itself). In model B, since its trailing wake is more complicated, several explanations can be given. Cases in model B certainly contain several auxiliary vortices due to their "sharp" angles. Note that, since intial conditions of vortices are values of winglets, they may have some imprecisions due to slightly high Y^+ values on winglets of model B. Despite this problem, velocity in model B are quite coherent with reality.

Z-component reveals same conclusions as Y-one. But these analyses lead to realize that span path for measurements is taken a little bit too early in the chord position (at $0.3\,m$). A path further (let's say $0.5\,m$ or $0.8\,m$) along the wing would have been much more accurate. $0.3\,m$ was taken because it is, in model A, the highest profile point which is crucial for flow (adverse pressure gradient). But it reveals not to be the best choice afterwards. A rotation motion is found in plane parallel to the wing. For model B, same conclusions of Y-component are valid.

Those analysis lead to conclude that with the winglet, fluid flow over and behind the wing seems to stay unchanged while without winglet, flow is widely perturbed due to vortex creation directly behind. Unfortunately, model B does not bring so much information due to its complex trailing wake at high angle of incidence and the mesh accuracy that is not optimal everywhere.

3.4 Vortex pattern

This section presents pattern of vortices. The purpose is more qualitative than quantitative. Indeed displays of vortices are shown in different sections behind the wing. From those, it is possible to determine the size of the vortices and how fast they grow (or rather vanish). This section is divided in four parts: one for each case (without winglet, with simple, blended and shifted downstream winglet). For each case, a streakline plot is created, by which it is possible to determine the location of the vortices. Then a Y and Z (please refer to section 3.3 to know axis) velocities analysis for each cross section behind the wing is done. This aims to know the intensity of vortices. Those components are also helpful to determine how fast vortices vanish.

Indeed vortex is a rotation motion in planes perpendicular to the fluid flow, namely to X. One can see vortex as a cylindrical motion. Even if it is growing, the cross section of the vortex tube would correspond to a dilating circle with primarily tangential motion. Figure 3.40 indicates (from [15]) corresponding velocities in cylindrical motion.

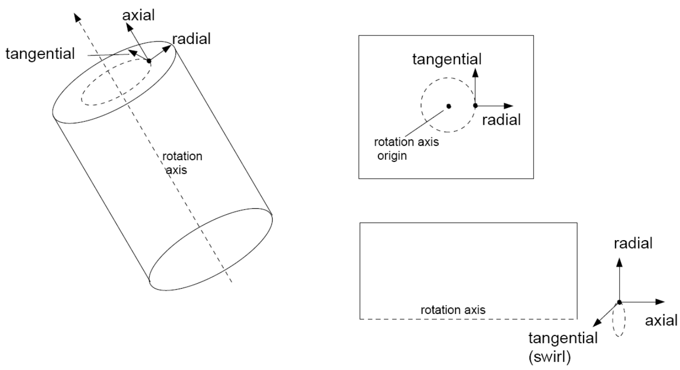

Figure 3.40: Corresponding axis in case of cylindrical motion

In this investigation, the model does no contain any swirl. But one can assimilate the axial component to X (direction of flow), tangential to Y (vertical) and radial to Z-component (parallel to the wing).

3.4.1 Case without winglet

Figure 3.41 displays the streak lines in both models: front and rear views.

For both models, angle of incidence is taken at 10° since the more important is the difference in pressure between both surfaces the larger is the vortex. The wing alone presents only one large vortex at the wingtip as expected. The rotation sense is easily deductible from pathlines and it is like theory describes. From it, one can realize that effectively fluid has a wide trend to go from lower to upper surface.

In model B vortex nearly seems not to be created, but this is an impression due to the picture and the domain in which it is depicted. Indeed pathlines run from the trailing edge to the end of the simulated domain. Then while in model A, several particles have already done a complete rotation, in model B none of them have. Firstly the domain is smaller ($5\,m$ long after the trailing edge for model B against $9\,m$ for model A) and secondly vortex in model B is effectively slightly smaller than in the full-3D-wing. Because wing is a simple plate in model B and then has a smaller vorticity (lower lift or lower circulation leads to lower vorticity) while

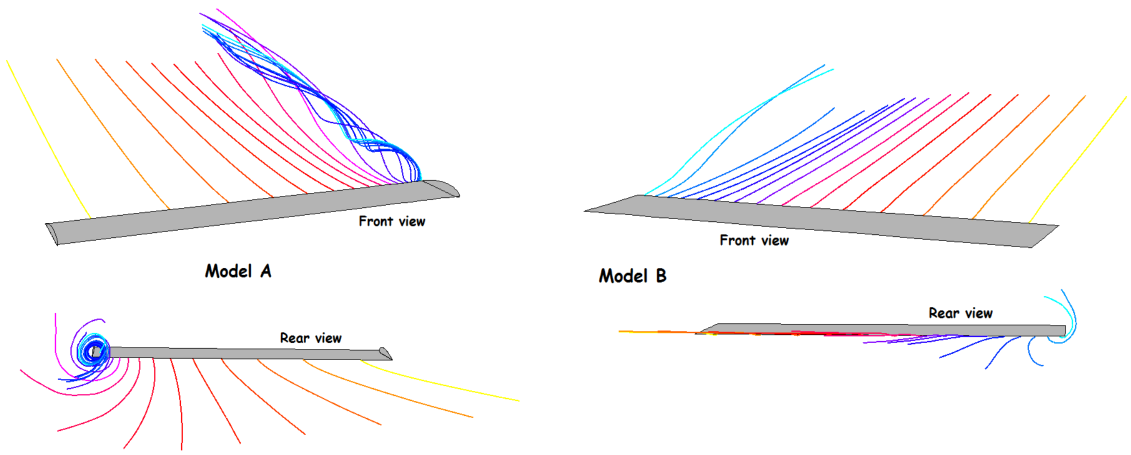

Figure 3.41: Particles pathlines in case without winglet: underlining of vortices situation in both models with front and rear views at $\alpha = 10°$

wing in model A, due to its shape has a higher one. Figure 3.42 depicts vorticity value on wings.

Indeed, more than 75 % of elements have a Z-vorticity higher than $78154\, s^{-1}$ (absolute value) in model A while only 70 % higher than $3034\, s^{-1}$ (still absolute value) in model B. Since vorticity can be seen as the circulation per unit area (around an infinitesimal loop) or the local angular rate of rotation, one can conclude that the circulation is lower around wing B. Lift is thus lower and lead to a lower pressure gradient between lower and upper surface. Vortex at wingtip is then reduced.

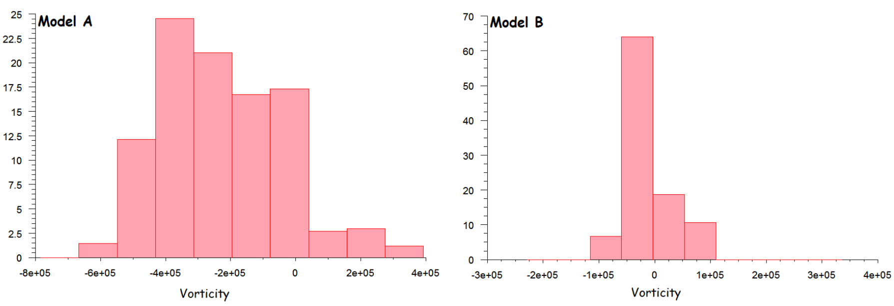

Figure 3.42: Z-vorticity distribution on upper surface wings of both models at $\alpha = 10°$

While it is quite difficult to visualize the expansion of the vortex on previous pathlines windows, figure 3.43 depicts Y-velocities field in both models at 10° of incidence. Both Y and Z components can be used to visualize vortices. In this report, Y-ones is used, but please refer to appendices F to have figures of vortex evolution with Z-component. Obviously, conclusions are the same since each of them create the given motion. Cross sections behind the wing, at which velocity field is depicted, are $0.5\, m$, $3\, m$ and $6\, m$ behind the trailing edge. One can see a grey line at each wingtip. It a path coming from the wingtip trailing edge to the end of the domain. This path is parallel to the fluid flow (namely 10° of inclination in these cases).

Figure 3.43 depicts iso-surface for Y-components behind the wing. Both together, upwards and downwards iso-surfaces situate vortices. They lead to a rotation motion. One can observe

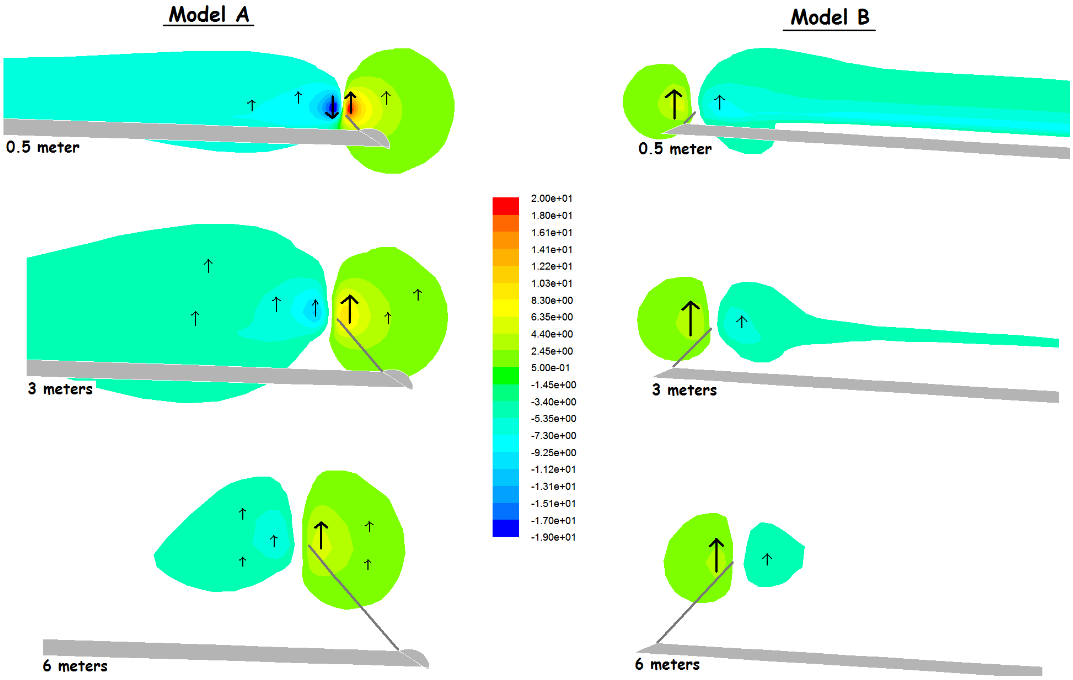

Figure 3.43: Comparison of the evolution of vortex in case without winglet thanks to Y velocities evolution along cross sections behind the wing: 0.5, 3 and 6 m behind for both models at $\alpha = 10°$

that in model B, none of cross sections contains negative velocities. This is because the whole vortex is going up due to the angle of incidence, and then simply a velocity gradient between the two sides can create the vortex. Obviously the center of rotation of the vortex is situated between those two components.

In one has a look at Z-velocities field in appendices F, there is no negative velocities because vortex does not have any overall motion in the Z-direction. Analysis on this field lead exactly to the same conclusions. On these figures, one can see clearly that vortex extends in this direction as well.

Immediately it is clear that the vortex in model A is stronger than in model B because there are negative velocities. Non-negative velocities lead to a slower vortex. From first to last cross section, intensity seems to decrease noticeably because of the viscous diffusion. The bigger is the viscosity the faster the vortex vanishes. In the present work, viscosity is the one at sea level, and $15°C$. According to Sutherland law (please refer to appendices A), viscosity increases with temperature. Then the higher an aircraft flies the slower is the vanishing of vortices, if one considers only this factor (viscosity).

Center vorticities (with respect to center line (grey line)) are still more lowering. That means vortex is still larger and larger. Let us consider that when center vorticity is the same as boundary conditions, vortex has totally disappeared. Objectively, table 3.45 summarizes maximum absolute values of X-vorticity (center vortex) at each cross section for both models. And figure 3.44 illustrates vortex seen thanks to X-vorticity.

This table underlines this fact: the weaker is the vortex the slower it vanishes. Indeed vortex in model A is stronger than in model B and its X-vorticity is divided by more than 12 from

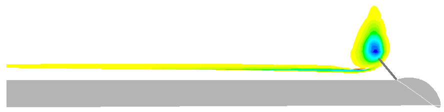

Figure 3.44: Illustration of vortex through X-vorticity at first cross section at $\alpha = 10°$ in case without winglet

	Model A	Model B
Cross section at $0.5\,m$	$686.4\,s^{-1}$	$109.6\,s^{-1}$
Cross section at $3\,m$	$185.0\,s^{-1}$	$75.2\,s^{-1}$
Cross section at $6\,m$	$56.6\,s^{-1}$	$37.9\,s^{-1}$

Figure 3.45: Maximum absolute value of X-vorticity for each cross sections at $\alpha = 10°$ in case without winglet (round to one decimal places)

first to last cross section while in model B, it is only divided by less than 3. At infinity, it must reach boundary conditions values which is $0\,s^{-1}$ since no initial rotation is set. With respect to the center line (trailing path), it is pretty clear that vortex extends in this direction.

3.4.2 Case with simple winglet

In purpose to situate vortices, figure 3.46 depicts streak lines in the case of a simple winglet for both models. There is a big difference between them. In model A, vortex is created at winglet tip, namely it is displaced from wingtip in case without winglet to winglet tip in this case. While in model B, the vortex is still created at wingtip. In both models, particles from wingtip (model A) or winglet tip (model B) seem to join the motion like if they are attracted. Since in model B, there is no pressure gradient between lower and upper surface of the winglet, it could be logical that there is no vortex at winglet tip. That fact could underline that in model A, vortex is well displaced to winglet tip, but when the angle is too sharp, a wide auxiliary vortex is created and lead to a lost in induced drag.

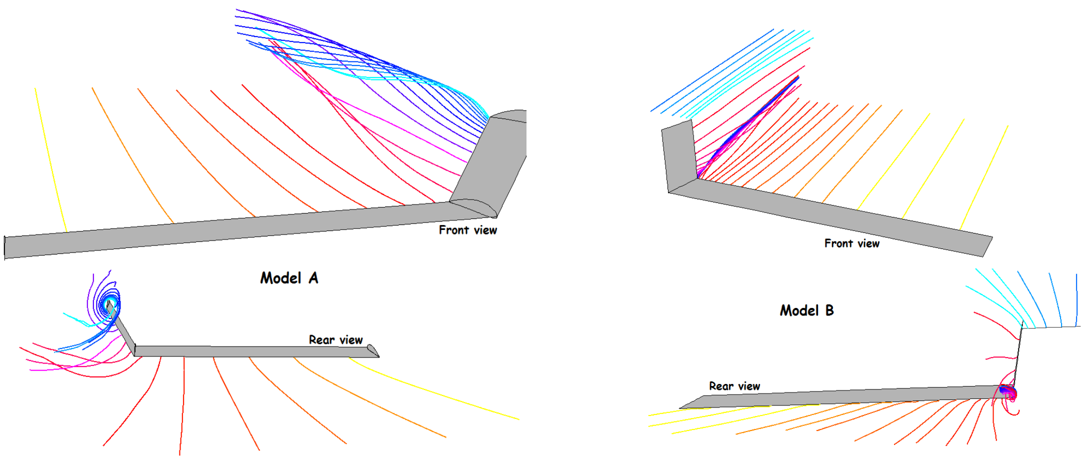

Figure 3.46: Particles pathlines in case with simple winglet: underlining of vortices situation in both models with front and rear views at $\alpha = 10°$

On figure 3.47, evolutions of the vortex velocities behind the wing are shown. Already on these, one can guest that vortex is less strong than in case without winglet (confirmed by vorticity below). Indeed, one can compare Y-velocities field behind the wing between both models. Obviously model B presents lower components and then should create a weaker motion.

Conclusions are confirmed by table 3.49. Vortex A stays effectively stronger than the B one. Vortex A is weaker compared to the case without winglet while the vortex B is stronger. And

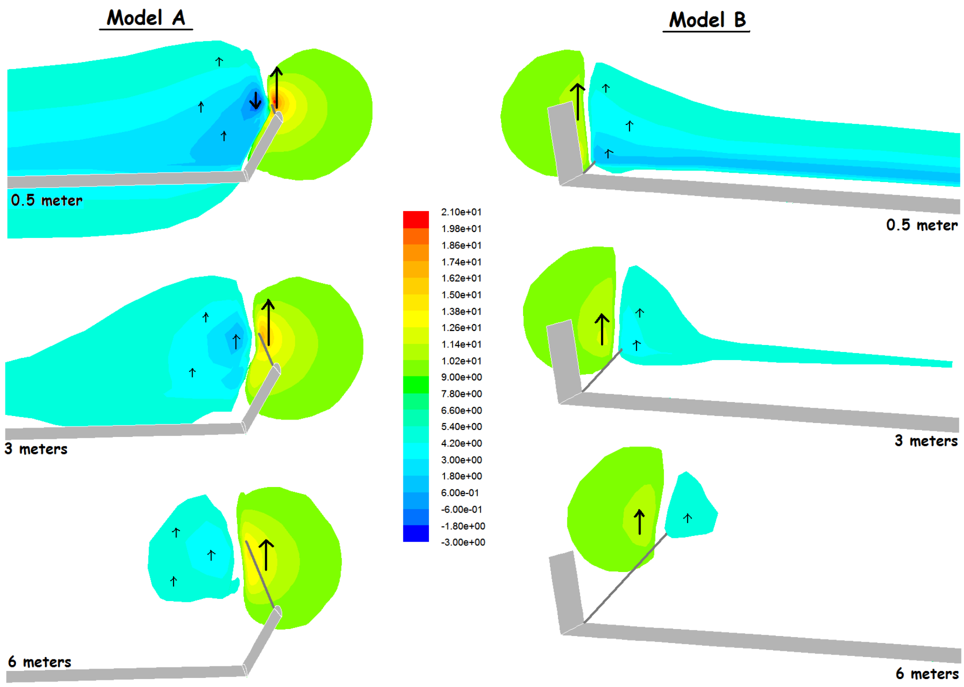

Figure 3.47: Comparison of the evolution of vortex in case with simple winglet thanks to Y velocities evolution along cross sections behind the wing: 0.5, 3 and $6\,m$ behind for both models at $\alpha = 10°$

clearly, the vanishing is once again much slower in model B. Actually, vanishing is asympotic as close as one approaches the far-field value. This is very visible in model A, where from first to second cross section, vorticity is divided by 3.1 and then from second to third, only by 1.9.

In appendices F vortex velocities in Z-direction are placed. Conclusions could be the same, but it is more difficult to see that vortex is weaker because in each cases, there are negative and positive velocities. Otherwise, those pictures indicates that vortex is well extending in all directions.

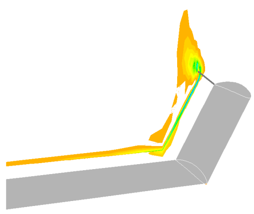

Figure 3.48: Illustration of vortex through X-vorticity at first cross section at $\alpha = 10°$ in case with simple winglet

	Model A	Model B
Cross section at $0.5\,m$	$397.7\,s^{-1}$	$155.8\,s^{-1}$
Cross section at $3\,m$	$128.3\,s^{-1}$	$72.3\,s^{-1}$
Cross section at $6\,m$	$67.2\,s^{-1}$	$33.3\,s^{-1}$

Figure 3.49: Maximum absolute value of X-vorticity for each cross sections at $\alpha = 10°$ in case with simple winglet (round to one decimal places)

3.4.3 Case with blended winglet

Figure 3.50 depicts streak lines in both models from rear view. This case is totally similar to the case with simple winglet. One can see that in model A, vortices are placed at winglet tip while in model B, there are created at wingtip and even more, along the winglet! Indeed they do not seem to be really due to the wingtip. In this case, blended winglet should create a smaller vortex than the simple one. Any real circular path of particles are found, only a trend to join such a motion.

Figure 3.50: Particles pathlines in case with blended winglet: underlining of vortices situation in both models with rear view only at $\alpha = 10°$

If one has a look at Y-velocities through cross sections, one can realize vortex is not at wing or winglet tip at all. These displays are placed in appendices F because there are very similar to other cases and would decrease readability of the report. On these, two trailing pathlines are depicted: from wingtip and winglet tip. Vortices are exactly between those two. One can think the blended winglet maybe still generates vortices, although not due to its junction like the simple winglet. But if one refers to appendices B, one can realize that mesh around (and over) winglet in both cases is not really optimal. Indeed this especially true in model B as explained below.

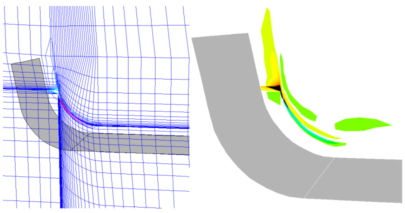

Figure 3.51: Illustration of the mesh problem to calculate the vorticity in case with blended winglet ($\alpha = 10°$)

	Model A	Model B
Cross section at $0.5\,m$	$430.3\,s^{-1}$	–
Cross section at $3\,m$	$142.3\,s^{-1}$	–
Cross section at $6\,m$	$72.0\,s^{-1}$	–

Figure 3.52: Maximum absolute value of X-vorticity for each cross sections at $\alpha = 10°$ in case with blended winglet (round to one decimal places)

Table 3.52 indicates maximum absolute values of X-vorticity. This give an idea of the intensity of vortices. And the conclusion is that vortices in this case have slightly higher intensities than simple winglet. In model A, this could come from the non-optimal geometry which has some sharp angles due to the discretization of the blended transition. One can say that the blended winglet is maybe not so well drawn in model A and then has similar performances than the simple one. In model B, no physical value can be extracted. This is clearly due to the mesh around the winglet itself as depicts on figure 3.51. One can see that the mesh is quite chaotic in this region and the black hole (on right side of figure 3.51) is an extreme value of vorticity which is not really physical. Section 2.2.3 informs about a non optimal Y^+ along the wing and winglet. And moreover section B reports a very high EAS (EquiAngle Skew) of 0.96 around the blended winglet. Those elements are nearly totally degenerated and then could lead to large imprecisions. That might be an explanation of the problem. Then vortex from model B in case with blended winglet should not totally be like reality due to this mesh problem.

3.4.4 Case with shifted downstream winglet

Figure 3.53 and table 3.54 summarize the case with the shifted downstream winglet (only in model B). The streak lines shows that there is a little vortex situated on the downstream surface. Indeed in this model, due to high pressure on lower surface, at winglet tip, flow tends to go to low pressure region (not to upper surface, but to the far-field actually). This trend is reinforced by the fact that in absolute value, high pressure is much more important than low pressure on upper surface (in model B!). So vortex is more present near the downstream part than near the upstream one. Exactly like in simple and blended winglet: winglet is not at upstream winglet tip, but at "lowest" place, namely wingtip or downstream part. This location is confirmed by Y and Z displays (in appendices). On these three trailing paths are drawn: wingtip path, upstream and downstream surface path.

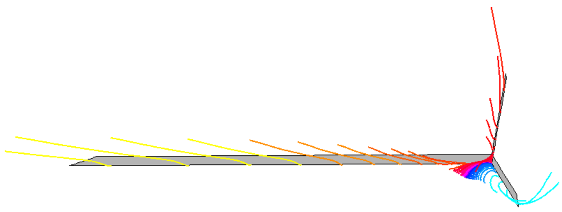

Figure 3.53: Particles pathlines in case with shifted downstream winglet ($\alpha = 10°$)

	Model A	Model B
Cross section at $0.5\,m$	–	$104.8\,s^{-1}$
Cross section at $3\,m$	–	$67.6\,s^{-1}$
Cross section at $6\,m$	–	$35.3\,s^{-1}$

Figure 3.54: Maximum absolute value of X-vorticity for each cross sections at $\alpha = 10°$ in case with shifted downstream winglet (round to one decimal places)

In general, this vortex is slightly weaker than in previous cases (see table 3.54). And once again, it vanishes very slowly.

3.4.5 Conclusions on vortex

Thanks to several fields depicting and streak lines, this sections aims to conclude what are differences between vortices in different winglet cases and models. Every analysis are done with fluid flow arriving at angle of incidence of 10°. Indeed at this angle, pressure gradient and Z-vorticity (rotation axis of wing circulation) are the highest and then should create the strongest and largest vortex.

The vortex created in case without is surely the strongest one in model A while in model B the sharp winglet leads to stronger vortex. It could be due to the "too sharp" angle of the winglet. They vanishe quite more quickly in model A since they are the biggest due to the real wing profile. Vanishing is inversly proportional to the vorticity value (difference between far-field value (0) and current one). In this case, streak lines indicates that vortex is situated exactly at same place in both models: at wingtip. It is effectively what theory reports.

When adding the simple winglet, vortex is considerably reduced in model A while it is higher in model B. The vanishing follows the same law. In this case vortices are not situated at the same places. Effectively, in model A, it is displaced to winglet tip where low and high pressure meet. While in model B, there is no really high and low pressure continuation on winglet, so there is no vortex at winglet tip. It is still created at wingtip. Upper and lower surfaces values are the initial conditions for vortex creation. In case of winglet, they are winglet surfaces values. In model B, Y^+ is not optimal on any winglet. That might lead imprecise intial conditions and then to displacements of vortices.

The blended winglet should reduce still more vortex sizes, but it does not really. Maximum vorticity values are pretty similar, even higher. In model A, this could come from sharp angles to create the blended transition and lead to very similar (or worse) performances than simple winglet. It is still situated at winglet tip. In model B, poor mesh quality around winglet brings extreme and unphysical values in the trailing vortex.

The shifted downstream (only in model B) reports a vortex more centered at downstream surface than at wingtip. Its intensity is similar to the one with simple winglet. Its displacement could come from initial conditions on the winglet surfaces.

Vortices created come from the circulation around the wing. Here are analysed two extreme cases. One with real wing profile until the winglet tip, and the other one with no wing profile at all (for the winglet neither). Those give different results that should be carefully understood. In general winglet does not have a wing profile. Then circulation (or pressure gradient) around them is very limited. They act more as a fence at wingtip. Model B presents such a winglet with an unreal wing while in model A, a real wing is used, but with an unphysical winglet. Comparisons are done in both extreme cases: reality should be between those. In model A vortex seems to be only translated to winglet tip while in model B, vortex seems to be created by the junction. Since winglets are not profiled in reality, vortices should not be strictly translated like in model A, and model B underlines a important feature: junction is an essential element in winglet building. Unfortunately the whole blended case in model B is useless due its mesh problem and more generally in model B, vortices power should be taken carefully due to Y^+ values on its winglets.

3.5 Mesh Independancy

This last part aims to determine if results are independant of the mesh. It is then possible to know exactly the influence of the mesh on them. This study is performed in model A with case without winglet. This mesh contains 286400 elements. For the mesh independancy, a grid of 3.6 millions cells is built. Around the airfoil, precision is increase by a factor 10 (size of last element) and there are more than 3 time more elements in the vertical direction. In the span direction (third dimension), there are more than 3 times elements as well.

Figure 3.55 presents the results for only two angles of incidence with the new grid (very long time of calculation!). Lift is slightly higher (5 to 8 % more) while the drag is almost equal (only 1 % at 10°). The main discrepancy between numerical's and litterature is especially in the drag. And one can conclude that the solution is pretty independant of the mesh at this level.

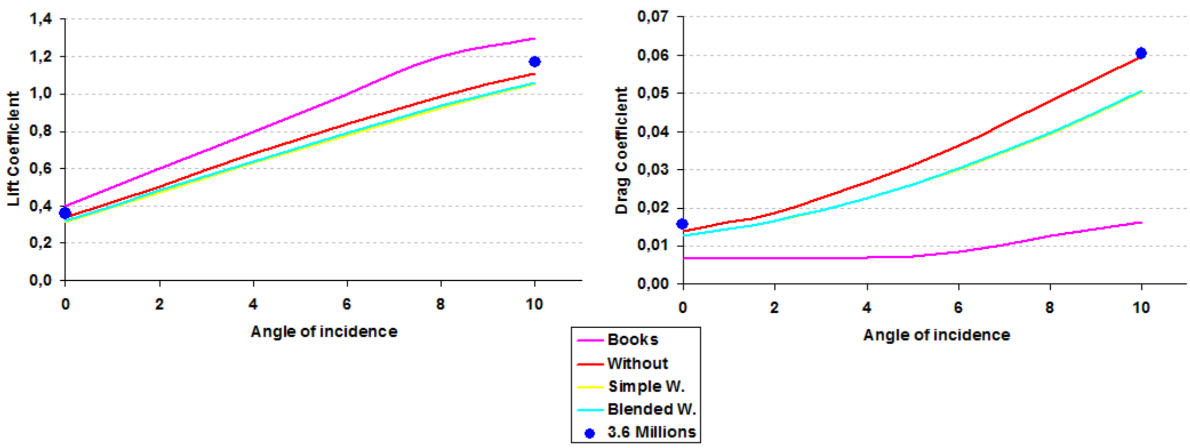

Figure 3.55: Lift and drag coefficient at 0° with 3.6 millions elements

For this study, all directions of discretization are modified while the main problem met in the mesh quality (and especially in Y^+, section 2.2.3) is around the winglet itself (or wingtip). A nice study should to increase number of elements in the span direction only (namely increase around winglet). This might refine the solution for induced drag phenomenon.

Chapter 4

Conclusions and Discussions

4.1 Assumptions and Limitations

Before taking final conclusions about the results and the tool used in this investigation, let us present/summarize main assumptions and limitations in models. Table 4.1 recalls which simulation is performed in which model.

	Full 3D-model (Model A)	2D wing in 3D (Model B)	2D simulation
Wing alone	x	x	x
Simple winglet	x	x	
Blended winglet	x	x	
Wingtip fence		x	

Table 4.1: Summary of simulations done

The main assumption is: **no chord and thickness variation for the winglet.**

Indeed it would have been very complicated and time consumming to build such a winglet. Moreover with the lack of data on winglet geometry, building would have been very approximate. Nothing could be done about the chord variation. But thanks to two different models, a thickness variation was made.

Each model has a different "real thickness feature". Model A has a real wing profile but its winglet as well. It means that the winglet creates as lift as the wing and it is even thick than the wing. While in model B, the wing and winglet are simple plates, meaning that wing does not behave like a real one but then the winglet becomes thin like a real one. This way to work was the only one to try to capture features of winglet with a real wing but also when winglet does not create big lift.

This assumption and the way of avoiding the problem mainly comes from the building the geometry. No special assumption was done for the simulations themself (in Fluent) since it is simple air coming with different angles of incidence. This split problem leads to "extreme" conclusions.

Results are limited to "gross" features because real case is a combination of both models. Moreover wing in model B can be seen like a very very unefficient wing.

4.2 Final Conclusions

Effects of blended winglet were investigated in this work. The investigation was lead numerically. In addition to comparisons between the blended winglet and the case without winglet, other analysis were performed. Each case was compared to cases without winglet, with the simple winglet, the shifted downstream winglet and obviously the blended winglet.

Fluent was used to model phenomenons around the wing and winglet. Although in classic aerodynamics, several models already exist like *the thin airfoil theory*, *the finite wing theory* and *computational method of panels*, they have some difficulties to include winglet effects. Numerical's can be the first step to include empirical influences of winglets in such models.

Two models were used. The model A is a NACA 4412 profile at which is added the winglet with the same profile (and same thickness). In model B, the wing and the winglet are simple plates fitted together. Mesh quality is very good in model A, while Y^+ values over the winglets in model B are rather high. Those lead to some imprecisions in vortex patterns. Moreover the mesh around the blended case is pretty bad (EAS up to 0.96). Then results from this case could not be deeply interpreted.

Forces performance (lift and drag) are pretty well enhanced thanks to the winglets. A maximum of 18 % drag reduction is reported in case with simple winglet of model A. This same winglet in model B decreases the drag in the same order but rather constantly through angles of incidence.

There is a wide pressure lost at wingtip in all cases: either there is a wingtip vortex creation or the low pressure from wing is added to the low pressure from winglet. Thanks to the winglet, the pressure gradient stays homogenous until the end of the wing, keeping the wing operational on its whole span. Along the chord, no special adverse pressure gradient could be simulated near the leading edge as reported in theory.

In linking with the pressure lost at wingtip, the X-velocity component falls drastically, when there is no winglet, decreasing lift at this region. Also there is rotation motion in Y-plan above and below the wing centered at vortex center. Y-velocity reveals that vortex feels still less as far as one is from wingtip.

Vorticity analysis confirms that strength of the vortex is the biggest without winglet and the addition of the simple winglet considerably reduces it. Unfortunately real effects of the blended winglet are not totally underlined. In model A, vortices are displaced to the winglet tip while model B has still vortex at the wing tip since there is no pressure gradient between upper and lower surfaces of the winglet.

The final word is that model A highlighted very well the vortex reduction and its feeling along the wing. And model B could be taken to illustrate effects of the "sharp" angle when adding the winglet because it presents some mesh problems and imprecisions.

4.3 Further Work

Since no chord variation was modelled for the winglet and the thickness variation was very limited, it is clear that very deep researches about winglets geometry should be done. Then a real wing (like model A) and, with those geometry data, a real winglet could be drawn. If a complete model with real data for the whole winglet could be built, conclusions on aerodynamic effects of winglet could be really more trusted.

Even if mesh in model A is reported as very good (according to [12]), some regions got troubles: region after wingtip (in the span direction), stagnation point at leading edge, ... Improving this mesh and drawing a very accurate winglet geometry could be a proposal for a further work.

About simulations, going up to the stall angle of incidence could also be interesting to see potential effect(s) of winglet at/on this angle.

Part II

Appendices

Appendix A

Fluent Program

Fluent is a Computational Fluid Dynamic (CFD) software. It simulates from simple fluid flows to complex combustion reactions passing by heat and mass transfers, multiphase flows, species transports and chemical reactions among others.

Geometries and domains could be built with its geometry and mesh generation software which is Gambit. Meshes can be imported (from SolidWorks, Catia, ...) into Gambit before generating it into suitable file for Fluent. This is one of the powerful interest of Gambit. This geometry and mesh builder is not discussed here. It is just the Fluent associated software and not the compulsory step before running Fluent since others softwares could be used to shape and mesh.

A.1 Basic equations in Fluent

For all flows, Fluent solves two basic conservation equations: continuity and momentum equations. Of course, when heat transfer are involved, energy equation conservation equation is also solved ([15]). These three equations are the only ones in the case of our project: an airfoil. But obviously, when modeling a combustion, chemical reaction, ... others equations like species, mixture fraction, ... conservation are solved as well.

Mass Conservation equation:

The continuity equation can be written as follows ([15]):

$$\frac{\partial \rho}{\partial t} + \nabla \cdot (\rho \vec{v}) = S_m$$

where the term S_m is the source term. One can derive this form for a two dimensional flow as well as for a three dimensional or axisymmetric, ...

Momentum Conservation equation:

This equation is written for a inertial (constant velocity) reference frame ([15]):

$$\frac{\partial}{\partial t}(\rho \vec{v}) + \nabla \cdot (\rho \vec{v} \vec{v}) = -\nabla p + \nabla \cdot (\overline{\overline{\tau}}) + \rho \vec{g} + \vec{F}$$

where p is the static pressure, $\overline{\overline{\tau}}$ the stress tensor (see below), $\rho\vec{g}$ the gravitational body and $\vec{F}$ is external body forces.
Recall that the stress tensor $\overline{\overline{\tau}}$ has the form in equation (A.1) ([15]).

$$\overline{\overline{\tau}} = \mu[(\nabla\vec{v} + \nabla\vec{v}^T) - \frac{2}{3}\nabla\cdot\vec{v}I] \tag{A.1}$$

where μ is the molecular viscosity, I the unit tensor and the last term on the right hand side shows effect of volume dilatation.
Once again, with a few mathematical development, one can derive this conservation equation for specific cases like 3D, axisymmetric, ...

Energy Conservation equation:

Energy conservation equation is given by ([15]):

$$\frac{\partial}{\partial t}(\rho E) + \nabla\cdot(\vec{v}(\rho E + p)) = -\nabla\cdot(\sum_j h_j J_j) + S_h$$

These three basic equations are solved in the case of the airfoil in this work.

A.2 Models

A.2.1 Solver

Segregated or coupled:

Fluent suggests two different solver: The *segregated* solver or the *coupled* solver. Those are the names in previous version of Fluent (Version 6.2 or lower). In the new version (6.3, the one used in this project) they are named *pressure* or *density* based solver respectively. In each of these method, Fluent solves governing equations and a control-volume-based technique is used. Namely division of the domain into discrete control volume according to the grid, integration of governing equations on the individual control volumes and then linearization of discretized equations and solutions ([15]). There is two ways of linearization: implicit and explicit. It is detailed a little bit more below.

The segregated method (or pressure based) is such that each governing equation (continuity, momentum, ...) is solved "sequentially". Of course, each equation is non-linear and then requires more than one iteration before it converges. At each iteration, several distinct steps are run. These are made in a diagram on figure A.1 left ([15]). For more detailed about each step, please refer to Fluent User's Guide [15].

The coupled solver (or density based) solves every governing equations "at the same time". They are coupled each together. On figure A.1 right, one can compare differences with segregated solver. Even if the iteration scheme is smaller in this case, the convergence time is longer ([18]).

Still from [18], "*Choice of solvers depends heavily on the model being solved. The segregated*

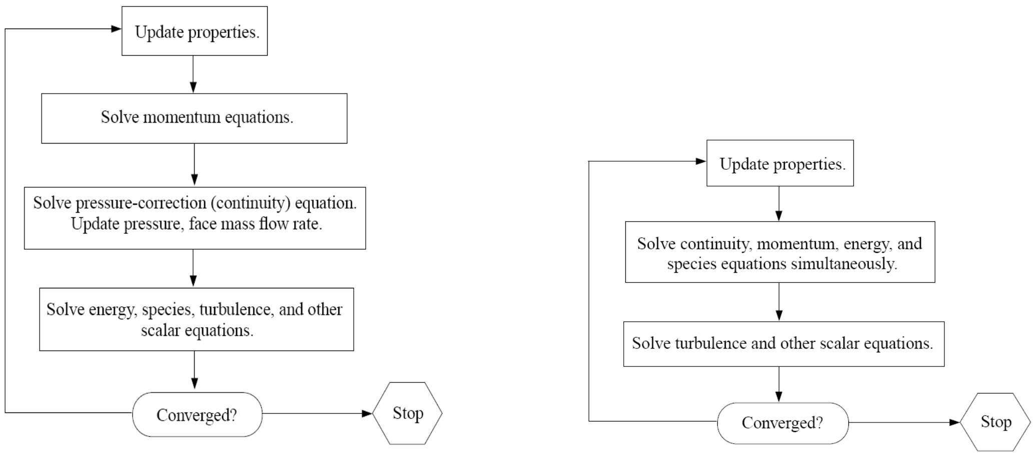

Figure A.1: Segregated and coupled iteration scheme comparison [3]

solver solution is based on the pressure, while the coupled solver solution is based on density. This makes the segregated solver better at low speed flows and the coupled solver better at solving transonic / supersonic cases". It is also recommanded not to use the coupled solver for a flow speed below Mach 0.4. The airspeed in simulations, done in this frame, is $45\,m/s$. It is why the segregated solver was chosen in this project.

Implicit or explicit linearization:

Non-linear governing equations are, in both pressure or density based case, linearized. This can be done by an *implicit* or *explicit* scheme with respect to the set of variable. [15] gives following definitions for both schemes:

- implicit: unknown values are found thanks to both existing and unknown value from neightboring cells. So each unknown appears in more than one equation and then the system must be solved at once (every equations at the same time)
- explicit: unknown values are found thanks to only existing values.

In segregated solver, no choice is given to the user between implicit or explicit.

Discretization scheme:

Recall that Fluent divides the whole domain in little control volumes. Then it intergrates on each control volume governing equations. This gives a discretization of the whole domain. By default, Fluent stores values ϕ for each cell at its center (C0 and C1 on figure A.2), where ϕ is a scalar quantity of which one wants to calculate its transport. But to determine convection terms, one needs to get face values (let's say its name: ϕ_f).

Figure A.2 presents centered cell values and surface A through which one wants to determine scalar ϕ_f. Fluent must interpolate values from center cells and it does that in different ways, named upwind schemes. "Upwind" means that it is computed thanks to upstream cells, according to the direction of the normal velocity v_n. Let us present the *First-order Upwind Scheme* and the *Second-Order Upwind Scheme* which are the ones used in this work for rough results and accurate results respectively.

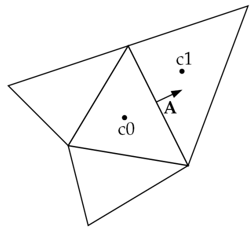

Figure A.2: cell scheme for calculation of face value of scalar ϕ

- First-Order: Values at cell faces are determined by assuming that they are equal to value at center.
- Second-Order: Values at cell faces are computed with a *multidimensional linear reconstruction approach.* This means that a Taylor serie expansion of cell-centered solution is done. It stated that face value ϕ is calculated with the following expression:

$$\phi_f = \phi + \nabla\phi \cdot \Delta\vec{s}$$

where ϕ is cell-centered value, $\nabla\phi$ is its gradient and $\Delta\vec{s}$ is the distance from upwind cell centroid to the face centroid.

A.2.2 Turbulence

In simple fluid flow, one important model is the turbulence one, especially in airfoil. Indeed, this determine viscous strength and then viscous drag, which is a relevant component of the total drag.

The chosen model is the *Shear-Stress Transport (SST) $k-\omega$ Model.* Here is presented a brief introduction to this model. The Standard $k-\omega$ Model might be used for low Reynolds number effects, compressibility and shear flow spreading. It is based on Wilcox $k-\omega$ model ([15]) and then is especially dedicated for modeling wakes, mixing layers and plane, round and radial jets. It is why this is applicable to wall-bounded flows and free shear flows. In others words, it is typically designed for boundary layers resolution.

A variation of this Standard Model is developped. It is the SST $k-\omega$ model. That model is used in the present work. The SST model was developped in order to blend the robust and accurate Standard model $k-\omega$ in the near-wall region with the $k-\epsilon$ model in the far field.

The $k-\epsilon$ model is a two-equations model which gives the solutions of two separate transport equations that allows to determined independently the turbulent velocity and the length scales. It is a semi-empirical model, said to be robust, economic and reasonably accurate.

The Standard $k-\omega$ Model:

This model solves two transport equations for k and ω which are the turbulence kinetic energy and the dissipation rate respectively. They are obtained from equations (A.2) and (A.3) respectively (transport equations).

$$\frac{\partial}{\partial t}(\rho k) + \frac{\partial}{\partial x_i}(\rho k u_i) = \frac{\partial}{\partial x_j}(\Gamma_k \frac{\partial k}{\partial x_j}) + \tilde{G}_k - Y_k + S_k \tag{A.2}$$

$$\frac{\partial}{\partial t}(\rho \omega) + \frac{\partial}{\partial x_i}(\rho \omega u_i) = \frac{\partial}{\partial x_j}(\Gamma_\omega \frac{\partial \omega}{\partial x_j}) + G_\omega - Y_\omega + D_\omega + S_\omega \tag{A.3}$$

where ([15]) $\tilde{G}_k$ represents the generation of turbulence kinetic energy due to mean velocity gradients. G_ω represents the generation of ω. Γ_k and Γ_ω represent the effective diffusivity of k and ω. Y_k and Y_ω represent the dissipation of k and ω due to turbulence. D_ω represents the cross-diffusion term and finally S_k and S_ω are source terms.

For all these terms, one can find in Fluent User's Guide ([15]) the way to calculate them.

Wall Functions or Near-Wall Model:

Obvisouly flows are affected quite a lot by walls. Close to the wall, velocity should decrease due to the no-slip condition satisfied at the wall. This effect has a significative impact on fidelity of numerical's ([15]). So it has to be well simulated.

For models such $k - \epsilon$ which are valid in the far field (or at least not really in the near-wall domain), one is not so intersted in the near-wall behaviour since one has chosen this model to simulate far field behaviour. For the case of this project, the purpose is really to compute very accurately near-wall effects since boundary-layers of an airfoil determine the main behaviour of the wing.

Willing capture near-wall behaviour requires very refined mesh at this location. And then it is time and memory consumming. So when one is not interested in this region, *wall functions* are useful. Wall functions are a kind of "black box" to bridge cells and the wall itself. An illustration of this technique can be found on figure A.3 ([15]).

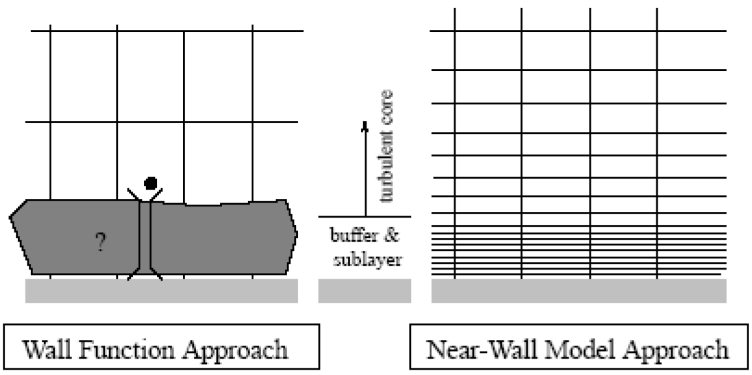

Figure A.3: Wall function illustration from [15]

Indeed, no need to refine the mesh in the near-wall region if one is not interested in the behaviour in this part. Otherwise, one need to refine it in order to capture desired effects. This is obviously time and cost consumming. Wall functions are, in a certain way, cost and time saving. In the case of an airfoil, one uses the near-wall model approach. Typically this black box, that offers wall functions, is used for high Reynolds number. In this project airfoil is subjected to quite low airspeed. It is then advised, from [15], not to use wall functions treatment.

In the case of wings, one chooses *transitional flow* in the $k-\omega$ Model panel since one works at low Reynolds number. In this case, [15] recommends to use Y^+ on the order of 1. Note that Y^+ is defined as dimensionless distance from the wall (see equation (A.4)).

$$Y^+ \equiv \frac{\rho u_\tau y}{\mu} \equiv \frac{u_\tau y}{\nu} \tag{A.4}$$

With this criterion, one is able to model the viscous sublayer where the fluid is nearly linear (figure A.4).

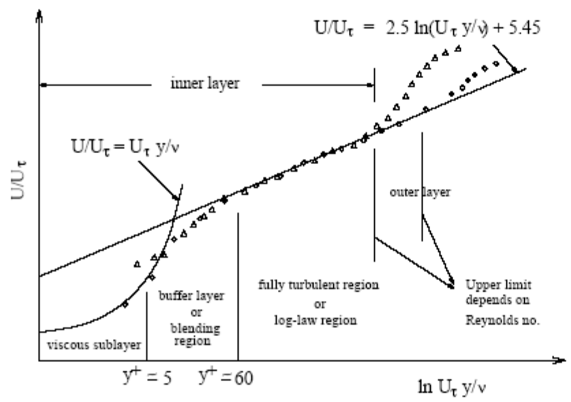

Figure A.4: Boundary layer illustration from [15]

These considerations are checked in the report.

Viscosity law:

The used viscosity law is *Sutherland* law. It uses an idealized intermolecular-force potential. The implemented formula must be specified through two or three coefficients. In this work, only the three coefficients based law is used (default one). Formula is presented by equation (A.5).

$$\mu = \mu_0 (\frac{T}{T_0})^{3/2} \frac{T_0 + S}{T + S} \tag{A.5}$$

where

- μ is the viscosity $(kg/m-s)$
- T the static temperture (in Kelvin)
- μ_0 the reference value (in $kg/m-s$ as well)
- T_0 is the reference temperature (in Kelvin, too)

- S is an effective temperature ([15]). This is Sutherland constant

Fluent has default values of these three constants for air at moderate temperatures and pressures. This the case in the investigation. So those values are kept. (Please refer to [15] for precise figures).

Appendix B

Modeling procedure

The geometry is built exactly at the same time of the mesh. Indeed, the cooper scheme is used. With this technique (please refer to section B.1), it is possible to extract an existing 2D geometry with mesh to create a complete three dimensional meshed geometry.

A 2D profile is drawn and meshed. Then the profile is extract along a defined path which is chosen in order to create a given winglet (simple, blended, shifted downstream). The path is meshed itself and then gives the discretization in the third dimension.

First of all the cooper scheme is briefly presented, then the way of creating the geometry (and the mesh) and finally a mesh quality analysis is performed.

B.1 Cooper scheme

This scheme works with so-called *source* and *non-source* faces. One can understand easily by means of a cylinder analogy presented here.
Figure B.1 shows the analogy.

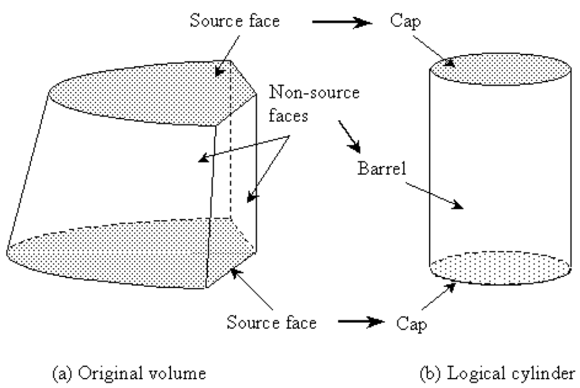

Figure B.1: Analogy with the cylinder for the cooper scheme from [15]

One can see that *source* face are associated with two closing disks of the cylinder and the *non-source* faces with the revolved rectangle. Then with this analogy, it is possible to imagine that if the two *source* faces are meshed in the same, one can mesh the whole volume according to these faces. The vertical (third dimension) discretization is controlled by the path (see section B.3). Then one has total control on the precision of the mesh inside the volume. The disavantage is the need to have two same meshes on both (or more) *source* faces.

B.2 2D geometry

A general view of the 2D geometry is depicted on figure B.2.

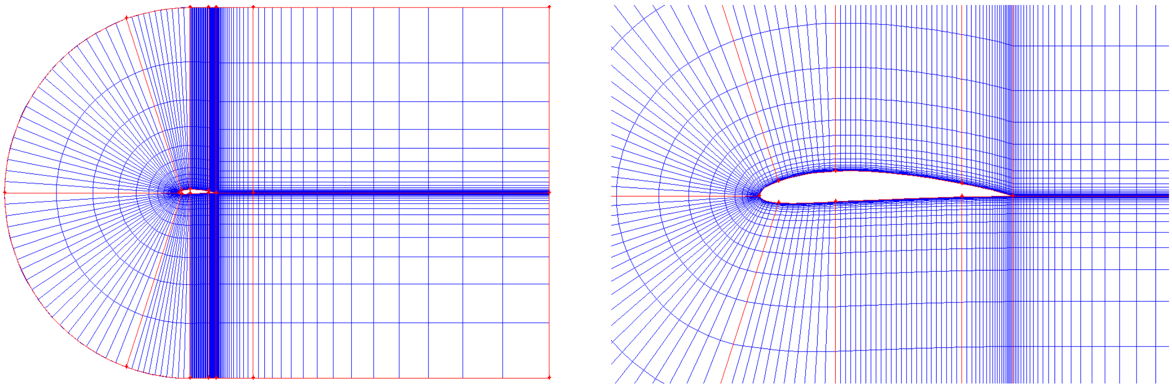

Figure B.2: Left: General view of the 2D geometry and mesh - Right: Zoom onto the wing

Obviously the mesh is still more refined as one approaches the wing (left picture on figure B.2). Near boundaries of the domain, cells are quite big since one doesn't care about what happens at these boundaries. Nevertheless, boundaries near the wing are very important. Indeed boundary layers at the wing involve viscosity drag, high pressure gradients, ... In this region, the mesh should be very refined to be able to capture these effects as one can see on right figure B.2.

The wing chord is $1\,m$, the domain is $14.7\,m$ long and $10\,m$ high. The first height of cells at the wing boundaries is $5e^{-5}\,m$ (to get a good Y^+, see section B.4). The profile itself contains 76 nodes on both upper and lower surfaces, namely 152 for the whole wing. From this discretization (on and perpendicular to the profile), the mesh is extended for the whole 2D domain as illustrated on figure B.3.

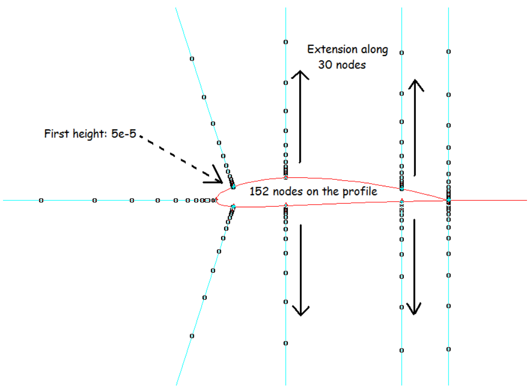

Figure B.3: Extension of the mesh for the whole 2D domain

The way of working is very similar to the *cooper scheme*. From a 1D discretization, one can create a 2D mesh (or from a 2D, creating a 3D mesh as explained later). In this case, the

2D mesh contains 6960 elements. Each boundary of the domain is set as *pressure farfield* to be able to set velocity components and the wing as *wall*.

B.3 3D geometry

Exactly like for the 2D case, one is able to extend the $n-1$ dimesional mesh to create a n dimensional mesh. So from the 2D mesh generated before, it is now possible to create the 3D one. Figure B.4 shows the path along which the 2D mesh is extended (case of the blended winglet).

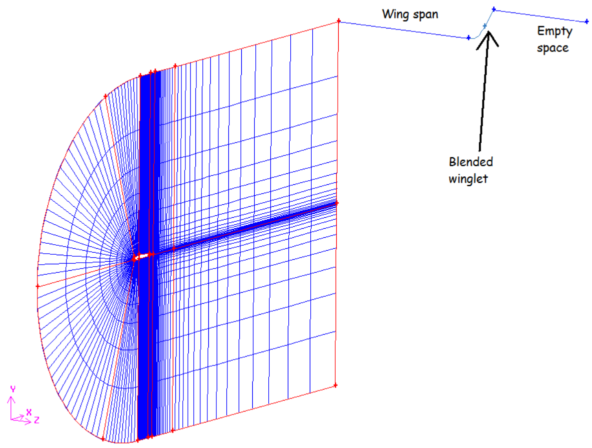

Figure B.4: Path for extension of the mesh for the whole 3D domain (case of the blended winglet)

The wing span is $4.5\,m$, then following cases, the path simulates a *simple*, *blended* or *shifted downstream* winglet. Finally a length of $3\,m$ is still horizontally extended without any winglet and wing. This allows 3D effects to be generated, i.e. vortices. Indeed, they are born at the wingtip and grow in the trailing wake. Without any empty space, vortices couldn't be created. The discretization along the path is done in such a way that at crucial regions, it is refined enough. Namely at the junction between wing and winglet and at the wingtip. The total number of node in the third dimension is 56 for the case with blended winglet.

In the 3D case, boundaries stay the same as in the 2D one. Each surface is set as *pressure farfield* except for the face at the fuselage side. It is *symmetry* in order to forget the fuselage effect. Obviously wing and winglet are set as *wall*. So far, only the full 3D model were discussed. For the 2D-wing-in-3D-environment model, the procedure was exactly the same: From a 1D discretization building a 2D mesh, then extending according to a divided path to create the whole 3D model. Table B.1 summarizes the total number of elements in each model.

	Without winglet	Simple winglet	Blended winglet	Shifted downstream w.
Full 3D model	286400	293360	425600	–
2D-wing-in-3D	63000	52500	86625	52500

Table B.1: summary of the number of elements for each model

It seems clear that the big model is the Full 3D. The second one is, as already talked, just to underline winglet effects and then has a smaller size for time consumming priority. For both models, the blended winglet needs more elements. Simulating properly the curve junction requires a certain number of elements. Indeed this special junction is the only feature that distinguishes other winglets in this work. It is obvious that if it is bad discretized, it is simple winglet like (too high angle between two elements). Figure B.5 illustrates this need in high density of element at that place.

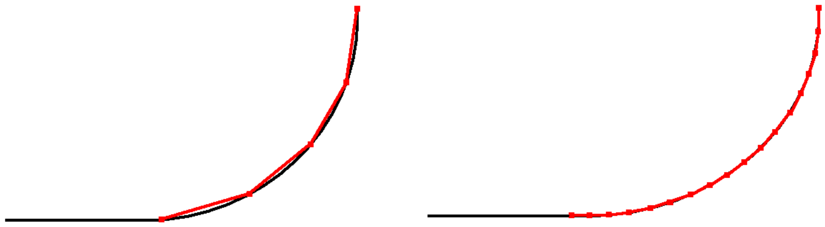

Figure B.5: Comparison between low and high density of elements for the blended winglet

In the case of high density of element, the blended transition is well modeled while with a few elements, one has still sharp corners between elements which can leads to comparable effects of the *simple* winglet. Recall that the 2D mesh contains about 7000 elements. So one more node in the third dimension leads to 7000 elements more in total! This explains this big difference.

B.4 Quality Analysis

The mesh quality analysis is an important part of the work. This informs if the mesh is good enough to start simulations. To have reference values, Fluent gives some criterions with tolerances to be respected. This leads to an objective analysis.

The way to get the mesh is explained previously. Clearly it is more refined in the neighbourhood of the wing since it is a crucial place to solve the problem. Along the span, the wingtip is also a crucial point to solve. It is why there, the mesh is refined as well. Every elements are *quad* elements, namely four sided elements (2D). There are the most structured ones. Several relevant criterions are retained for the analysis and presented here. For each of them, each case is compared (withtout winglet, with *simple* and *blended* winglet). The quality analysis is firstly performed on the 2D mesh. This mesh is extended through the third dimension. Then this analysis is an important step. 3D elements are also studied, especially for winglets.

B.4.1 2D elements in the Full-3D-Model

Area:

The area is a simple criterion giving the area of elements. Obviously as small is area as refined is the mesh. This confirms regions where the discretization is smallest. Figure B.6 illustrates smallest and largest areas region.

Smallest areas go from $0\,m^2$ to $0.02\,m^2$ and largest ones from $0.3\,m^2$ to $2\,m^2$. It is clearly visible that the most refined mesh is around the wing and especially behind the wing where lies the trailing wake. This region is crucial for the present investigation since the purpose

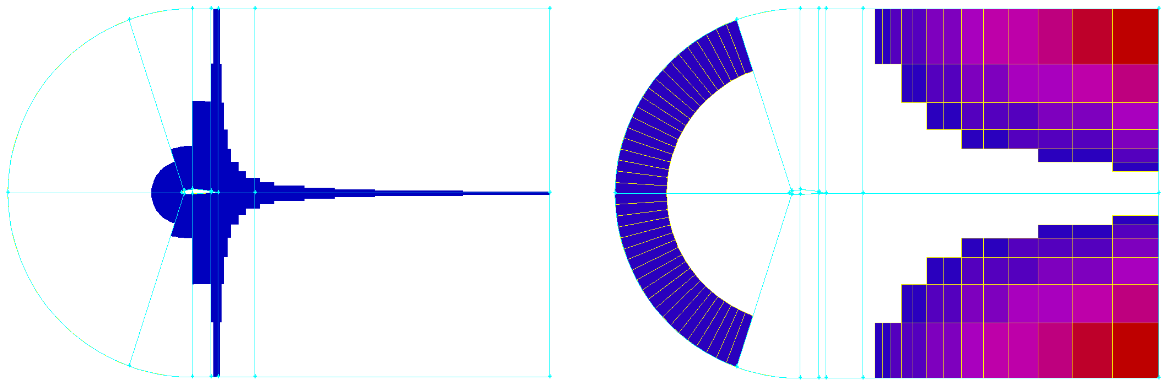

Figure B.6: Left: Smallest area regions (from $0\,m^2$ to $0.02\,m^2$) - Right: largest areas region (from $0.3\,m^2$ to $2\,m^2$)

of winglet is to lower induced drag. Largest elements are, in a certain way, the opposite of smallest ones. Left side of figure B.6 underlines that the four corners are less refined as well as places before the wing, where it is less important to have accurate solutions.

Aspect Ratio:

Several definitions of the aspect ratio (AR) are established. According to quadrilateral and hexahedral elements, the definition (B.1) is given.

$$Q_{AR} = \frac{max[e_1, e_2, ..., e_n]}{min[e_1, e_2, ..., e_n]} \tag{B.1}$$

where e_i is the average length in the direction i as shown on the figure B.7. n is the number of different directions associated with this element.
The aspect ratio gives an absolute value of the ratio between sides while the *stretch* criterion gives a relative value (please refer to the next criterion).

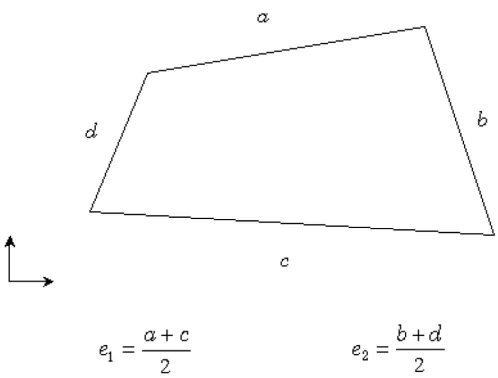

Figure B.7: Example of calculation of the aspect ratio

A perfect equilateral element has a $Q_{AR} = 1$. According to [12], the AR in regions of interest should be at maximum of $[20 - 100]$. Figure B.8 shows aspect ratios from 0 to 20 which leads to a quite good quality.

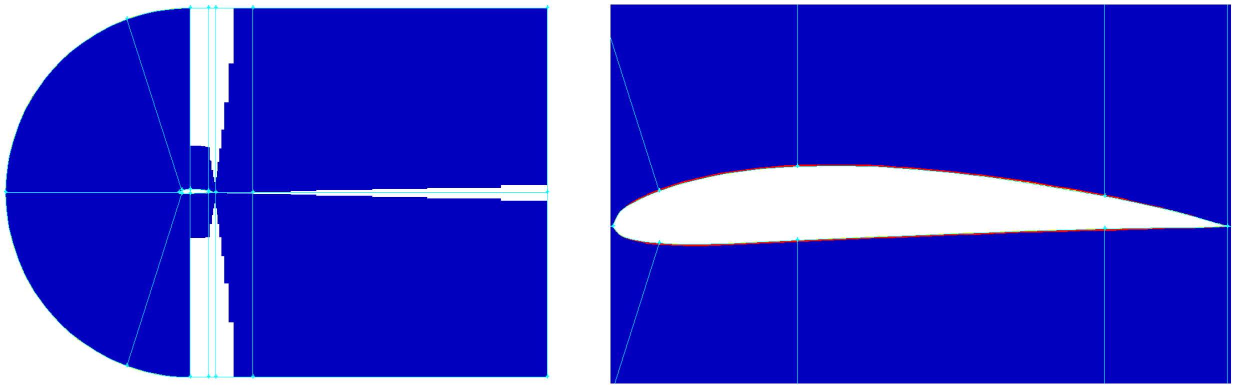

Figure B.8: Aspect ratio (from 0 to 20): Left: general view - Right: Zoom onto the wing

The left side of this figure confirms that the aspect ratio is rather good in regions of interest (< than 20), except the few cells simulating the boundary layers at the wing surface as one can see in red on right side of the figure. Red zones are cells having aspect ratio up to 100. The last four cells in this red part have a value between 100 and 400 for the very last one.

400 seems to be very large. Indeed it is large according to quality criterions given by [12]. But it is a kind of compromise between refined mesh at the wing and not much node in the whole domain. Only 5.85 % of elements have values between 400 and 30000, which is the maximum aspect ratio value in the 2D domain.

Stretch:

The stretch criterion is defined thanks to the formula (B.2).

$$Q_s = 1 - \sqrt{\frac{K min(s_1, s_2, ..., s_n)}{max(d_1, d_2, ..., d_n)}} \tag{B.2}$$

where d_i and s_j are the lengths of the diagonal i and the edge of element j, respectively. n and m are the total number of diagonals and edges. For quadrilateral elements, $n = 2$, $m = 4$ and $K = 2$. For hexahedral elements, $n = 4$, $m = 12$ and $K = 3$.

While the aspect ratio gives values for the ratio between edges, stretch gives a kind of relative value: from 0 to 1. With this unity based criterion, it is easy to know in an relative way if elements are good between each other, even though it gives the same " quality window" as the aspect ratio. By definition (B.2), $0 \leq Q_s \leq 1$. When $Q_s = 0$, it describes equilateral elements (perfect) and when $Q_s = 1$, it stands for completely degenerated (poorly shaped) elements.

One can understand stretch criterion as the regularity of elements. If it equals to zero then elements are very regular, or as much as it tends to one, elements are very unregular and poorly shaped.

Due to the high density of elements, a large quantity (nearly 50 %) of elements are poorly shaped with high stretch values. Even if elements have quite good aspect ratios, they can have

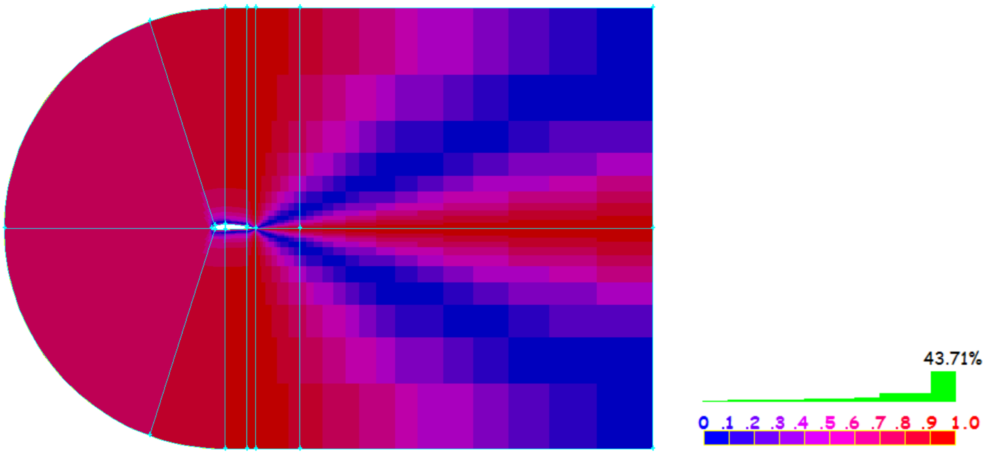

Figure B.9: Stretch repartition and its legend

large stretch numbers due to their unregularities. The average value is 0.8563. This is very high, but fortunately good values are kept near regions of interest like in the near-wing regions and in the beginning of the trailing wake (figure B.9). It is a kind of compromise. Every criterions could not be very good together.

EquiAngle Skew:

The EquiAngle Skew (or EAS) indicates the skewness of elements. This is calculated by (B.3).

$$Q_{EAS} = max\{\frac{\theta_{max} - \theta_{eq}}{180 - \theta_{eq}}, \frac{\theta_{min} - \theta_{eq}}{\theta_{eq}}\} \tag{B.3}$$

where θ_{max} and θ_{min} are maximum and minimum angles (in °) between edges and the elements. θ_{eq} is the characteristic angle corresponding to an equilateral cell. In the case of triangular or tetrahedral elements, $\theta_{eq} = 60°$ and for quadrilateral or hexahedral ones, $\theta_{eq} = 90°$.

By (B.3), $0 \leq Q_{EAS} \leq 1$, where $Q_{EAS} = 0$ stands for an equilateral elements and $Q_{EAS} = 1$ for a completely degerated (poorly shaped) element. One can find in table B.10 general guidelines for values of EAS (from [12]).

Q_{EAS}	Quality
$Q_{EAS} = 0$	Perfect
$0 < Q_{EAS} \leq 0.25$	Excellent
$0.25 < Q_{EAS} \leq 0.5$	Good
$0.5 < Q_{EAS} \leq 0.75$	Fair
$0.75 < Q_{EAS} \leq 0.9$	Poor
$0.9 < Q_{EAS} \leq 1.0$	Very Poor
$Q_{EAS} = 1.0$	Degenerated

Figure B.10: Quality scale with the EAS [12]

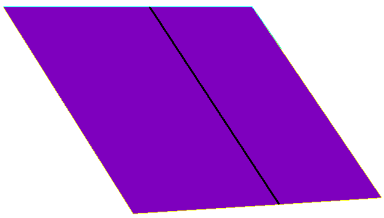

Figure B.11: Worst elements (EAS of 0.37)

For high quality 2D mesh, [12] advises to have an average EAS of 0.1, namely all elements should be *excellent* according to table B.10. In the 2D mesh, 82.5 % of elements have EAS between 0 and 0.1, meaning that the average EAS is well below 0.1. Worst elements are situated at the stagnation point of the wing with an EAS of 0.37, which is very good for "worst" ones.

They are depicted on figure B.11.

B.4.2 2D elements in the 2D-wing-in-3D-environment Model

The quality of the mesh in this second model is briefly presented. Recall that the second model is only performed to confirm/reinforce effects the winglet with a higher angle of winglet. This model contains less elements than the Full-3D one. For this model, the third dimension is different than the one from the other model. It is why each case of winglet is studied separately. Figure B.12 depicts all four cases in this model and their mesh.

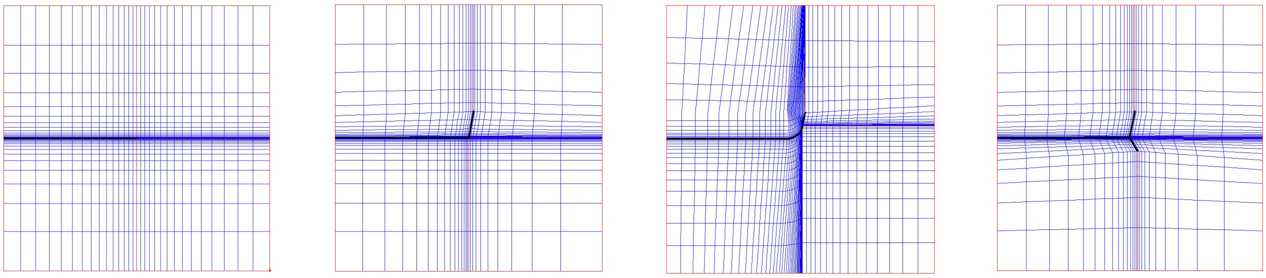

Figure B.12: The four cases in the second model: Without, Simple, Blended and Shifted downstream winglet (from left to right)

One can see the wing and winglet (if the case) in black. This illustrates the fact observed in table B.1 and on figure B.5: one needs more elements to modelize the blended winglet. Only two main criterions are quickly analysed. These are the Aspect Ratio (AR) and the EquiAngle Skew (EAS). They can give a picture of lengths ratio and a kind of regularity of elements. The area criterion is deductible from figure B.12.

Aspect Ratio:

The Aspect Ratio (AR) criterion gives a value more representative, in an absolute way, of the quality of elements. One can find on figure B.13 the stretch criterions depicted for all four cases of this model.

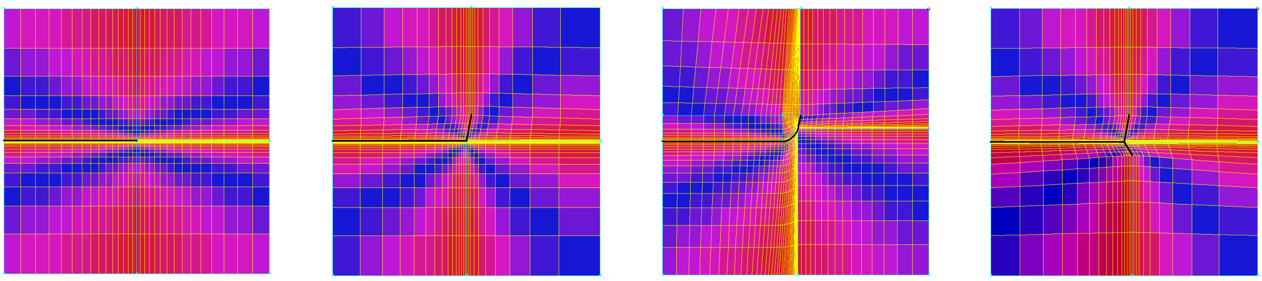

Figure B.13: Stretch criterions for all four cases: Without, Simple, Blended and Shifted downstream winglet (from left to right)

The AR is rather good in each case. Indeed for everyone, about 60 % (except for the blended case where it goes up to more than 75 %) of elements have an AR less than 100 which is the maximum recommanded value by [12]. However, near-wing regions get, for all cases, AR up to 2000. This is high but comes from a compromise between size and accuracy. Although, as shown on figure B.13, the stretch criterions is not optimal. This is because stretch criterion is a kind of comparison between all elements. Then regios of interest are not optimal compared to other regions. Please note that yellow parts are mesh concentrations. Nothing to do with colors code. In conclusion, the AR is rather good even if the repartition of good elements is not optimal (stretch).

EquiAngle Skew:

The EquiAngle Skew has a very acceptable range. In the case without any winglet, all elements are perfect, namely an $Q_{EAS} = 0$. For others, the highest average value of EAS is 0.1062 while the recommanded average value by [12] is 0.1. According to that, meshes are very high quality. Worst elements are generally good (± 0.3) except in the blended case where the worst ones reach 0.96! They are situated near winglet. One can find on figure B.14 worst elements for all three cases (since all elements are perfect for the case without winglet).

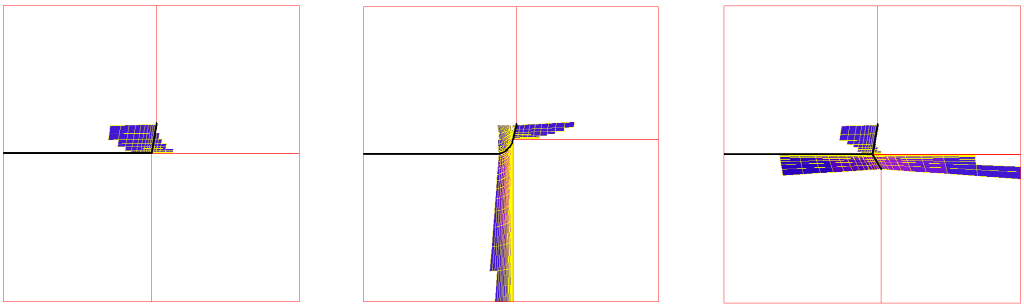

Figure B.14: Worst EAS regions for these three cases: Simple, Blended and Shifted downstream winglet (from left to right)

Generally they are situated near the winglet itself. This is however one of crucial places.

B.4.3 Conclusions on 2D elements:

Full-3D Model:

The 2D mesh quality analysis is performed since the whole 3D mesh is generated from this 2D domain. So it is important to have a rather good quality mesh before building the 3D one. If the 2D discretization is well made, then the 3D one depends only on the third dimension discretization. Thanks to the four criterions used in the analysis, some conclusions can be underlined.

The area criterion confirms places where mesh is more refined. These places are indeed regions of interest, namely the near-wing regions and trailing wake (figure B.6). The four corners and areas before the wing are not relevant in this investigation.

The aspect ratio and stretch criterion give informations on lengths and regularity of elements. Aspects ratio works with lengths ratio. All regions of interest are kept in acceptable range (maximum of 100), except for the four last cells at the wing boundary. They go up to 400 for the very last one (figure B.8). This is quite large but it comes from a kind of compromise. The stretch criterion evaluates the regularity of each element. This criterion is not the best respected. Indeed the average value is 0.8563 and nearly 50 % (43 % on figure B.2) stand beyond a value of 0.9. But fortunately regions of interest (near-wing and the beginning the trailing wake) get reasonable values between 0 and 0.5.

Finally the EquiAngle Skew measures a kind a regularity as well. This criterions is the most respected in the 2D mesh. Indeed more than 82 % stand below 0.1 which is the recommanded average value by [12] for a high quality mesh.

The 2D mesh is globaly well created. Except for the stretch criterion which is, in average but not localy, too high. Every other stay in very acceptable ranges to get a good quality mesh.

2D-wing-in-3D-environment Model:

The purpose of this model is rather for confirming or reinforcing trends than for getting accurate results. But a good starting 2D mesh is even essential than in the previous model.

Aspect ratios are acceptable in average, although they are a slightly too high in last cells near the wing (up to 2000). It is a pity that good shaped elements are not optimally allocated (Stretch).

The EquiAngle Skew is very very good, except for a few elements near the blended winglet. Otherwise, the average values tell that meshes are *good* to *excellent*, according to [12].

B.4.4 3D elements in the Full-3D Model

The 3D mesh is generated from the 2D mesh analysed just above. Following the case, mesh features stay the same or not. The analysis is divided in two part: the case without winglet and the case with it.

Case without winglet:

Since for this case, the 2D mesh is simply extracted in the third dimension, without any changes in direction (no winglet). Then changes in the quality come only from the extraction. Indeed, figure B.15 shows the elements with highest AR. They lie in a thin layers in the trailing wake. Already in the 2D, highest AR elements were in this region, although this time, values are greater than 11000! This is tremendous but once again comes from a kind of compromise: accuracy at boundary layers and size of the problem. Fortunately scales of vortices are such that this thin layer should appear nearly *inviscid* for them and it lies not totally next to the wing, but a few chords further. Accuracy of the vortices calculations should be affected in a minute way.

The third dimension has 36 divisions. This compromise is also seen on figure B.16 where one can see more refined parts where stretch criterion is not really optimal. Effectively, at these regions of interest, density of nodes is higher to increase accuracy but by care of memories, one can not increase density in all dimensions. It is why stretch criterion is so. The EquiAngle Skew (EAS) is pretty good. The average value is 0.025 which is an excellent mesh according to [12]. Elements with higher EAS (up to 0.82) are situated on right hand (from front view) of the wingtip . Any of those elements are in the trailing edge where vortices are developped (figure B.17). Please note that this space with that kind of mesh is also present in winglet cases.

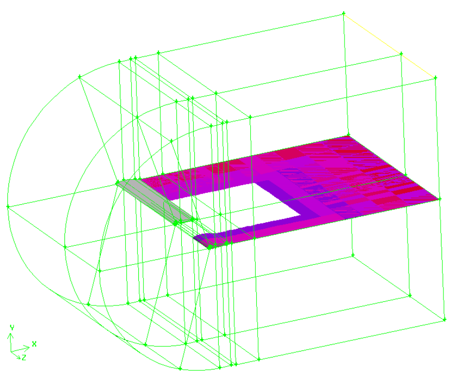

Figure B.15: AR greater than 11000

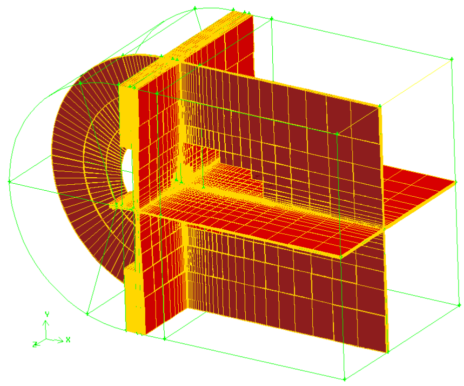

Figure B.16: Stretch in [0.96 – 1]

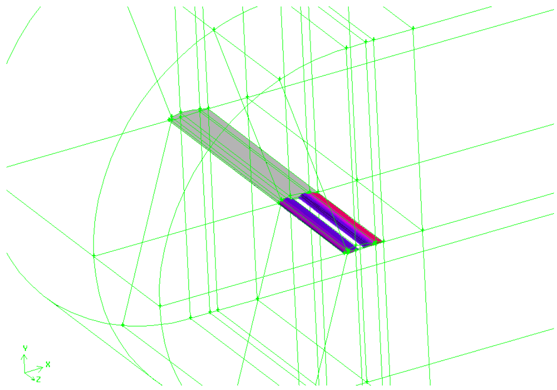

Figure B.17: Stretch in [0.96 – 1]

Cases with winglet:

Meshes in cases with winglet have exactly the same quality as the mesh without, except for the EquiAngle Skew. Most elements (more than 50 %) have an aspect ratio smaller than 100. It still exists a layer with relatively high AR in the far trailing wake.

Stretch criterion also still indicates the higher nodes density in crucial places for calculations. EAS is different in only one place: the winglet. Indeed, meshes are exactly the same except around the winglet and in its trailing wake. Since the whole 2D domain is cooped along the third dimension path, elements with non-optimal EAS are placed on the whole length of the 3D domain as shown on figure B.18. Values at these places are between [0.6 – 0.7] as one can see on figure B.19 where distributions of the EAS are depicted for each cases. For both cases with winglet (simple and blended), there is a new peak between 0.6 and 0.7 which corresponds to elements shown on figure B.18.

B.4.5 3D elements in the 2D-wing-in-3D-environment Model

Since this model is built from the complete 2D geometry, the mesh quality in three dimensions is exactly the same as the one in 2D. Indeed the whole wing and winglet are built in 2D then extended in 3D. Then the 2D mesh doesn't meet any curved path and then does not complicate the mesh structure. It is why every conclusions made in the 2D mesh for this

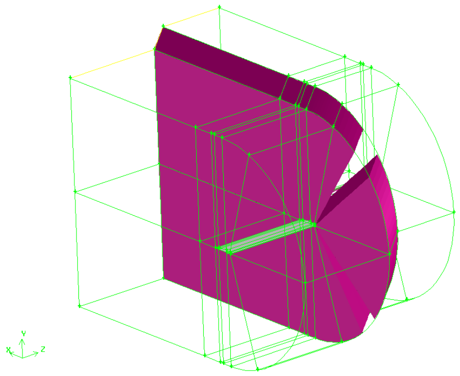

Figure B.18: EAS of [0.6 − 0.7] for the simple winglet

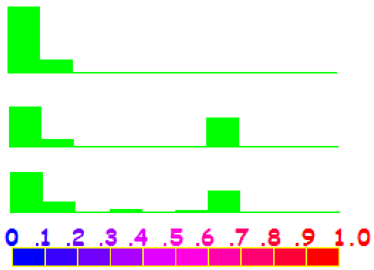

Figure B.19: EAS distribution for the case withtout winglet, simple and blended winglet (from top to bottom)

model are completely valid for the 3D mesh. The third dimension discretization doesn't affect the quality.

B.4.6 Conclusions on 3D elements

Full-3D Model:

One can distinguish the case with winglet and the case without. They are different from the partial curved path. In the case without, it is a straight line, otherwise it is curved at the level of winglet. This curve leads to some modifications in features of meshes and especially in quality.

Without winglet, the aspect ratio (AR) reaches very high values but only in the far trailing wake. Otherwise, it stays at an acceptable range according to [12] (at about 100 in average). Even if it stays quite low, regions of interest are not optimally deserved by elements with high AR (stretch criterion). EquiAngle Skew (EAS) is very good with an average value of 0.025. Like in the 2D mesh, it should be 0 (perfect elements). But an additional mesh, other than the 2D extracted mesh, is created. It is the mesh after the wingtip along the thrid dimension path. It is filled by quadrilateral elements with poorer quality ($[0.96-1]$). Fortunately those elements are not present in the trailing wake where accurate solutions are needed since this investigation studies *induced drag by wingtip vortices* which develop mainly after the wing (figure B.17). This space is also present in cases with winglet (after the winglet thus).

With winglet, AR and stretch criterions examinated in the case without winglet are still correct. Only the EAS gets changes due to the curved path in the third dimension. At the winglet position on the extracting path, elements have non optimal values as shown on figure B.18. This is confirmed by the comparison between EAS values distribution of cases of figure B.19. A new peak appears in the case with winglet. This is the winglet region. Range of these values is $[0.6-0.7]$, which is fair according to [12]. One should take this as a compromise once again, because keep in mind that average EAS for each case is below 0.4 which is the maximum recommended value for high quality mesh in 3D.

Meshes are rather good. They have kept main characteristics of the 2D mesh, except around winglet regions (when the case) where EAS is poorer and spaces after the wing tip (or winglet tip) where EAS is bad. Fortunately this should not affect calculations in a large way.

2D-wing-in-3D-environment Model:

Meshes characteristics are in this model the same as in the 2D analysis since the extracting path is only a straight line.

Appendix C

Data extraction

When willing diplaying evolutions of a given parameter along given cross section, one has two possibilities. The first one is to display in a colorful map what happens in the given cross section. The second one is to extract data from Fluent simulations, to work on them and to plot them in a smart way to illustrate properly the given fact. Obviously the second one is more "speaking" and accurate. But it is not always possible to use that one because Fluent itself is limited. So in this particular case, colorful display are used.

Sections below present why data extraction is not always so accurate as expected.

C.1 Along the wingspan

To be able to get data from Fluent at specific cross section, one had to create a straight line. Indeed, Fluent allows to create a real cross section plane, but in this case one gets, in addition to data for the wing, data for the whole domain upwards and downwards the wing. Those data are totally useless since one wishes to analyze what occurs on the wing. Then graphs are pretty unreadable. In case without winglet, simple or shifted downstream, there is no problem since every winglet evolution is straight. But in the case of blended winglet, one can not fit perfectly with the winglet with straight line. One has to divide the curve line into straight lines. So due to this lack of precision in Fluent, a big assumption is done.

Fluent allows only to enter starting and ending point coordinate. It is very time consumming. So figure C.1 illustrates what was done in the case with blended winglet.

Figure C.1: Non-fitted path in case of blended winglet to measure pressure distribution

So at the beginning of the winglet, data does not fit really with the one undergone by the winglet itself. For example it is why one can observe a kind of bumb in pressure distribution in the case with blended winglet.

C.2 Along the chord

Along the chord, the same problem of imprecision occurs. If one extract data for a entire cross section plane, there are too much useless data. For example on lift side of figure C.2, if one wishes to plot data in the red cross section, Fluent allow to do it only in the whole red plane. And so, there are too much useless data up and downwards the wing.

Moreover along this direction (x), it is totally impossible to interpolate in several point the profile since it is only curve line. It would be too time consumming. But Fluent allows to select a surface from which data are extracted. So for example upper surface can be selected and then be plotted. Once again, all data in the perpendicular direction are plotted and not especially in the given cross section. But since in cases with winglet, pressure does not change a lot on the wing along the span, it is quite coeherent. While in the case without, pressure varie quite significantly along the span and then it gives unreadable evolution as shown on right figure of C.3.

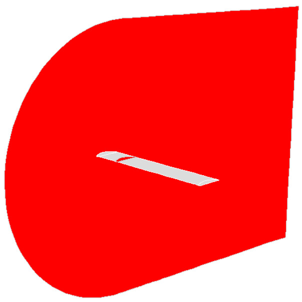

Figure C.2: Example of a plane in Fluent

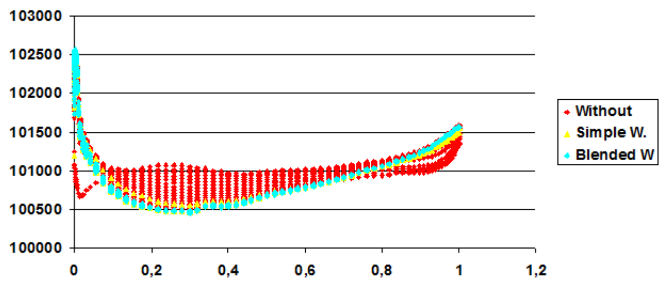

Figure C.3: Example of unreadable pressure evolution due to useless data

For example, pressure in red is the pressure in the case without winglet. This pressure is measure for the whole upper surface along each point of the wingspan since the whole upper surface is selected. That makes red pressure unreadable. While in case with winglet, pressure does not vary so pressure is quite readable[1].

[1]Please refer to suitable section to know more about pressure evolution

Appendix D

Pressure figures

One can find all figures about pressure analysis not displayed in the main report. These figure are not essential to be placed in the analysis itself. But a quick look at them could bring more information and make analysis easier to understand.

Pressure distribution along the wingspan and the chord:

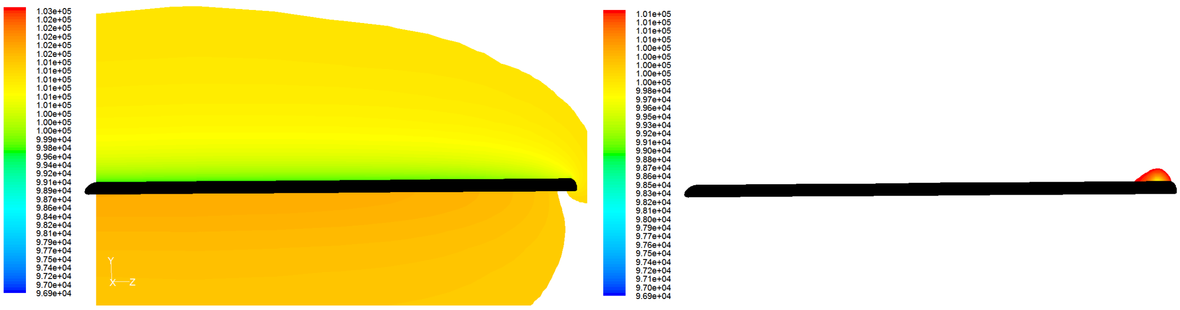

Figure D.1: Model A: Pressure distribution along the span at $\alpha = 10°$ in the case without winglet

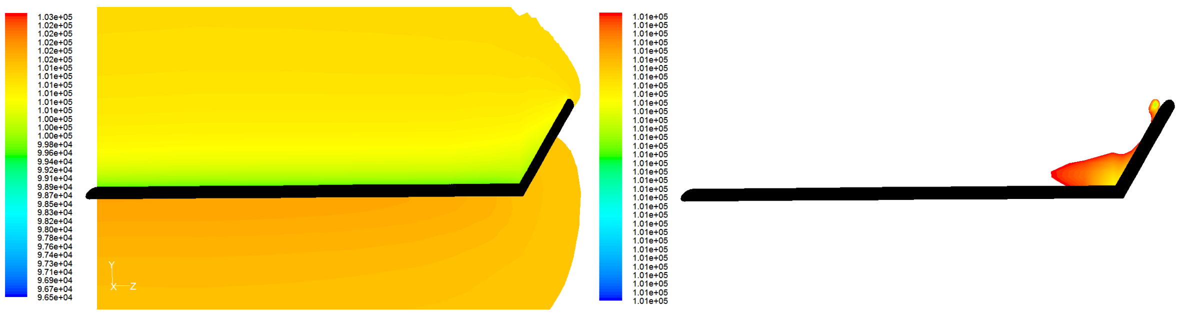

Figure D.2: Model A: Pressure distribution along the span at $\alpha = 10°$ in the case with simple winglet

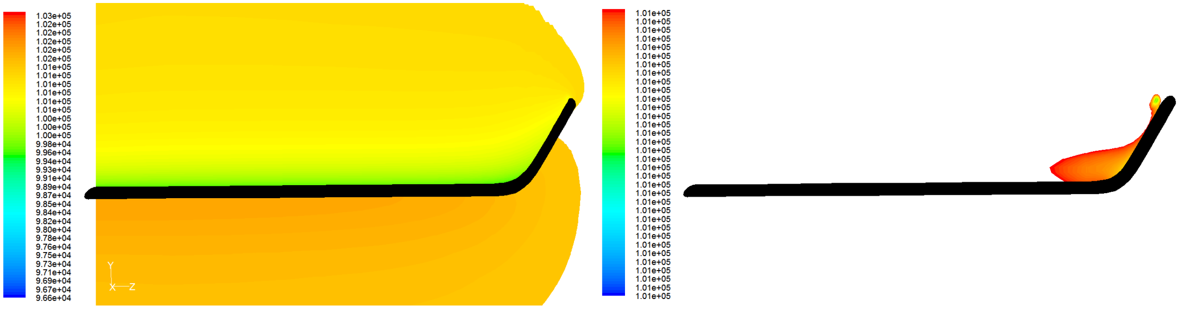

Figure D.3: Model A: Pressure distribution along the span at $\alpha = 10°$ in the case with blended winglet

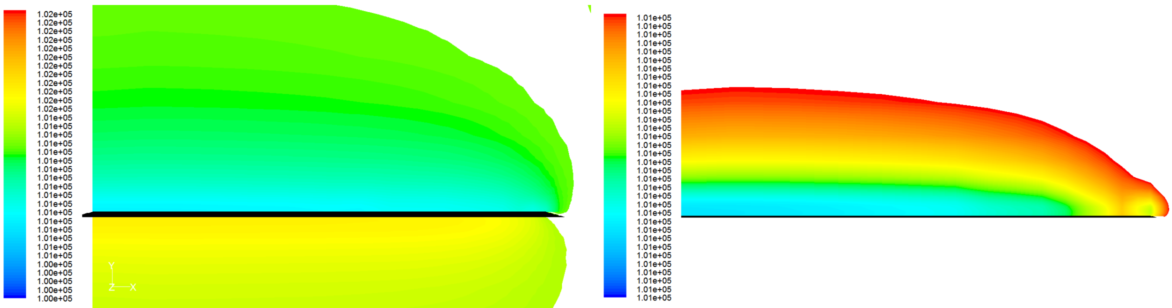

Figure D.4: Model B: Pressure distribution along the span at $\alpha = 10°$ in the case without winglet

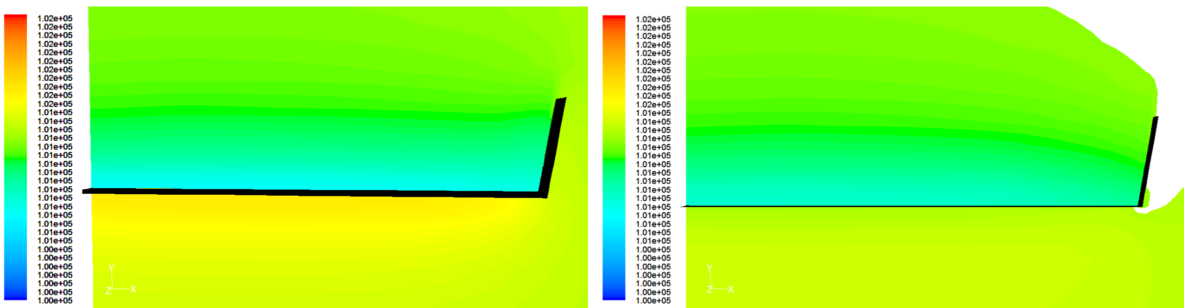

Figure D.5: Model B: Pressure distribution along the span at $\alpha = 10°$ in the case with simple winglet

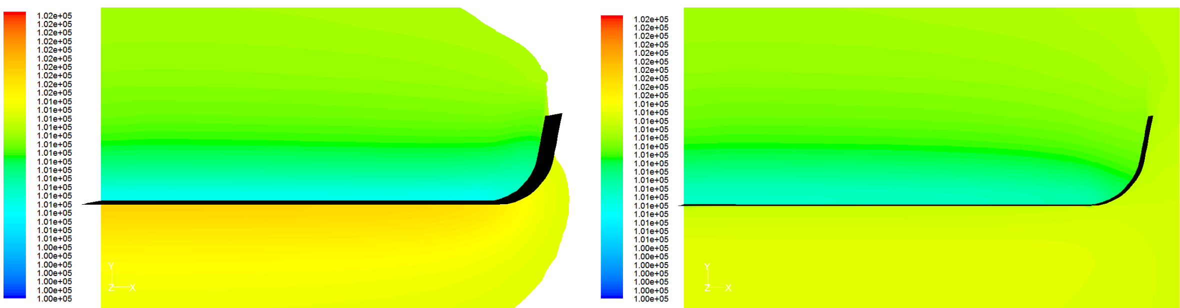

Figure D.6: Model B: Pressure distribution along the span at $\alpha = 10°$ in the case with blended winglet

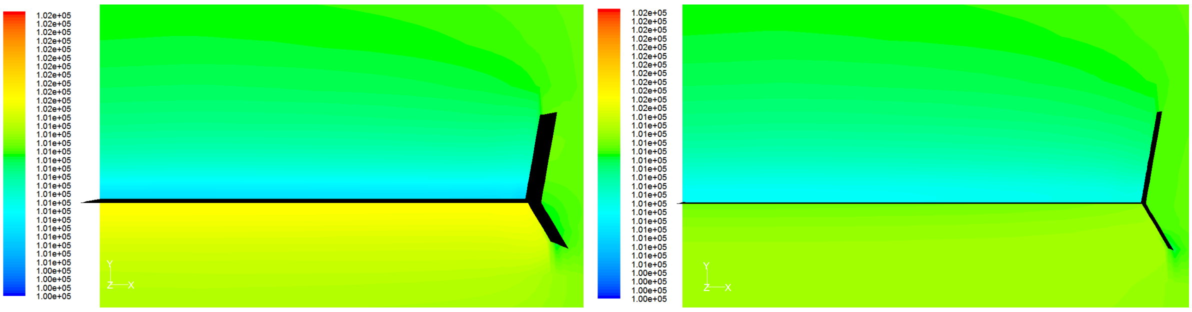

Figure D.7: Model B: Pressure distribution along the span at $\alpha = 10°$ in the case with shifted downstream winglet

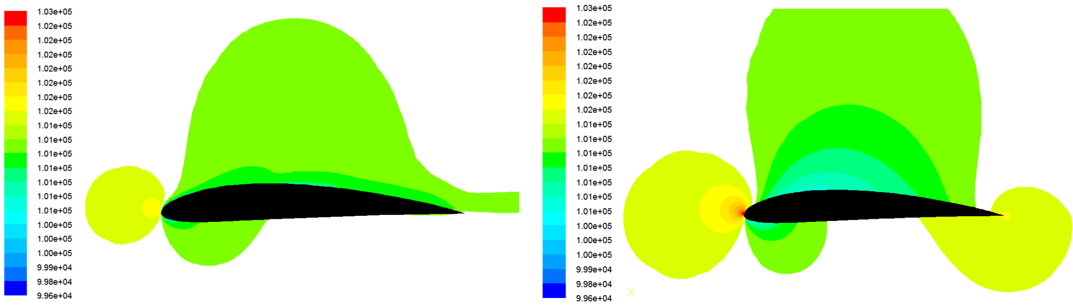

Figure D.8: Model A: Pressure distribution along the chord at $\alpha = 0°$ in the case without winglet at wingtip and $0.5\,m$ before respectively

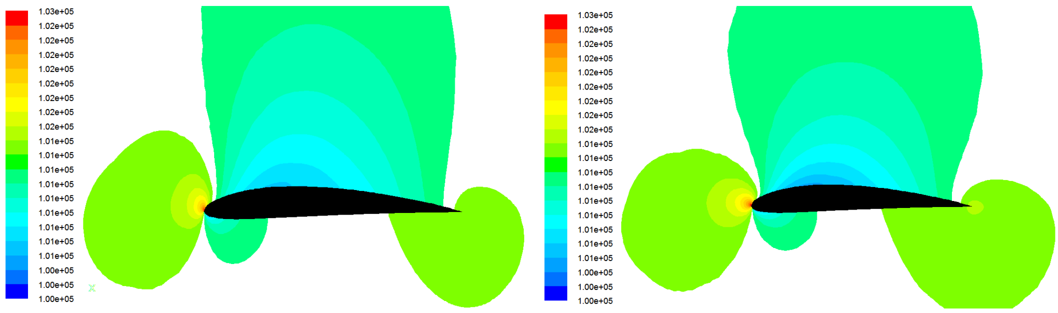

Figure D.9: Model A: Pressure distribution along the chord at $\alpha = 0°$ in the case with simple winglet at wingtip and $0.5\,m$ before respectively

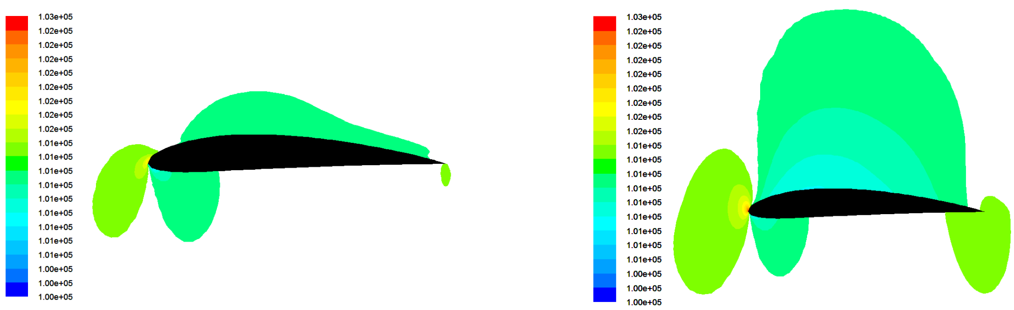

Figure D.10: Model A: Pressure distribution along the chord at $\alpha = 0°$ in the case with simple winglet at winglet tip and $0.25\,m$ before respectively

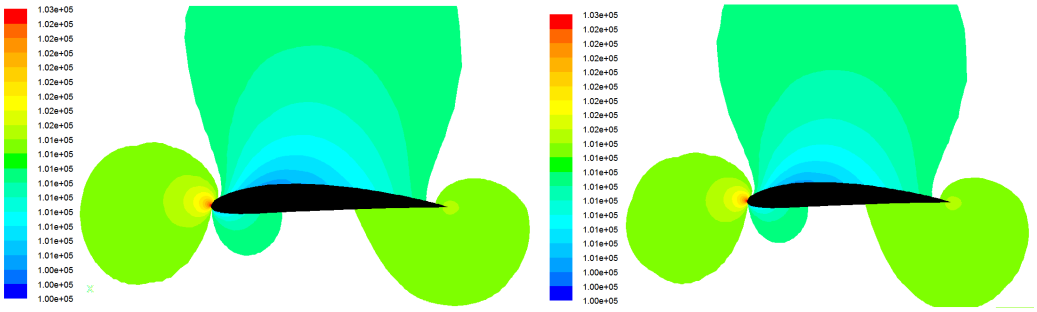

Figure D.11: Model A: Pressure distribution along the chord at $\alpha = 0°$ in the case with blended winglet at wingtip and $0.5\,m$ before respectively

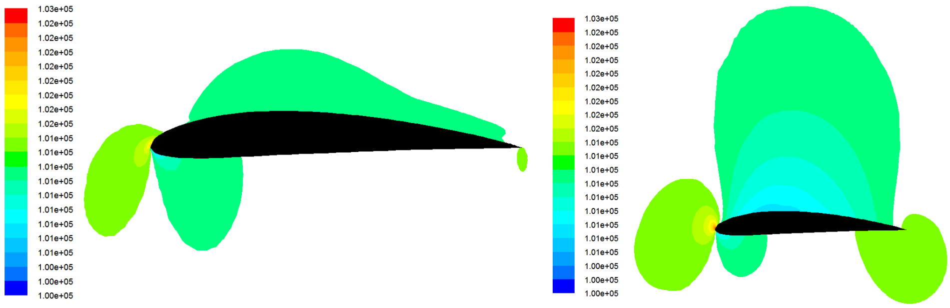

Figure D.12: Model A: Pressure distribution along the chord at $\alpha = 0°$ in the case with blended winglet at winglet tip and $0.4\,m$ before respectively

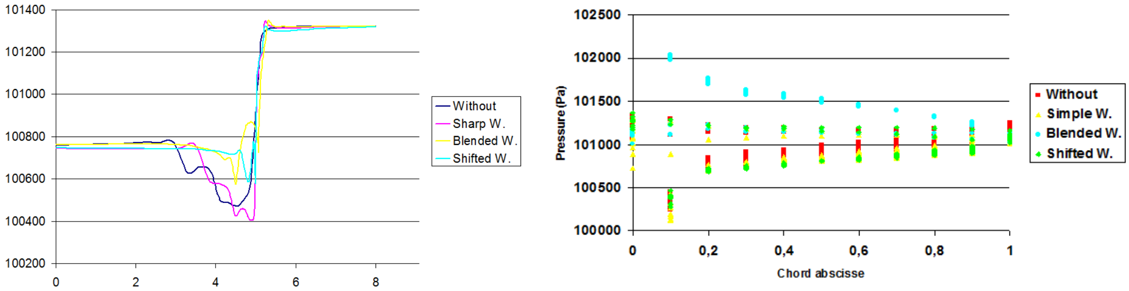

Figure D.13: Model B: Comparisons of pressure distribution along the span ($\alpha = 10°$) and along the chord respectively between cases

Appendix E

Velocity figures

One can find all figures about velocity analysis not displayed in the main report. These figure are not essential to be placed in the analysis itself. But a quick look at them could bring more information and make analysis easier to understand.

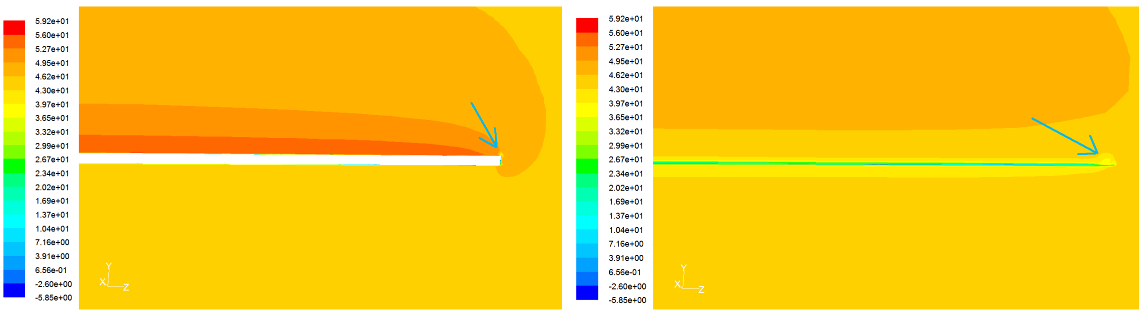

Figure E.1: Model A: Evolution of X velocities lost at wingtip when vortex is creating ($\alpha = 0°$): cross section at chord of $0.5\,m$ and $1\,m$ (trailing edge)

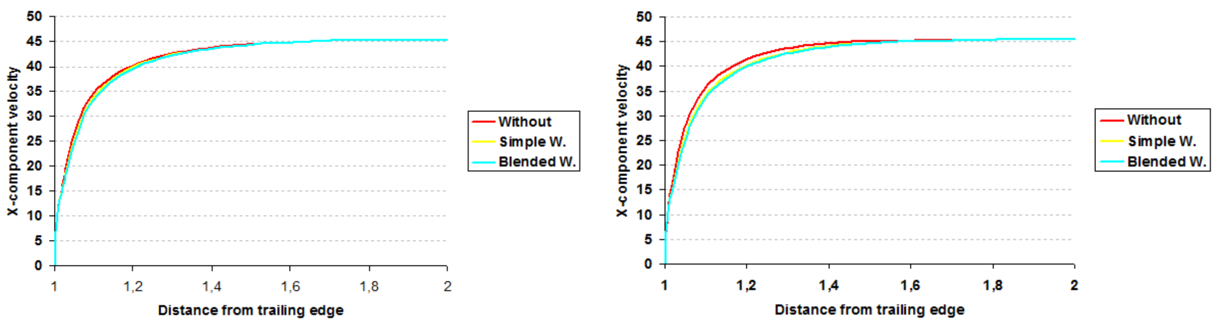

Figure E.2: Model A: Evolution of X velocities in the trailing wake: at span of the middle of the wing and at $0.5\,m$ from wingtip

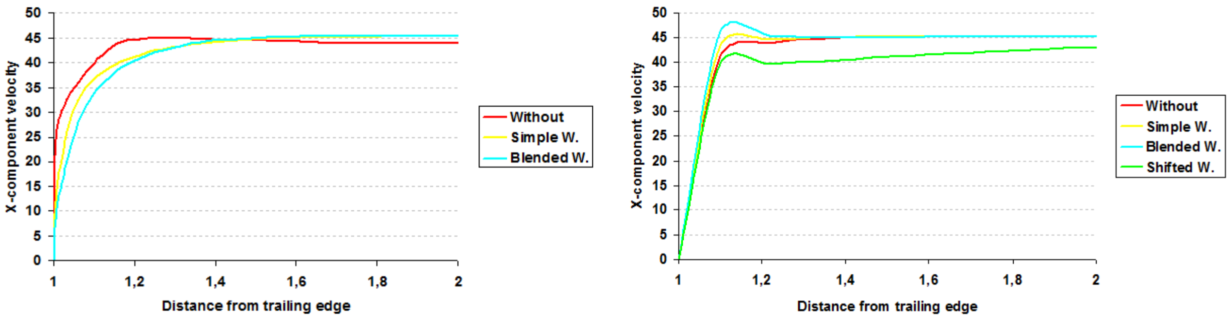

Figure E.3: Comparison of the evolution of X velocities in the trailing wake at wingtip for both models

	Without	Simple W.	Blended W.	Shifted W.
Upper limit Model A	83.3	85.7	85.5	–
Lower limit Model A	−38.8	−40.3	−38.8	–
Upper limit Model B	26.1	26.5	25.6	25.5
Lower limit Model B	−3.2	−2.8	−5	−3.5

Table E.1: Limits of Y-component velocity for each case at 10° for both models in m/s (round to one decimal places)

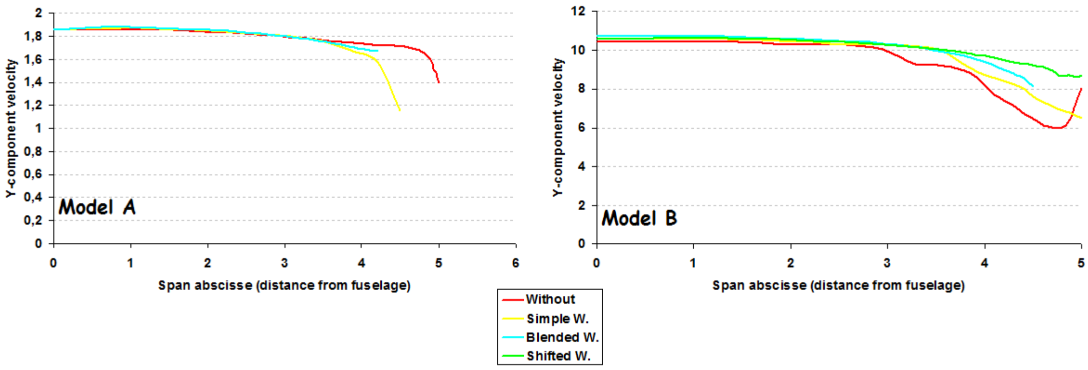

Figure E.4: Evoution of Y velocities on upper surfaces of model A and B at 0° and 10° respectively

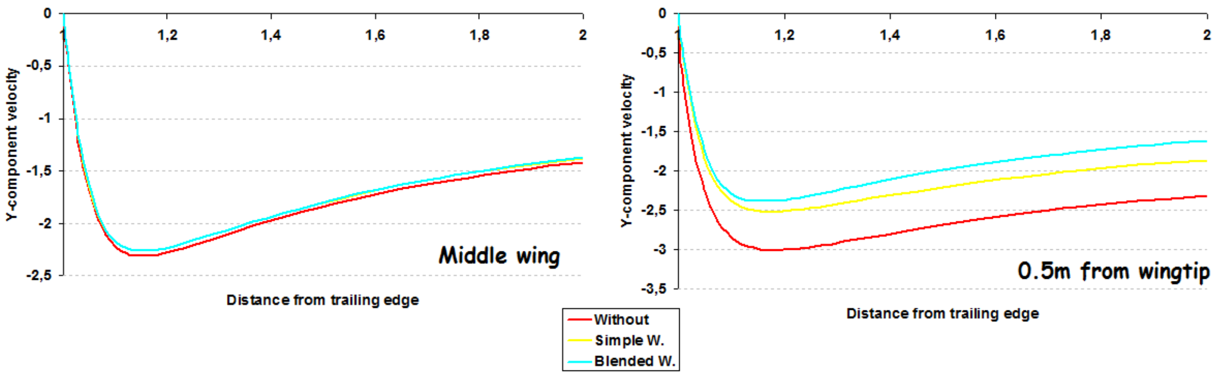

Figure E.5: Comparison between evolutions of Y-component in trailing wake between middle wing and at $0.5\,m$ from wingtip

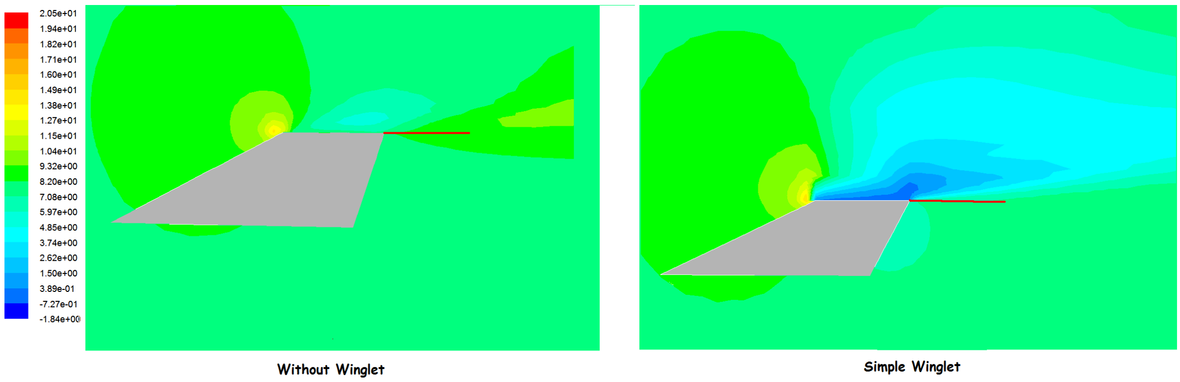

Figure E.6: Model B: Comparison between traling wake at wingtip in Y-component for each case: without and simple winglet respectively at $10°$

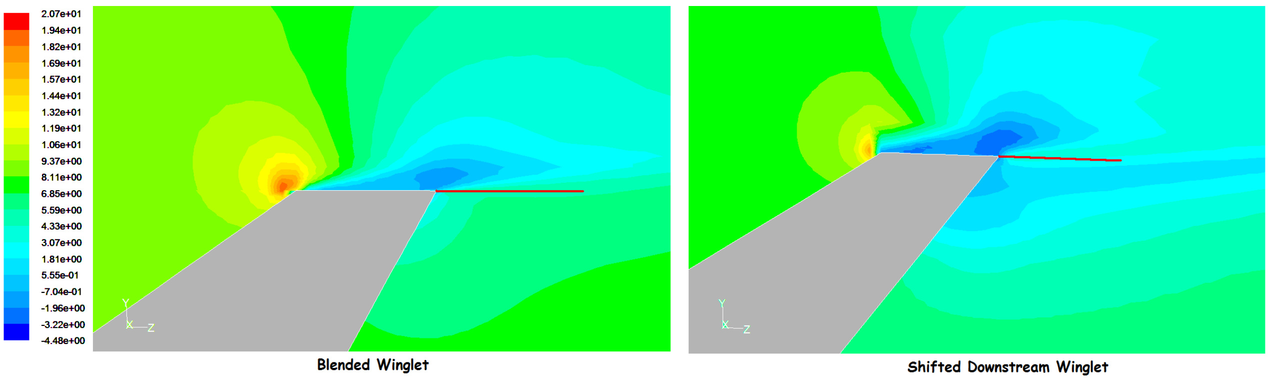

Figure E.7: Model B: Comparison between traling wake at wingtip in Y-component for each case: blended and shifted downstream winglet respectively at $10°$

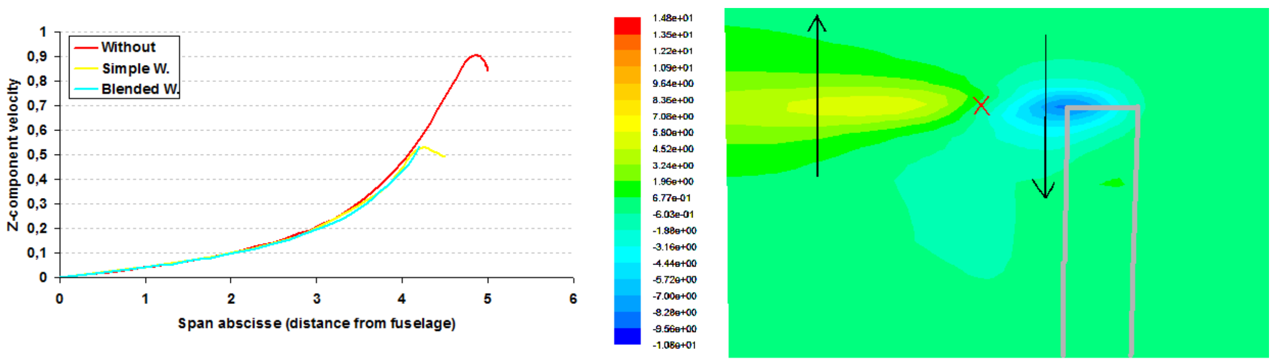

Figure E.8: Left: model A: Evolution of Z-component on the lower surface at $\alpha = 0°$ - Right: model B: rotation in Z-plane with its translated rotation center due to incidence ($10°$)

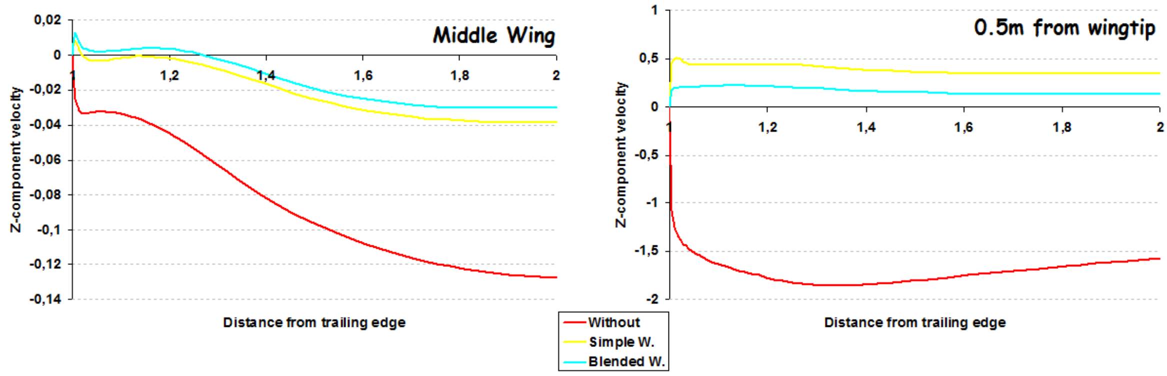

Figure E.9: Model A: Evolution of Z-components along the trailing path at middle wing and $0.5\,m$ from wingtip at $\alpha = 0°$

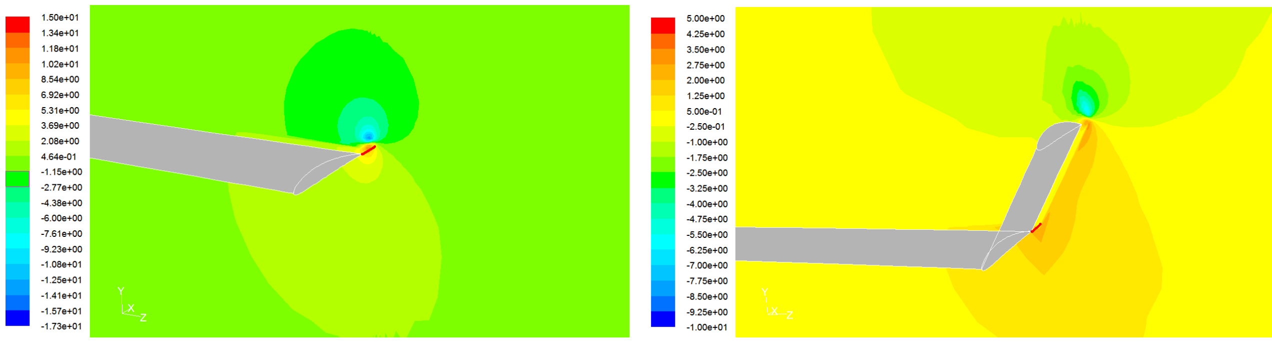

Figure E.10: Model A: Position of trailing path line in Z-components field for case without and with winglet, respectively, at $\alpha = 0°$

Appendix F

Vortex pattern figures

One can find all figures about vortex pattern analysis not displayed in the main report. These figure are not essential to be placed in the analysis itself. But a quick look at them could bring more information and make analysis easier to understand.

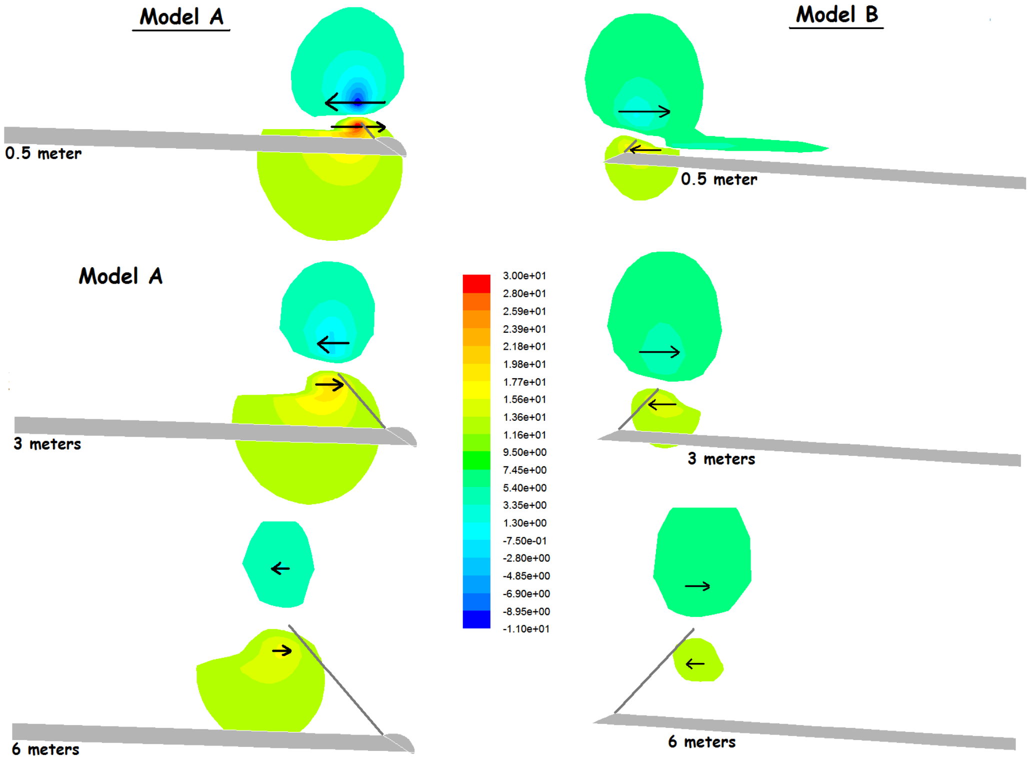

Figure F.1: Comparison of the evolution of vortex in case without winglet thanks to Z velocities evolution along cross sections behind the wing: 0.5, 3 and 6 m behind for both models $\alpha = 10°$

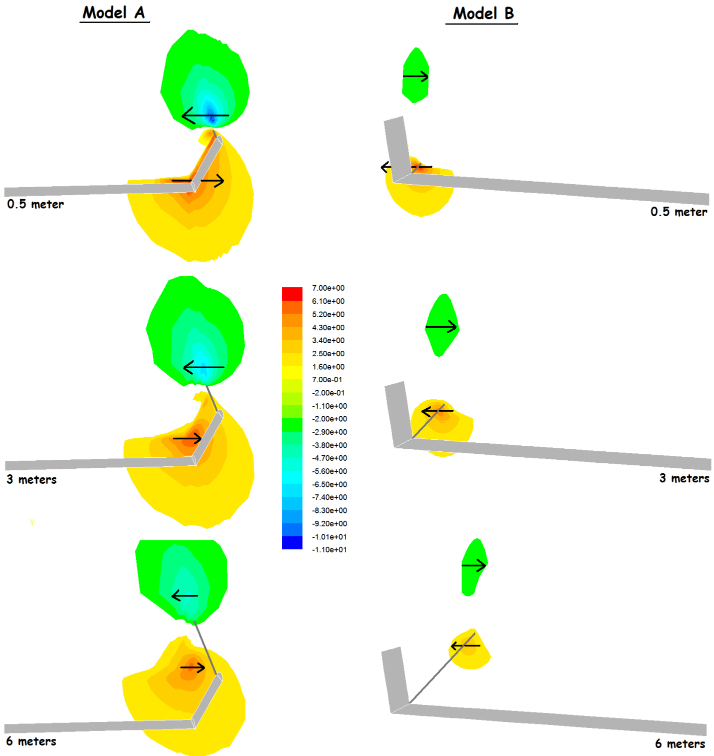

Figure F.2: Comparison of the evolution of vortex in case with simple winglet thanks to Z velocities evolution along cross sections behind the wing: 0.5, 3 and $6\,m$ behind for both models $\alpha = 10°$

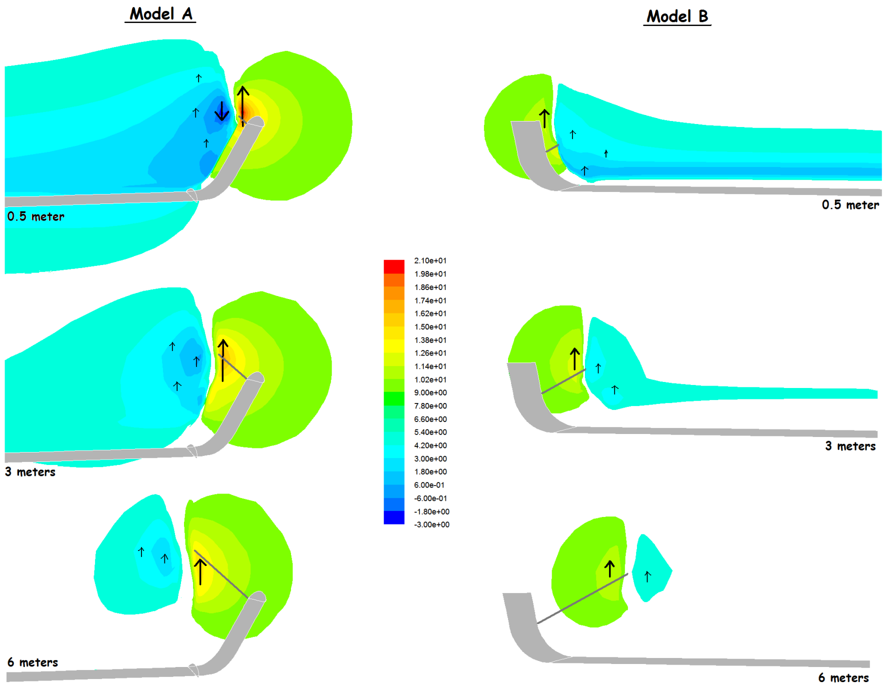

Figure F.3: Comparison of the evolution of vortex in case with blended winglet thanks to Y velocities evolution along cross sections behind the wing: 0.5, 3 and $6\,m$ behind for both models $\alpha = 10°$

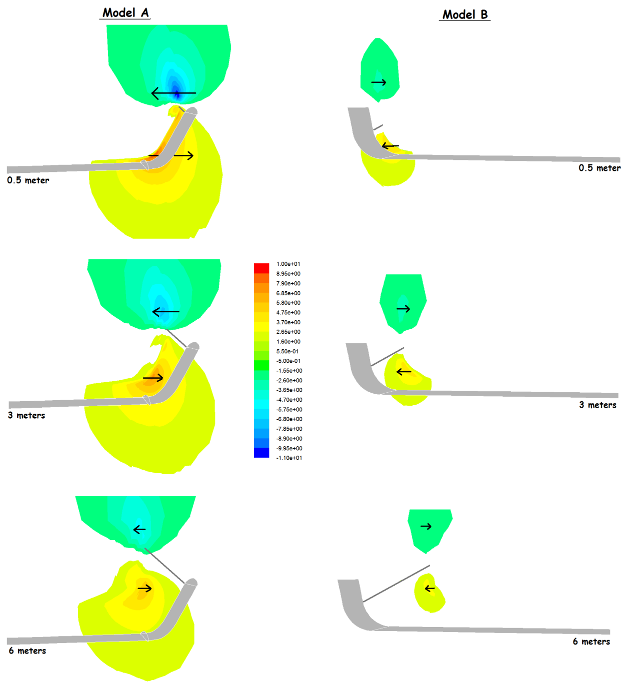

Figure F.4: Comparison of the evolution of vortex in case with blended winglet thanks to Z velocities evolution along cross sections behind the wing: 0.5, 3 and 6 m behind for both models $\alpha = 10°$

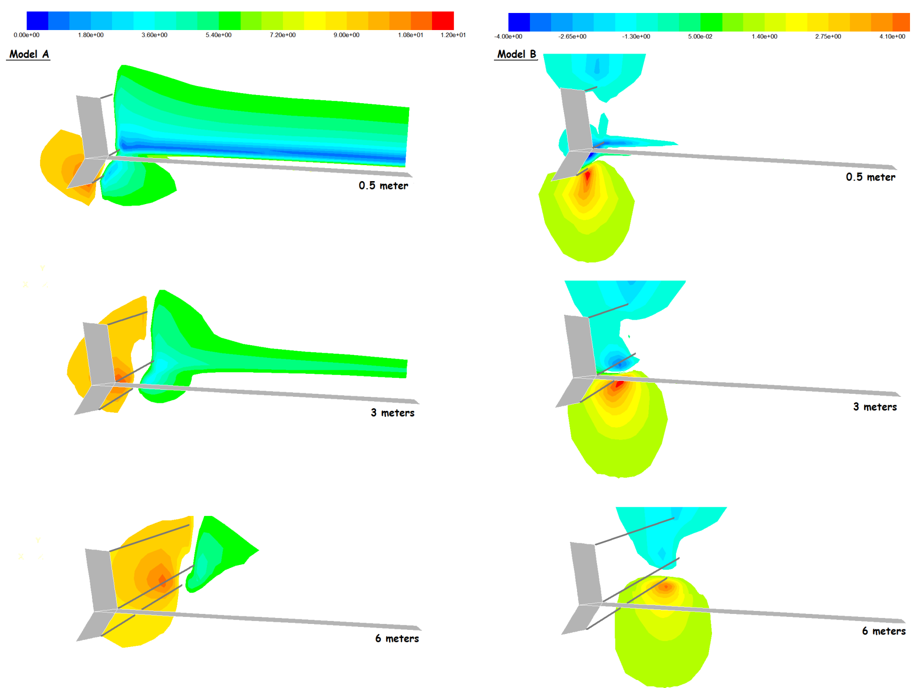

Figure F.5: Comparison of the evolution of vortex in case with shifted downstream winglet thanks to Y (Left) and Z (Right) velocities evolution along cross sections behind the wing: 0.5, 3 and 6 m behind for model B at $\alpha = 10°$

Part III

Bibliography

Bibliography

[1] *A. Filippone (1999-2001) "Wing-tip devices"*; Retrieved March, 2008 from http://aerodyn.org/drag/tip_devices.html

[2] *Winglet range performances*; Retrieved March, 2008 from http://www.b737.org.uk/winglets.htm

[3] *Prices evolutions study*; Retrieved March, 2008 from http://www.wtrg.com/prices.htm

[4] *Oil production*; Retrieved March, 2008 from http://www.energybulletin.net/primer.php

[5] *T.J. Craft, A.V. Gerasimov, B.E. Launder, C.M.E. Robinson*; A computational study of the near-field generation and decay of wingtip vortices; School of Mechanical, Aerospace and Civil Engineering, The University of Manchester, UK; 2006

[6] *Alexander Büscher, Rolf Radespiel, Thomas Streit*; Modelling and design of wing tip devices at various flight conditions using a databased aerodynamic prediction tool; Braunschweig, Germany; 2006

[7] *J. Leyser*; Accurate computation of lift and induced drag at lifting surfaces; AIAA Paper 96-2405-CP; 1996

[8] *A.Chr. Olesen, J.R. Jensen, S.H. Olesen and T. Meldgaard*; Investigation of Blended Winglets effect on Wing Performance; Aalborg University Denmark; FACE 7 semester, Autumn 2007

[9] *F. George*; Understanding Winglets Technology; Retrieved April, 2008 from http://www.smartcockpit.com

[10] *Vortex page*; Retrieved March, 2008 from http://www.wikipedia.org

[11] *Gratzer*; Blended winglet; United States Patent; Sept. 20 1994

[12] *Chungen Yin*; Numerical Fluid Dynamics lectures; Fall 2007; Institute of Energy Technology, Aalborg University

[13] *Fluent presentation*; Retrieved March, 2008 from http://www.erdc.hpc.mil/hardSoft/Software/fluent

[14] *Fluent models characteristics*; Retrieved April, 2008 from
http://down.cd/info_852.html
http://down.cd/info_1912.html

[15] *Fluent 6.2 User's guide*; January 2005

[16] *Cornell University Tutorials*; Retrieved April, 2008 from http://courses.cit.cornell.edu/fluent

[17] *http://www.fluent.com/software/fluent/fluent63.htm*

[18] *http://www.cfd-online.com* and *http://www.cfd-online.com/Wiki*

[19] *Ira H. Abbott and Albert E. Von Doenhoff*; Theory of wing sections (including a summary of airfoil data; Dover Publications inc.; 1960

[20] *B. Desauvage, D. Lambert, D. Renauld*; Travail intégré partie aérodynamique; 2e Epreuve du grade d'ingénieur civil électromécanicien en aéronautique; Liege University; 2007

[21] *E.L. Houghton, P.W. Carpenter*; Aerodynamics for Engineering Students (Fifth edition); Oxford, Great Britain: Butterworth-Heinemann; 2003